EFFECTS OF A TRANSVERSE ELECTRIC FIELD ON THE CHARACTERISTICS AND HEAT TRANSFER OF A DIFFUSION FLAME

Edwin R. Pejack and Henry R. Velkoff

Department of Mechanical Engineering

The Ohio State University
Research Foundation
Columbus, Ohio

Technical Report No. 8

November 1967

U. S. ARMY RESEARCH OFFICE - DURHAM
Box CM, Duke Station
Durham, North Carolina 27706

Contract No. DA-31-124-ARO-D-246

DISCLAIMER

The findings in this report are not to be construed as an official Department of the Army position unless so designated by other authorized documents.

****

The citation of trade names and names of manufacturers in this report is not to be construed as official Government endorsement or approval of commercial products or services references.

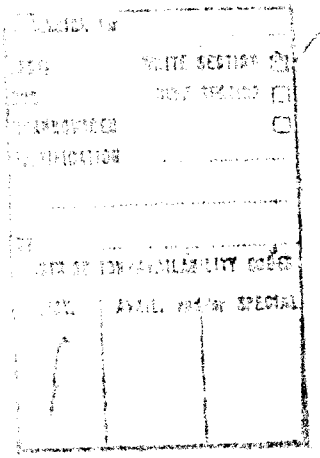

EFFECTS OF A TRANSVERSE ELECTRIC FIELD ON THE CHARACTERISTICS AND HEAT TRANSFER OF A DIFFUSION FLAME

Edwin R. Pejack and Henry R. Velkoff

Department of Mechanical Engineering

The Ohio State University
Research Foundation
Columbus, Ohio

November 1967

DISTRIBUTION OF THIS DOCUMENT IS UNLIMITED

U. S. ARMY RESEARCH OFFICE - DURHAM
Box Cm, Duke Station
Durham, North Carolina 27706

Contract No. DA-31-124-ARO-D-246
RF Project No. 1864

FOREWORD

The work reported herein was partially sponsored by the United States Army Research Office, Durham, under Contract No. DA-31-124-ARO-D-246. This re ort was presented by Edwin R. Pejack as partial fulfillment of the requirements for the Doctor of Philosophy degree at The Ohio State University.

The author wishes to thank H. R. Velkoff, project supervisor; C. D. Jones, faculty advisor; and M. Wineaz, C. Meacham, I. Anderson, and W. Graham, student assistants; for their help in the completion of this research.

ABSTRACT

Effects of a transverse electric field on a parallel flow diffusion flame in a flat combustion chamber were investigated. Various mixtures of propane, nitrogen, and air were introduced separately at the base of an experimental combustion chamber and burned in a diffusion flame sheet located between flat walls of the chamber which served as anode and cathode. The electrode walls were instrumented to measure the local heat transfer rate, local current density, and pressure.

It was found that the application of a voltage difference across the electrodes moved ions out of the burning zone and resulted in a current at the electrode walls. The heat transfer rate near the base of the flame was considerably increased on the cathode and decreased on the anode; at positions further from the base of the flame the electric effect was lessened.

Flame distortion was thought to be caused by electrically induced gas motion derived from a gradient in current density in the flow direction and by the onset of an electrically induced flame flickering. An analysis of the products of combustion revealed that the applied electric field acted to increase the amount of unburnt solid carbon and decrease the quantities of unburnt fuel and carbon monoxide.

TABLE OF CONTENTS

TABLE OF CONTENTS (continued)

LIST OF TABLES

LIST OF FIGURES

LIST OF FIGURES (continued)

LIST OF FIGURES (continued)

LIST OF FIGURES (continued)

LIST OF SYMBOLS

A	flame thickness, inch
a	position of interface, inch
C	concentration, lbm $inch^{-3}$
D	diffusion coefficient, $inch^2 sec^{-1}$
E	electric field strength, volt $inch^{-1}$
F	body force per unit volume, lbf $inch^{-3}$
G	stability parameter
i	number of air molecules combining with one of fuel
J	current density, amp $inch^{-2}$
J_o	current density at electrode
k	mobility, $inch^2$ $volt^{-1}$ sec^{-1}
L	distance from anode to flame
L_o	L at y = 0
n	Number density, charges per cubic inch
p	pressure, lbf $inch^{-2}$
q	heat transfer per area, BTU $hr^{-1}ft^{-2}$
Q	heat transfer, BTU hr^{-1}
r	charge generation rate, charges $sec^{-1}inch^{-3}$
R	width of combustion chamber, inch
s	x-L, inch
t	time, sec
U	uniform gas velocity, inch sec^{-1}
u	gas velocity in y direction, inch sec^{-1}
v	ion velocity, inch sec^{-1}
V	voltage, volt

w	induced velocity, inch sec^{-1}
x	coordinate across chamber
y	coordinate along chamber
α	recombination coefficient, $inch^3$ sec^{-1}
ϵ	dielectric permittivity, $coulomb^2$ lbf^{-1} $inch^{-2}$
ρ	density, lbm $inch^{-3}$

Subscripts and Superscripts

A	air
f	flame
F	fuel
s	saturation
x	component in x direction
y	component in y direction
+	positive charge carrier
-	negative charge carrier
'	nondimensionalized quantity
1	fuel zone
2	ionization zone
3	air zone

CHAPTER 1

INTRODUCTION

The area of study known as electrofluidmechanics is concerned with the behavior of a fluid in an electric field when the fluid is responsive in some way to the electric field. One such fluid-field interaction has as its basis the force exerted on charged particles distributed within a region of the fluid, which, because of molecular collisions, result in forces on the fluid. In this type of interaction the electric field couples with the fluid mechanic system through the inclusion of an electric body force in the equations of fluid motion. Since it transpires that combustion flames by their nature are sources of partially ionized gas, a mechanism for the flame-field interaction is established and provides the basis for the study in this investigation.

The physical situation considered is that of a flat parallel flow diffusion flame of propane/nitrogen and air burning at atmospheric pressure in a flat combustion chamber. Opposing walls of the combustion chamber serve as anode and cathode by which an electric field is impressed transverse to the diffusion flame sheet. The walls of the chamber are instrumented to measure the internal local heat transfer rates with electrode voltage, gas mixture, and gas velocity as operating parameters. The electrical measurements of local current density, ion density, and electric pressure are also made to elucidate the ways by which the field interacts with the flame. Exhaust temperatures and compositions are measured for all values of the operating parameters so that an overall heat balance can be set up for the combustion chamber. The objects of the investigation are first of all to determine the physical effects of the electric field on the flame, with a particular emphasis on the local heat transfer rates, and secondly, by an analysis of experimental data and theoretical principles to determine the mechanisms responsible for the physical effects observed.

The range of voltages encountered in this study are low enough such that the processes of electrical arcing, surface ionization, and secondary ionization do not occur, and that the field induced ion velocity is small compared to the random thermal velocity of molecular motion. The gas velocities are sufficiently low that compressibility and magnetic effects are not considered.

CHAPTER 2

SURVEY OF PREVIOUS WORK IN THE AREA OF FLAME-FIELD INTERACTIONS

Many experiments have shown that certain flames respond to an applied electric field; a review of the earlier literature on the subject is given by Wilson (1)* The typical experiment may be represented by a candle or Bunsen flame located in a horizontal electric field showing distortion of the flame toward the negative electrode. General agreement has developed that the major flame-field effects are caused by a great disparity in the size and mobility between the positive and negative charge carriers which, in an electric field, results in net forces on the flame gases in the direction of the drift of the ion with the lowest mobility (2).

Since the antecedent for the flame response to an electric field is the production of ion pairs within the flame, it is not surprising that much research has been performed to establish, for a given flame system, the source of the ionization, the identification of the ions, and their number density.

With respect to the source of the ionization, two processes are considered: nonequilibrium or chemi-ionization resulting from the chemical reaction and equilibrium thermal ionization as predicted from Saha's equation (3) which expresses the degree of ionization as a function of the temperature and ionization potential of the molecule. Many investigators (4,5,6,7) have measured ion concentrations in flames much higher than predicted by Saha's equation and therefore concluded that chemi-ionization was important. However, in flames where material with a relatively low ionization potential is present, such as carbon particles or metallic salts, then thermal ionization may be large enough to dominate chemi-ionization (8,9,10).

Identification of flame ions and determination of their number density is still a relatively current area of research. Mass spectrometer and electrostatic probe studies (6,11,12) have shown for certain hydrocarbon flames that the most numerous positive ion is H_3O^+, with significant numbers of $C_3H_3^+$. Number densities of positive ions have been measured from 10^8 to 10^{14} ions per cubic centimeter in the reaction zone (3,5,13,14,15,16,17,18,19,20). Negative ions O^- and OH^- have been found to be present in quantities two orders of magnitude lower than the positive ion (11), which indicates that most of the negative charges are present as electrons, in agreement with other investigations (4,6,7,16);

* Numbers in parentheses refer to references in the reference list

in some cases electron attachment to molecules may also act to produce negative ions (18). Considerable increases in the level of ionization have been achieved by the injection of metallic salts of metals with low ionization potentials, such as cesium or potassium (1,21) with a consequent greater electric field interaction (22).

In the particular case of hydrocarbon flames, carbon formation plays an important role in contributing to flame ionization. Nakamura (10) showed that there is a close relationship between ion concentration and carbon formation in a diffusion flame. Others (9,23) have similarly found that flames rich in hydrocarbon fuel produce much more ionization than lean flames. One mechanism put forth is that while the carbon molecule has a relatively high ionization potential, the ionization potential of an aggregate of carbon molecules would approach the much lower value of solid carbon, and, therefore, thermal ionization would increase. The phenomenon of carbon ionization has been suggested as a means of electrically controlling flame carbon (2,24).

Although Sir J. J. Thompson suggested as early as 1909 (7) that combustion processes could be controlled by the application of a magnetic or electric field, only recently has research been initiated concerned with practical effects of flame-field interactions, in distinction to purely diagnostic or combustion kinetics oriented research. Payne and Weinberg(2,25) in a preliminary investigation discussed potential applications to heat transfer control and carbon deposition. A later paper (23) discussed the limitations of flame-field interactions imposed by electrical breakdown of the gases in the electrode space and by the rate of ion generation within the flame. It was noted that the breakdown limitation could be optimized by suitable geometric configurations, and that the ion limitation could be circumvented by seeding with metallic salts.

Some interesting work has been performed showing that electric fields can under some conditions support a flame that, if the field were removed, would be extinguished. Both blow-off limits (26) and lean extinction limits (27,28) were found to be increased by the application of an electric field. The maximum volumetric heat release rate was also increased in an opposed-jet diffusion flame system by the application of a field perpendicular to the flame surface (29).

Ionization and a consequent electric field interaction was demonstrated to exist for detonation waves (30). The detonation velocity could be either increased or decreased by electric fields, or even quenched (31,32).

The energy supplied to the flame through the application of the field in the cases discussed above is small compared to the chemical energy release and is not a direct influence in the interaction. There has been some interest, however, in augmenting the chemical energy release in flames with electrical energy by means of a superimposed

electric discharge (33,34,35). The goal is to generally increase flame heat transfer and make more efficient use of the chemical energy, or to produce hotter flames than obtainable by combustion alone. This concept has the operational problem that the electrical discharge tends to localize in the flame rather than distribute over the region of combustion.

CHAPTER 3

ELECTRIC EQUATIONS OF A DIFFUSION FLAME BETWEEN FLAT PLATE ELECTRODES

3.1 ONE DIMENSIONAL ANALYSIS

3.1.1 Statement of the Problem - The physical configuration considered is that of a flat diffusion flame parallel to and located between flat plate electrodes as shown in Fig. 1. For an approximate one dimensional analysis taking into consideration only the variation in ion density and field strength across the combustion chamber in the x direction, the variation of physical properties in the y direction is neglected, and the flame is considered to be a flat sheet of uniform thickness.

For flames which are affected by electric fields, there will be ion pairs generated within the reaction zone because of either thermal or chemi-ionization. It would be expected that the ion generation rate would be a maximum at some point within the reaction zone and decrease in both directions. For the following analysis however, an ionization zone thickness, A, is taken as the thickness over which a constant ion generation rate, r, would produce the same number of total ion pairs as actually produced in the flame.

When no electric field is applied to the flame, the number density n_+ and n_- of the positive and negative ions, respectively, would be such a value that the loss of ion pairs by recombination would equal the production of ion pairs by the ion generation rate r. Then for no applied field,

$$r = \alpha n_+ n_- \tag{3.1}$$

where α is the recombination coefficient.

When an electric field is applied to the ionization zone, forces are exerted on the ions, which tend to move them out of the ionization zone. For the electrode configuration in Fig. 1 the positive ions that are moved out of the ionization zone would move across the air zone to the right of the flame, and the negative ions would tend to move across the fuel zone to the left of the flame. Except for a negligible amount of ions which may be present in the air and fuel zones because of random thermal ionization, the ions in the air and fuel zones are either all positive or all negative. Therefore, no recombination can occur in these zones, and the ions would drift across to the electrodes where they are measured as a current density, J_o.

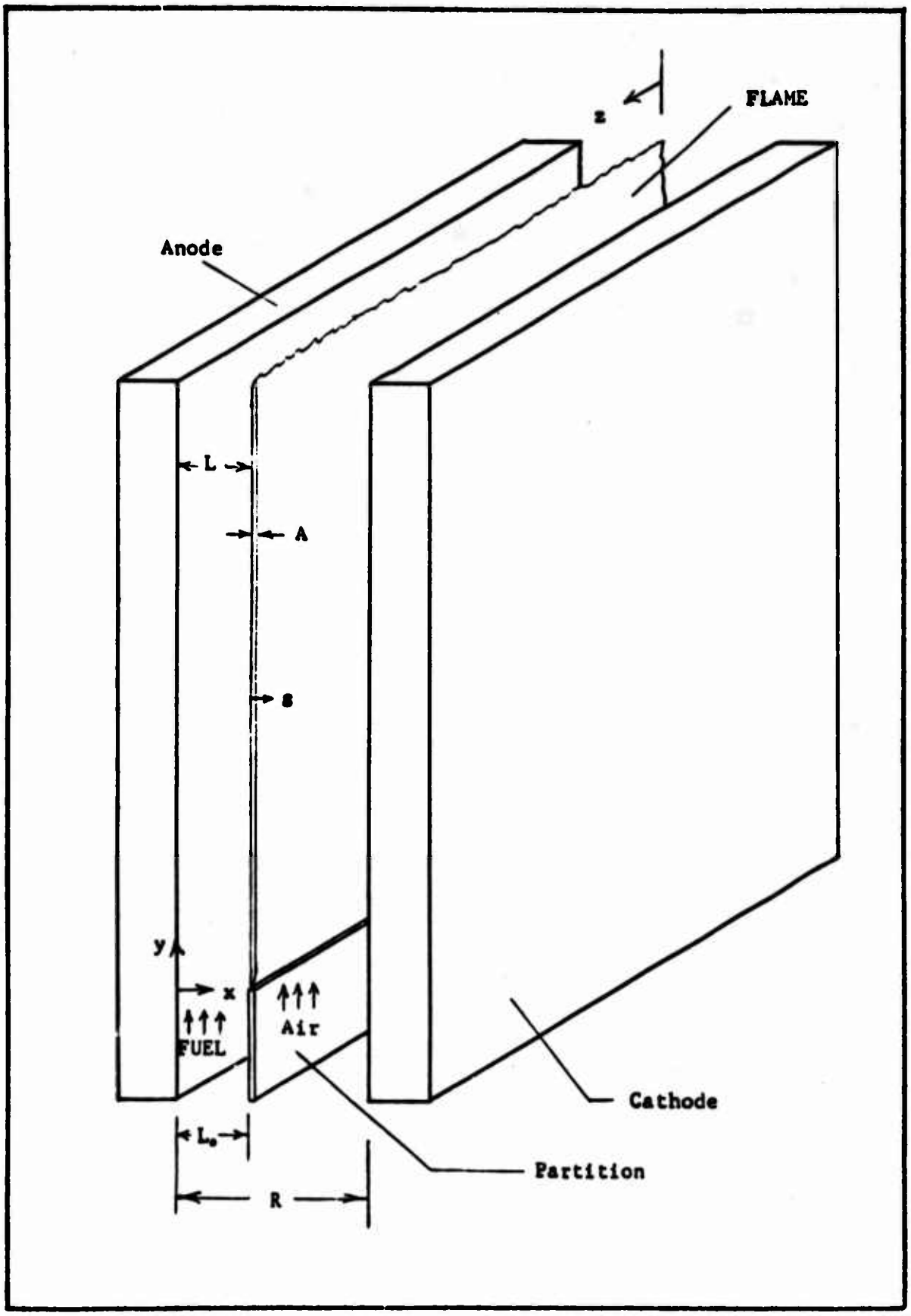

Fig. 1 Diffusion flame between electrodes

It is assumed as an approximation that the ion generation rate, r, and the ionization zone thickness, A, are properties of the flame and not affected by the electric field. It is clear then that an upper limit on the ion current density would exist when the field is strong enough to remove every ion pair from the ionization zone at a rate sufficiently high that recombination is negligible. At field strengths higher than this value no further increase in ion current could be expected as long as there were no secondary ionization occurring in the fuel or air zones or on the electrode surfaces. The point at which this condition is reached is termed the saturation point and the associated quantities, saturation current density, J_s, saturation field strength E_s, and saturation voltage, V_s, are thus defined.

At field strengths lower than the saturation field strength, both recombination and field removal are active in removing ion pairs from the ionization zone. In this case, the ion current density, J, would be expected to be dependent on the applied field strength. The electric analysis of the flame between electrodes can be, therefore, conveniently considered in two regimes, subsaturation and saturation, and three zones, the fuel zone, the air zone, and the ionization zone, as suggested by Weinberg (23).

3.1.2 Subsaturation: The Ionization Zone - Throughout this analysis, the field strengths in the gas are taken to be low enough that the ions may be characterized as having a constant mobility, k. This means that macroscopically the ions drift at a velocity

$$v_+ = k_+E \tag{3.2}$$

or

$$v_- = k_-E \tag{3.3}$$

for positive and negative ions, respectively, where k is the ion mobility and E is the field strength.

For the one-dimensional treatment, the drift velocity is considered high enough in relation to the air and fuel velocities that the ions move across the air and fuel zones with no appreciable motion in the y direction. In other words, it is taken that

$$J_{y+} = J_{y-} = 0 \tag{3.4}$$

The ion current density is then

$$J_+ = n_+v_+ \quad \text{for positive ions} \tag{3.5}$$

and

$$J_- = n_-v_- \quad \text{for negative ions} \tag{3.6}$$

By combining Eqs. (3.2) and (3.3) into (3.5) and (3.6) there results the ion density:

$$n_+ = \frac{J_+}{k_+ E} \qquad \text{for positive ions} \qquad (3.7)$$

and

$$n_- = \frac{J_-}{k_- E} \qquad \text{for negative ions} \qquad (3.8)$$

From published results on flame ionization (4,6,7,16) there is some evidence that the negative ions are composed largely of electrons and hence have a mobility very large in comparison to any conceivable positive ion. This means that in the presence of any electric field, the right side of Eq. (3.8) is small compared to Eq. (3.7) and hence the negative ion density is very small compared to the positive ion density. Consequently, the negative ion density is taken as zero in regions where an electric field exists.

A region of the ionization zone can have either a finite field strength or a zero field strength. Considering a region where the field is finite, continuity of positive ion flow gives

$$\frac{dJ}{dx} = r - \alpha n_+ n_- \qquad (3.9)$$

But for regions where there is a field n_- is negligible and Eq. (3.9) reduces to

$$\frac{dJ}{dx} = r \qquad (3.10)$$

For convenience, a coordinate system is placed at the left side of the ionization zone in Fig. 1; i.e., let

$$s = x - L \qquad (3.11)$$

Then Eq. (3.10) is written as

$$\frac{dJ}{ds} = r \qquad (3.12)$$

If the boundary condition on Eq. (3.12) is taken as $J = 0$ at $s = 0$, and r is considered constant, the solution to Eq. (3.12) is

$$J = rs \qquad (3.13)$$

Equation (3.13) above gives a maximum current density at the edge of the

ionization zone equal to rA. This current density, however, is the maximum current density obtainable from the flame, contrary to the assumption of subsaturation conditions. It must, therefore, be assumed that for subsaturation one part of the ionization zone has a zero field strength, and another part a finite field strength. Letting $s = s_1$ be the value of s that divides the ionization zone into the two parts, then for $s < s_1$, $E = 0$ and $J_+ = 0$, and for $s > s_1$, Eq. (3.12) applies. The details of the following analysis are carried out in Appendix 1 where it is shown that

$$s_1 = \left[1 - \frac{J_o}{J_s}\right] A \tag{3.14}$$

where J_o is the current density at the edge of the ionization zone, which is also the current density at the electrode surfaces.

For regions where $s > s_1$, Maxwell's relation

$$\frac{dE}{ds} = \frac{n_+}{\epsilon} \tag{3.15}$$

and the boundary condition $E = 0$ at $s = s_1$ leads to

$$E = \left[\frac{J_s A}{k\epsilon}\right]^{1/2} \left[\frac{J_o}{J_s} - 1\right] + \left[\frac{J_s}{Ak\epsilon}\right]^{1/2} s \tag{3.16}$$

$$(s > s_1)$$

where k without subscript will hereafter be taken as the positive ion mobility.

Equation (3.16) gives the field strength at any point within the ionization zone. The field strength at the edge of the ionization zone facing the cathode, E_f, is obtained by setting $s = A$ in Eq. (3.16).

$$E_f = \left[\frac{A}{J_s k\epsilon}\right]^{1/2} J_o \tag{3.17}$$

The potential drop across the ionization zone, V_2, is obtained by integrating Eq. (3.16) from $s = s_1$ to $s = A$.

$$V_2 = \frac{1}{2}\left[\frac{J_o^4 A^3}{J_s^3 k\epsilon}\right]^{1/2} \tag{3.18}$$

3.1.3 Subsaturation: The Air Zone - In this region no ionization or recombination occurs and $J = J_o$. From Appendix 1, using Maxwell's equation

$$\frac{dE}{dx} = \frac{n_+}{\epsilon} \tag{3.19}$$

and the boundary condition $E = E_f$ at $s = A$, from Eq. (3.16) there results

$$E = \left[\frac{2J_o}{k\epsilon}\left(x-L+\frac{J_oA}{2J_s}-A\right)\right]^{1/2} \tag{3.20}$$

The potential drop across the air zone, V_3, is obtained by integrating Eq. (3.20) from $x = L + A$ to $x = R$. Therefore

$$V_3 = \frac{2}{3}\left(\frac{2J_o}{k\epsilon}\right)^{1/2}\left[\left(R-L-A+\frac{J_oA}{2J_s}\right)^{3/2}-\left(\frac{J_oA}{2J_s}\right)^{3/2}\right] \tag{3.21}$$

3.1.4 Subsaturation: The Fuel Zone - The ions in the fuel zone are composed largely of electrons and as previously stated have a very high mobility and a negligible concentration. From Maxwell's equation

$$\frac{dE}{dx} = \frac{n_-}{\epsilon} = 0 \tag{3.22}$$

and therefore the field strength is constant across the zone. Since $E = 0$ at the edge of the zone, $E = 0$ everywhere in the fuel zone. The potential drop across the zone, V_1, is also zero as a result.

3.1.5 Subsaturation: Summary - The total potential drop across all zones must equal the voltage applied to the electrodes, V. Therefore

$$V = \frac{1}{2}\left[\frac{J_o^4A^3}{J_s^3k\epsilon}\right]^{1/2}+\frac{2}{3}\left(\frac{2J_o}{k\epsilon}\right)^{1/2}\left[\left(R-L-A+\frac{J_oA}{2J_s}\right)^{3/2}-\left(\frac{J_oA}{2J_s}\right)^{3/2}\right] \tag{3.23}$$

The ionization zone is very thin compared to the electrode spacing. (Calcote and King (36) measured an ionization zone of around one-half a millimeter thick.) So Eq. (3.23) can be reduced to

$$V = \frac{2}{3}\left(\frac{2J_o}{k\epsilon}\right)^{1/2}(R-L)^{3/2} \tag{3.24}$$

where small terms have been dropped. Taking the derivative of Eq. (3.24), we find

$$\frac{dJ_o}{dV} = \frac{9k\epsilon V}{4(R-L)^3} \tag{3.25}$$

which will be used later. Equation (3.17) and (3.24) can be written in nondimensional form as

$$E' = E_f \left[\frac{J_s A}{k\epsilon}\right]^{-1/2} = \frac{J_o}{J_s} \tag{3.26}$$

and

$$V' = \frac{3}{2}\left[\frac{2J_s}{k\epsilon}\right]^{-1/2} (R-L)^{-3/2} V = \left[\frac{J_o}{J_s}\right]^{1/2} \tag{3.27}$$

3.1.6 Saturation: The Ionization Zone - In the saturation regime all ion pairs generated in the flame are moved out of the flame by electric forces and measured as current density, J_s, at the electrode walls. The field strength in the zone is obtained from Eq. (3.15) as before; however, in this case the field at the edge of the ionization zone is unknown. From Appendix 1 the solution for the field strength is

$$E = \left[E_f^2 - \frac{J_s}{k\epsilon A}(A^2-s^2)\right]^{1/2} \tag{3.28}$$

where E_f, the field strength at the edge of the zone facing the cathode, is unknown at present and will be determined later. The potential drop across the zone, V_2, is obtained from integration of Eq. (3.28) from $s = 0$ to $s = A$. From Appendix 1,

$$V_2 = \frac{E_f A}{2} + \frac{1}{2}\left(\frac{J_s A^3}{k\epsilon}\right)^{1/2}\left[E_f^2 \frac{k\epsilon}{J_s A} - 1\right] \operatorname{csch}^{-1}\left[E_f^2 \frac{k\epsilon}{J_s A} - 1\right]^{1/2} \tag{3.29}$$

3.1.7 Saturation: The Fuel Zone - As before, the field strength is constant and equal to the value at the edge of the ionization zone facing the anode. Equation (3.28) at $s = 0$ is

$$E = \left[E_f^2 - \frac{J_s A}{k\epsilon}\right]^{1/2} \tag{3.30}$$

which gives the field strength at any point in the fuel zone. The potential drop across the zone, V_1, obtained by integration of Eq. (3.30) across the fuel zone is

$$V_1 = \left[E_f^2 - \frac{J_s A}{k\epsilon}\right]^{1/2} L \tag{3.31}$$

3.1.8 Saturation: The Air Zone - The boundary condition on Eq. (3.19) is $E = E_f$ at $x = L + A$. Then integrating Eq. (3.19),

$$E = \left[\frac{2J_s}{k\epsilon}(x-L-A) + E_f^2\right]^{1/2} \tag{3.32}$$

Integrating Eq. (3.32) across the air zone to find the potential drop V_3,

$$V_3 = \frac{k\epsilon}{3J_s}\left\{\left[\frac{2J_s(R-L-A)}{k\epsilon} + E_f^2\right]^{3/2} - E_f^3\right\} \tag{3.33}$$

3.1.9 Saturation: Summary - The total potential drop across all zones must equal the voltage applied to the electrodes. Therefore,

$$V = \left[E_f^2 - \frac{J_s A}{k\epsilon}\right]^{1/2} L + \frac{E_f L}{2} + -\left[\frac{J_s A^3}{k\epsilon}\right]^{1/2}\left[\frac{E_f^2 k\epsilon}{J_s A} - 1\right] \operatorname{csch}^{-1}\left[\frac{E_f^2 k\epsilon}{J_s A} - 1\right]^{1/2}$$

$$+ \frac{k\epsilon}{3J_s}\left\{\left[\frac{2J(R-L-A)}{k\epsilon} + E_f^2\right]^{3/2} - E_f^3\right\} \tag{3.34}$$

Again for $A < R$ and $A < R-L$, the potential drop can be simplified to

$$V = \left[E_f^2 - \frac{J_s A}{k\epsilon}\right]^{1/2} L + \frac{k\epsilon}{3J_s}\left\{\left[\frac{2J_s(R-L)}{k\epsilon} + E_f^2\right]^{3/2} - E_f^3\right\} \tag{3.35}$$

By nondimensionalizing Eq. (3.35) in the same way as Eq. (3.27), there results

$$V' = \frac{3}{2^{3/2}}\left[E'^2 - 1\right]^{1/2}\left[\frac{L}{R-L}\right]\left[\frac{A}{R-L}\right]^{1/2} + \left[1 + \frac{E'^2 A}{2(R-L)}\right]^{3/2} - \frac{E'^3}{2^{3/2}}\left[\frac{A}{(R-L)}\right]^{3/2} \tag{3.36}$$

Figure 2 is a plot of the nondimensional field strength at the flame surface versus the nondimensional voltage applied to the electrodes, for the particular case of $L/(R-L) = 1$ and $A/(R-L) = 0.04$. The general behavior of the flame field strength is that it increases slowly with increasing electrode voltage at low voltages, but at higher voltages the field strength increases more rapidly.

3.2 TWO DIMENSIONAL ANALYSIS

In the most general case, the flame ionization rate and the type of ion may be a function of distance y along the flame. Suppose that the quantity J_x/k varies in some way along the flame. That is, let

$$\frac{J_x}{k} = \text{function of } y \tag{3.37}$$

where a subscript x or y signifies the component of that quantity in the x or y direction, respectively. The one dimensional analysis of Section 3.1 will now be assumed to be valid at any y if the corresponsing J_x and k from Eq. (3.37) is used. Then

$$J_x = n_+ k\, E_x \tag{3.38}$$

is valid at any point. Writing Eq. (3.38) as

$$\frac{J_x}{k} = \text{function of } y = n_+ E_x \tag{3.39}$$

and substituting Eq. (3.19) yields

$$\frac{1}{2}\frac{dE_x^2}{dx} = \frac{\text{function of } y}{\epsilon} \tag{3.40}$$

Integrating,

$$E_x^2 = \frac{(\text{function of } y)x}{\epsilon} + \text{constant} \tag{3.41}$$

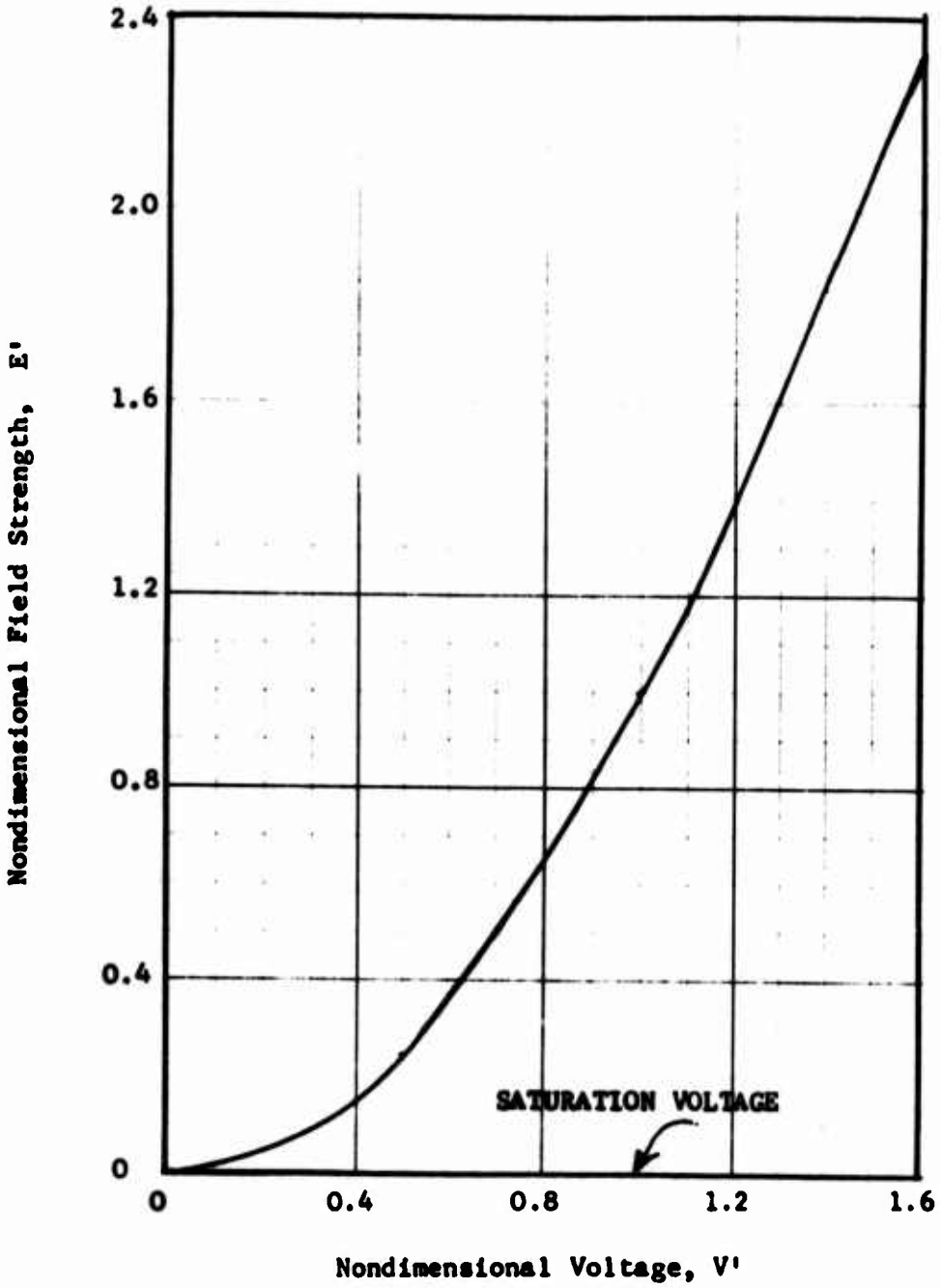

Fig. 2 Nondimensional field strength versus nondimensional voltage

which shows that E_x is a function of x and y. Substituting Eq. (3.41) into Maxwell's equation pertaining to irrotationality of the field,

$$\frac{\partial E_x}{\partial y} = \frac{\partial E_y}{\partial x} \tag{3.42}$$

there results

$$\frac{\partial E_y}{\partial x} = \text{a nonzero function.}$$

Therefore E_y is nonzero and $J_y = n_+ k E_y$ is also nonzero, contrary to the assumptions of the one-dimensional treatment. It is concluded then that if the current density or mobility k varies in the y direction, a component of J and E will result in the y direction. A component of E in the y direction will result in electric forces and induced motion in that direction, which will later be shown to affect the location of the diffusion flame in the chamber.

CHAPTER 4

MODEL OF A DIFFUSION FLAME BETWEEN FLAT PLATE ELECTRODES

4.1 DIFFUSION FLAME THEORY WITH NO ELECTRIC FORCES

The case considered first is the diffusion flame in Fig. 1 when no voltage is applied across the electrodes. The electrodes merely act as confining walls, and the flame can be analyzed by the method used by Burke and Schumann (37), or by modifications of this method (38).

The problem consists of determining the position and shape of the flame within the combusion chamber when the flow rates of gases are known. Following the simplified treatment of Burke and Schumann, the following assumptions are made:

1) Velocity is constant and in the y direction only;

2) The diffusion of the gases is one dimensional and can be described by Fick's law with a constant diffusion coefficient D;

3) The fuel and oxidant have the same density, so gravity effects are negligible.

Although assumption 1 is subject to question considering that viscous effects tend to reduce the velocity near the walls and that the high temperature generated by the flame tends to cause expansion and higher velocities near the flame, it is frequently mentioned that assumption 2 tends to counterbalance the inaccuracies of assumption 1 because the diffusion coefficient increases with temperature and tends to shorten the flame while the increased velocity near the flame tends to lengthen the flame. In any case, the simple diffusion flame theory is discussed here only as a basis for the discussion of a mechanism for an electric effect to be discussed later.

The physical situation involved is the interdiffusion of fuel and air which are initially separate at y = 0 and interdiffuse as the mixture flows up the combustion chamber at constant velocity U. The fuel and air are considered separately. Taking the air component first, the conservation of air in a differential volume element leads to the diffusion equation

$$\frac{\partial C_A}{\partial t} = D \frac{\partial^2 C_A}{\partial x^2} \qquad (4.1)$$

Since

$$y = Ut \tag{4.2}$$

and U is taken as constant, Eq. (4.1) can be written

$$\frac{\partial C_A}{\partial y} = \frac{D}{U} \frac{\partial^2 C_A}{\partial x^2} \tag{4.3}$$

which is the diffusion equation for the air concentration anywhere in the combustion chamber. The boundary conditions are

at $x = 0$, at $x = R$, $\quad \frac{\partial C_A}{\partial x} = 0$

at $y = 0$, $\quad C_A = 0$ from $x = 0$ to L_o

at $y = 0$, $\quad C_A = C_{Ao}$ from $x = L_o$ to R

Equation (4.3) with the above boundary conditions can be solved by the method of separation of variables. The solution is

$$C_A = C_{Ao}\,(1 - L_o/R) - \sum_{n=1}^{\infty} \frac{2C_{Ao}}{n\pi} \sin \frac{n\pi L_o}{R} \cos \frac{n\pi x}{R} \exp\left[-\frac{Dn^2\pi^2 y}{UR^2}\right] \tag{4.4}$$

The concentration of fuel, C_F, is determined in the same way, and

$$C_F = \frac{L_o C_{Fo}}{R} + \sum_{n=1}^{\infty} \frac{2C_{Fo}}{n\pi} \sin \frac{n\pi L_o}{R} \cos \frac{n\pi x}{R} \exp\left[-\frac{Dn^2\pi^2 y}{UR^2}\right] \tag{4.5}$$

The concentration of fuel and air having been found from Eqs. (4.4) and (4.5), the flame surface is determined by the values of x and y such that

$$iC_F = C_A \tag{4.6}$$

where i is the number of air molecules which combine with one molecule of fuel.

4.2 DIFFUSION FLAME IN AN ELECTRIC FIELD ONE DIMENSIONAL MODEL

In the completely one dimensional treatment of a diffusion flame, the current density, flame location, and electric field strength are not dependent on y. Following the results of Section 3.1, there exists within the gas containing the positive ion a body force per unit volume

$$F = n_+ E = \frac{J}{k} \tag{4.7}$$

The equations of motion then permit a solution

$$v_x = 0$$

$$v_y = U = \text{constant}$$

where v_x and v_y are the respective x and y component of velocity. The body force is effective in producing a pressure gradient

$$\frac{\partial p}{\partial x} = F \tag{4.8}$$

As long as the pressure generated is small enough to render the effects of pressure diffusion or density changes small compared to the effects of concentration gradients, which is the case here, the electric effect is seen to produce only a pressure gradient and have no first order effect on the shape or location of the flame. There is a question of whether this condition is stable and is taken up in a later section.

4.3 DIFFUSION FLAME IN AN ELECTRIC FIELD TWO DIMENSIONAL MODEL

The two dimensional treatment considers that the current density J obtained from the flame is a function of distance y along the flame. It was shown in Section 3.2 that a variation in J along the flame leads to a field strength, E_y, and a body force, F_y, in that direction.

It is now assumed that the impressed electric field strength in the x direction is large compared to the induced component in the y direction. The body force and the current density in the x direction are, therefore, large in comparison to the components in the y direction. From Eq. (4.7) the body force in the x direction is

$$F_x = \frac{J}{k} \tag{4.7}$$

The equation of motion is then

$$\rho \left[w \frac{\partial w}{\partial x} + u \frac{\partial w}{\partial y} \right] = - \frac{\partial p}{\partial x} + \frac{J}{k} \qquad (4.8)$$

where inviscid incompressible flow is considered and w is the induced velocity in the x direction. The induced velocity is small such that the left side of Eq. (4.8) is negligible compared to either term on the right. By integrating Eq. (4.8) the pressure can, therefore, be written approximately as

$$p = \frac{Jx}{k} + \text{constant} \qquad (4.9)$$

The reference pressure is taken as p = 0 at the flame sheet where x = L, so Eq. (4.9) is

$$p = \frac{J}{k} (x-L) \qquad (4.10)$$

The two dimensional aspect of the problem is maintained in an approximate sense by letting J be a function of y which could be determined by measuring the current density along the electrode. From Eq. (4.10) the pressure gradient in the y direction is

$$\frac{\partial p}{\partial y} = \frac{(x-L)}{k} \frac{\partial J}{\partial y} \qquad (4.11)$$

The physical significance of the term $\partial J/\partial y$ is now clear. A pressure gradient in the y direction arising as a consequence of the gradient in current density causes an acceleration of the gas on one side of the flame; an induced transverse velocity thereby results.

For steady inviscid flow where the velocity in the x direction is small, Euler's equation in the y direction reduces to

$$\frac{\rho}{2} \frac{\partial u^2}{\partial y} + \frac{\partial p}{\partial y} = 0 \qquad (4.12)$$

Substituting Eq. (4.11),

$$\frac{\rho}{2} \frac{\partial u^2}{\partial y} + \frac{(x-L)}{k} \frac{\partial J}{\partial y} = 0 \qquad (4.13)$$

For a case where $\partial J/\partial y$ is constant, Eq. (4.13) integrates to

$$\frac{\rho u^2}{2} + \frac{(x-L)y}{k}\frac{\partial J}{\partial y} = \frac{\rho U^2}{2} \tag{4.14}$$

The average value of (x-L) over the air zone is (R-L)/2; then on the average Eq. (4.14) is

$$\frac{\rho u^2}{2} + \frac{(R-L)y}{2k}\frac{\partial J}{\partial y} = \frac{\rho U^2}{2} \tag{4.15}$$

It is interesting to note that Eq. (4.15) can be obtained in another way by first assuming that the force field is irrotational. From irrotationality

$$\frac{\partial F_x}{\partial y} - \frac{\partial F_y}{\partial x} = 0 \tag{4.16}$$

where

$$F_x = n_+ E_x \tag{4.17}$$

$$F_y = n_+ E_y \tag{4.18}$$

Substituting Eqs. (4.17) and (4.18) into (4.16) results in

$$n_+\left[\frac{\partial E_x}{\partial y} - \frac{\partial E_y}{\partial x}\right] + E_x\frac{\partial n_+}{\partial y} - E_y\frac{\partial n_+}{\partial x} = 0 \tag{4.19}$$

The quantity in the bracket in Eq. (4.19) is zero because the field is irrotational, so Eq. (4.19) reduces to

$$E_x\frac{\partial n_+}{\partial y} - E_y\frac{\partial n_+}{\partial x} = 0 \tag{4.20}$$

As an approximation E_x and n_+ are taken to be the expressions developed in Chapter 3 for the one dimensional analysis, only now J is taken to be a function of y.

From Eqs. (3.19) and (3.20), $\partial n_+/\partial y$, $\partial n_+/\partial x$ and E_x are calculated and substituted into Eq. (4.20). For $A << L$, Eq. (4.20) reduces to

$$E_y = -\left[\frac{2(x-L)^3}{Jk\epsilon}\right]^{1/4}\frac{\partial J}{\partial y} \qquad (4.21)$$

The body force from Eq. (4.18) averaged over the air zone is then

$$(F_y)_{avg} = -\frac{(R-L)}{2k}\frac{\partial J}{\partial y} \qquad (4.22)$$

If the body force is the gradient of a potential, Euler's equation in the y direction reduces to

$$\frac{\rho u^2}{2} + \frac{(R-L)y}{2k}\frac{\partial J}{\partial y} = \frac{\rho U^2}{2}$$

which is Eq. (4.15).

A series of approximations will now be made to determine the order of magnitude of the induced transverse velocity. Consider that the entire gas flow initially with uniform velocity U at y = 0 retains its identity by assuming a hypothetical interface between the air and fuel streams. This is not true for the diffusion flame since the gases immediately interdiffuse, and of course the flame surface itself is not generally a streamline. As an order of magnitude approximation however, the analysis is continued.

For constant density the interface must move toward the cathode as the air stream is accelerated. If x = R - a is the position of this interface, the interface velocity w is approximately

$$w = -U\frac{da}{dy} \qquad (4.23)$$

and for continuity of mass

$$au = U(R-L_o) \qquad (4.25)$$

Combining Eqs. (4.15), (4.23), and (4.24), the transverse velocity of the interface is

$$w = -\frac{U^2(R-L_o)^2}{2k\rho}\left[y\frac{\partial^2 J}{\partial y^2} + \frac{\partial J}{\partial y}\right]\left[U^2 - \frac{(R-L_o)y}{k\rho}\frac{\partial J}{\partial y}\right]^{-3/2} \qquad (4.25)$$

If the velocity w represented by Eq. (4.25) is interpreted as a transverse velocity away from the flame in the gas on one side of the flame, then this velocity opposes the diffusion velocity of one species toward the flame and, therefore, the flame would be shifted toward the cathode.

In a real flame the question remains whether the effect of the electric field is a first order effect. Suppose for example that a diffusion flame in the combustion chamber of Fig. 1 is considered where the fuel mixture is 23.6% propane and 76.4% nitrogen, and both fuel and air flow at a velocity of 2.8 inches per second. For no electric field present, the concentration profile and flame surface can be determined by the method of Section 4.1. Once the flame surface is determined, the diffusion velocity of any specie can be determined for any position along the flame. If now an electric field is applied and the current density distribution is measured, the electrically induced transverse velocity can be determined by Eq. (4.25). Suppose that $\partial J/\partial y$ is constant and equal to a value of 0.2 microampere per square inch. It will be seen later that this value is representative of the flames investigated, and is in fact equal to the average value of $\partial J/\partial y$ over the first three inches of one of the flames later designated as flame 2. Listed in Table 1 are the values of the diffusion velocity and induced velocity for the particular flame mentioned.

Table 1

Diffusion and Induced Velocities for an Electro-Diffusion Flame

Height above Base of Flame, inch	Diffusion Velocity, inch/sec	Induced Velocity, inch/sec
1.48	0.045	0.14
2.9	0.036	0.14
3.0	0.024	0.14

The values in the table above show that under the assumptions made the electrically induced velocity is even greater than the diffusion velocity of air and, therefore, a first order effect would be produced on the diffusion flame. The formulation of the problem of determining the flame location in the electric field case is achieved by expressing continuity of specie at any point in the combustion chamber, whence

$$\frac{\partial c}{\partial y} = \frac{D}{U}\frac{\partial^2 C}{\partial x^2} - \frac{1}{U}\frac{\partial (Cw)}{\partial x} \qquad (4.26)$$

where time, t, is eliminated by $y = Ut$ as before, and C is the concentration of fuel or air. It is seen that the last term in Eq. (4.26) has appeared in the simple diffusion equation as a result of the electric effect. The solution of Eq. (4.26) requires a specification of the induced velocity which, in general, is a function of x and y. If w is constant, then Eq. (4.26) has constant coefficients and is solved by the method of separation of variables.

The main point of the preceeding discussion has been to establish that an electric field can be expected to produce first order effects on a diffusion flame by means of forces arising from a gradient in current density along the flame.

CHAPTER 5

THE QUESTION OF INSTABILITY OF THE FLAME

Chapter 3 considered a planar diffusion flame between parallel flat plate electrodes and the distribution of ion density, electric field strength, and electric potential were studied. Since only electric parameters were investigated, it was assumed for simplification in that analysis that the flame sheet was planar and stabilized in space. It is known hower (39), that under certain conditions electric forces can act to destabilize the primary flow in fluid motion, in analogy with several classical stability problems in fluid mechanics. The question considered at this time is the following: "Given a planar diffusion flame sheet stressed by a transverse electric field as in Fig. 1, can instability of the flame sheet be expected, and what parameters serve as the criterion for instability?"

When the flame sheet is in equilibrium at a certain distance from the anode, there are electrical forces on the flame sheet proportional to E_f, the field strength at the edge of the flame. To consider the stability, a perturbation in flame position at constant electrode voltage such as to increase L is assumed; then if the field strength E_f increases after the perturbation, the destabilizing electric forces will be increased and a possible condition for instability exists. Mathematically, if $\partial E_f/\partial L$ is positive, a condition for electric destabilization of the diffusion flame sheet would exist.

Since two sets of electric equations exist, one for subsaturation and one for saturation, the stability criterion is found for both sets.

Using Eq. (3.24) and substituting Eq. (3.17) results in an expression for V in terms of E_f for the subsaturation case.

$$V = \frac{2}{3}\left[\frac{4E_f^2 J_s}{Ak\epsilon}\right]^{1/4}(R-L)^{3/2} \qquad (5.1)$$

(subsaturation)

The equivalent equation for saturation is Eq. (3.35). Taking $\partial/\partial L$ at constant V of Eq. (5.1) and (3.35), we get after resubstituting Eq. (3.17)

$$\frac{\partial E_f}{\partial L} = \frac{27}{8}\frac{V^2}{(R-L)^4}\left[\frac{Ak\epsilon}{J_s}\right]^{1/2} \qquad (5.2)$$

(subsaturation)

and

$$\frac{\partial E_f}{\partial L} = \frac{\left[E_f^2 + \frac{2J_s(R-L)}{k\epsilon}\right]^{1/2} - \left[E_f^2 - \frac{J_sA}{k\epsilon}\right]^{1/2}}{E_fL\left[E_f^2 - \frac{J_sA}{k\epsilon}\right]^{-1/2} + \frac{k\epsilon E_f}{J_s}\left[\frac{2J_s(R-L)}{k\epsilon} + E_f^2\right]^{1/2} + \frac{k\epsilon E_f^2}{J_s}} \qquad (5.3)$$

(saturation)

E_f in Eq. (5.3) could be eliminated by using Eq. (3.35) which gives E_f implicitly in terms of V and J_s. Noting that $E_f > J_sA/k\epsilon$ in saturation, it is seen that $\partial E_f/\partial L$ in Eqs. (5.2) and (5.3) are always positive, consequently a possible condition for instability exists.

Consider now the flame sheet in an equilibrium position between electrodes with a field applied as in Fig. 1. If the flame undergoes a small displacement, δ, in the positive x direction while maintaining its equilibrium ion density, a destabilizing force, $n_+ (\partial E_f/\partial L)\,\delta$, tends to increase the perturbation. Let it be also assumed that during the perturbation the equilibrium profiles of air and fuel concentrations are not disturbed. Then, since the equilibrium position of the flame is specified as the surface of stoichiometricity, the flame after perturbation will find itself in a region where

$$C_A > iC_F \qquad (5.4)$$

The degree of departure from the equilibrium condition is proportional to the quantity

$$\delta\frac{\partial}{\partial x}[C_A - iC_F]$$

The flame stability is governed by the stabilizing influence of the term above and the destabilizing influence of the term $n_+(\partial E_f/\partial L)$. The stability is therefore related to the ratio of these terms, G, where

$$G = \frac{n_+ \frac{\partial E_f}{\partial L}}{\frac{\partial}{\partial x}\left[C_A - iC_F\right]} \tag{5.5}$$

Substituting

$$n_+ = \frac{J}{kE_f} \tag{5.6}$$

results in

$$G = \frac{\frac{J}{kE_f}\frac{\partial E_f}{\partial L}}{\frac{\partial}{\partial x}\left[C_A - iC_F\right]} \tag{5.7}$$

The numerator of Eq. (5.7) is different for subsaturation or saturation. For subsaturation, using Eqs. (5.2), (3.26), and (3.27), the numerator becomes

$$\frac{J}{kE_f}\frac{\partial E_f}{\partial L} = \frac{3J_s V'^2}{k(R-L)} \qquad \text{(subsaturation)} \tag{5.8}$$

and for saturation the result is, using Eqs. (5.3) and (3.26),

$$\frac{J}{kE_f}\frac{\partial E_f}{\partial L} = \frac{J_s}{k(R-L)} \left\{ \frac{\left[1 + \frac{2(R-L)}{A\,E'^2}\right]^{1/2} - \left[1 - \frac{1}{E'^2}\right]^{1/2}}{\frac{E'L}{(R-L)}\left[\frac{1}{E'^2-1}\right]^{1/2} + \left[\frac{2E'^2A}{(R-L)} + \frac{E'^4A^2}{(R-L)^2}\right]^{1/2} - \frac{E'^2A}{(R-L)}} \right\} \tag{5.9}$$

Where E' appears in Eq. (5.9), it may in principle be eliminated in favor of V' by Eq. (3.36) which gives a relation between the nondimensional field strength, E', and the nondimensional voltage, V', or by use of Fig. 2.

It is interesting to investigate how the electric destabilizing parameter given by Eqs. (5.8) and (5.9) varies with applied voltage.

Figure 3 is a plot of the nondimensionalized electric destabilizing parameters from Eqs. (5.8) and (5.9) for the particular case where $L/(R-L) = 1$ and $A/(R-L) = 0.04$. In the subsaturation regime the parameter increases with the square of the voltage. The curve for saturation, from Eq. (5.9), drops to zero very near the saturation point as indicated by the curving down of the curve near $E' = 1$ on Fig. 3. This behavior arises as a result of the assumptions leading to Eq. (5.9), namely, that as a consequence of taking the negative ion mobility as very high, the potential drop across the fuel zone is zero in subsaturation, but has a value, depending on E_f, above the saturation point.

The stabilizing influence on the flame sheet is the denominator of Eq. (5.7), related to the concentration profiles. In the flat diffusion flame of the type under consideration, this quantity will be a function of position along the flame. For the flame used as an example in Section 4.3 (Flame 2 of the experimental flames), the stabilizing parameter was determined from a plot of the concentration equations (4.4) and (4.5) and is shown in Fig. 4 in relative units as a function of distance along the flame. At lower parts of the flame the concentration gradients are high and the stabilization is greatest; at higher parts of the flame the stabilizing parameter decreases.

Other models of flame stability can also be considered; e.g., a flame surface tension, σV, can be assumed where σ is the flame surface charge density and V is the potential (40). Stability of such surfaces have been discussed in the literature (41). Experiments demonstrating the onset of flame instability are discussed in a later section.

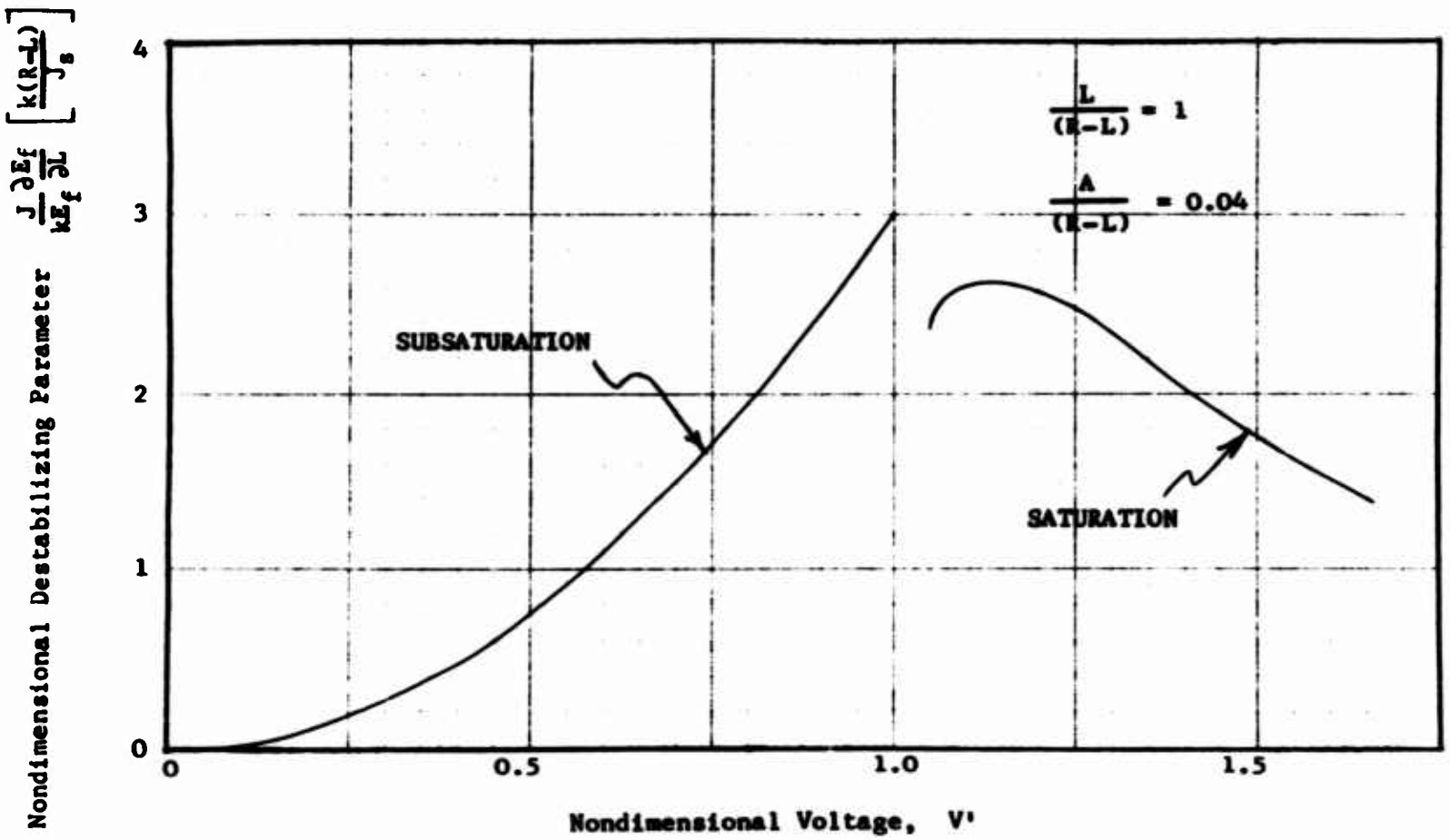

Fig. 3 Nondimensional destabilizing parameter versus nondimensional voltage

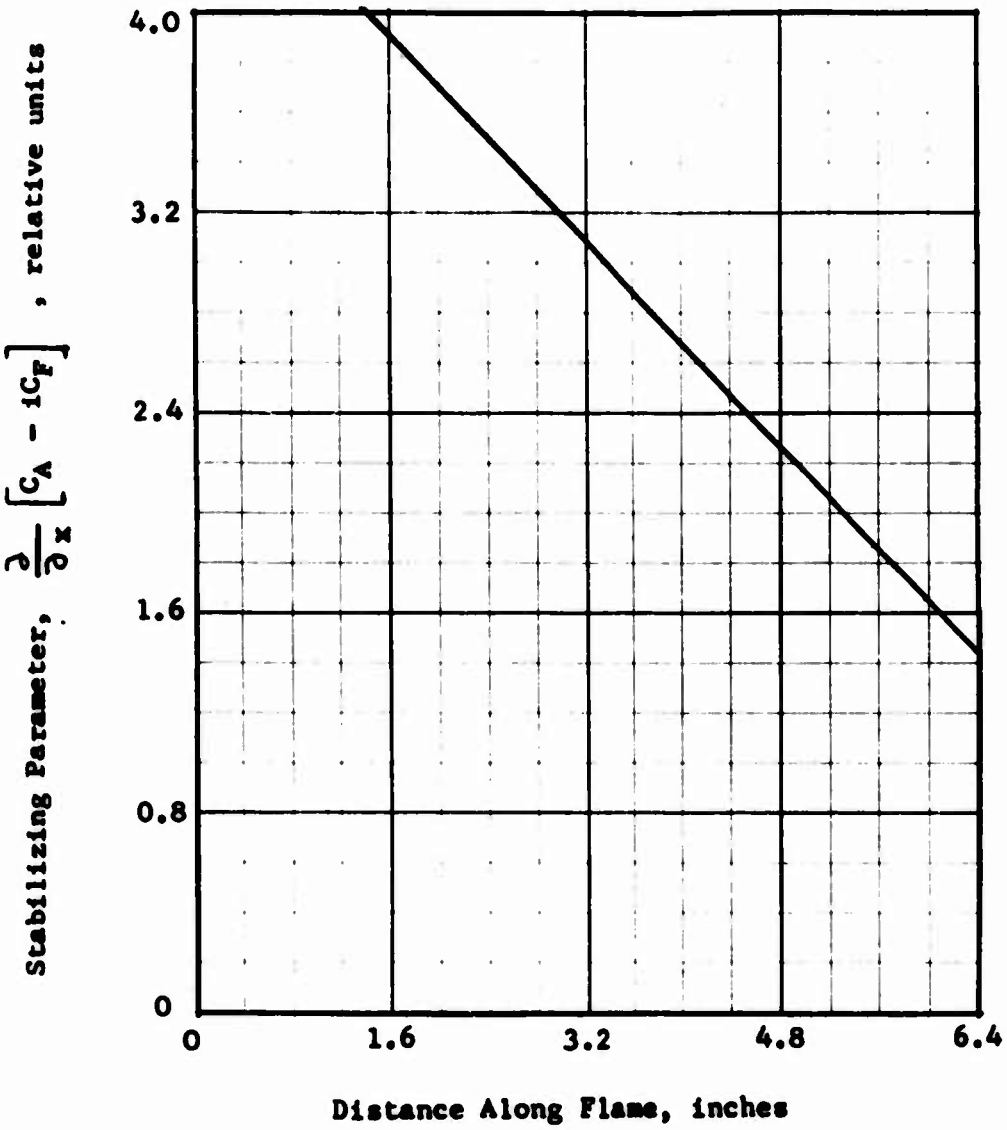

Fig. 4 Stabilizing parameter versus distance along the flame

CHAPTER 6

DESCRIPTION OF THE EXPERIMENTAL COMBUSTION CHAMBER

A parallel flow diffusion flame combustion chamber was constructed to determine experimentally the mechanisms and effects of an electric field applied transverse to the flow. The shape of the cross section in the flow direction was rectangular, with an aspect ratio of 5.5, so that a wide flat flame could be produced within the combustion chamber which would approximate the ideal flat diffusion flame discussed earlier. The gaseous reactants were propane mixed with controlled amounts of nitrogen as fuel, and air as the oxidant. The gases were introduced to opposite sides of the base of the combustion chamber as shown in the gas flow diagram in Fig. 5. As the gases flowed upward within the combustion chamber, the streams diffused together, producing a diffusion flame sheet when ignited.

The two walls facing the flame sheet were each constructed of individually cooled brass segments, each insulated from the adjacent one by a 1/8-inch thick strip of asbestos. Each brass segment was cooled by a separate stream of oil (General Electric 10C transformer type) recirculated by a pump. The inlet and outlet oil temperatures and flow rates could be measured for each segment, as well as the temperature of the segments themselves. Both walls consisted of eight such segments, each 1/2-inch thick and one inch wide. Above the top segment of each wall was an additional $1\frac{1}{2}$ inch wide segment which made a total height of $10\frac{1}{2}$ inches of cooled surface on each side. The cooled surface on the fuel side of the flame served as the anode, and the cooled surface on the air side served as the cathode.

The walls of the combusion chamber facing the edge of the flame were constructed of $\frac{1}{2}$-inch thick asbestos board lined with a 1/64-inch thick sheet of mica on the edges adjacent to the electrodes to prevent current leakage. One edge wall had sections cut out so that the flame could be observed in an edge view. The inside of this wall was fitted with a sheet of 1/16-inch thick Pyrex glass to contain the combustion gases.

It was desired that the flame sheet be not permitted to extend completely across the inside width of the chamber for two reasons. First, the boundary layer on the glass window might prevent an effective view of the flame in addition to the danger of cracking the glass, and second, since hydrocarbon gas was used, there is the possibility of carbon depositing on the edge walls and providing a path for current to flow between the electrodes. Consequently, a nitrogen gas buffer layer was introduced at each end of the chamber at the base of the fuel passage. When occasionally carbon deposits did form on the edge walls, it was noticed that

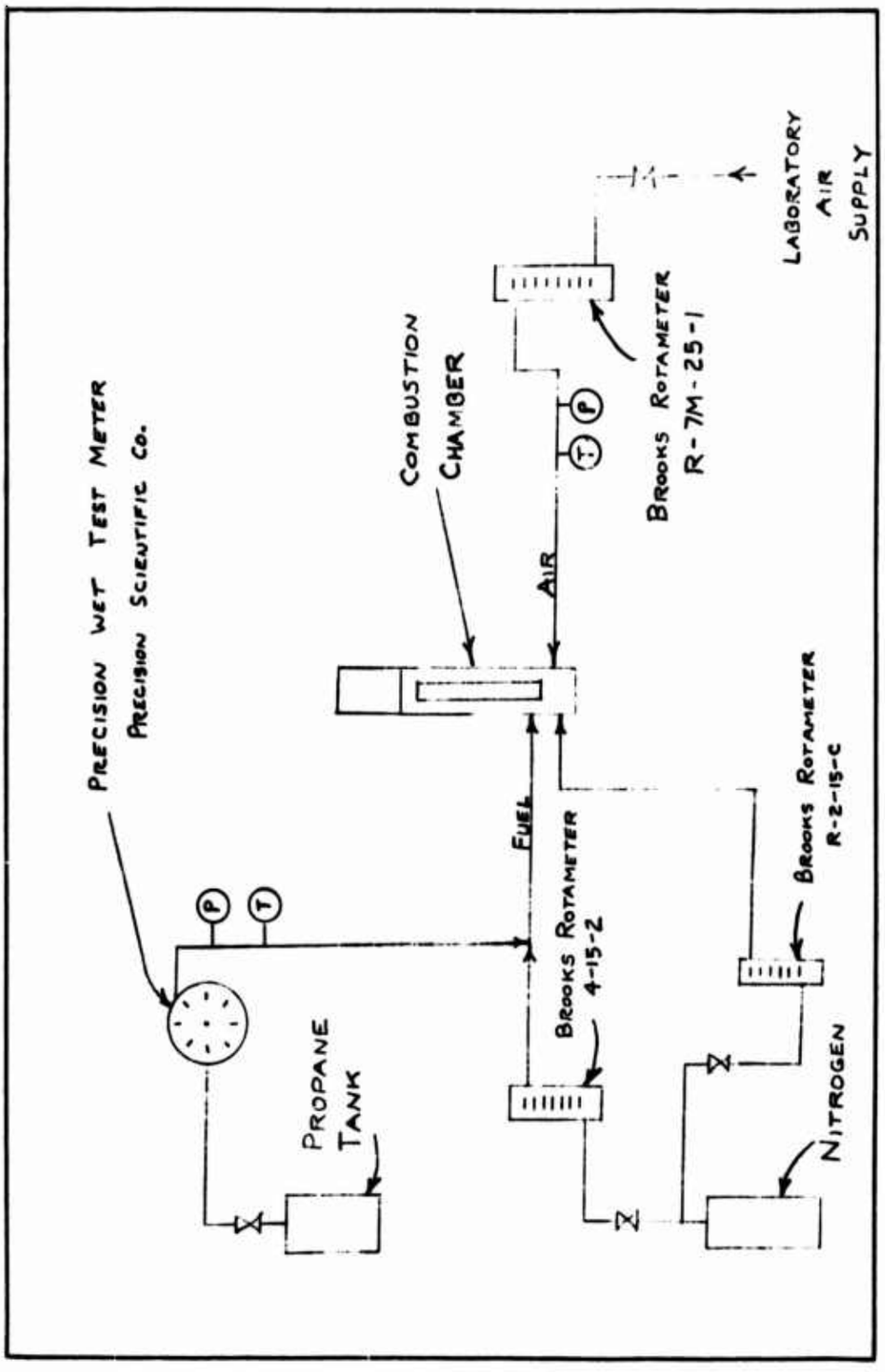

Fig. 5 Gas flow diagram

they were more easily wiped off the glass window, and for this reason the other edge wall was also lined with glass. The cross-sectional dimensions of the inside of the chamber were 1¼ inches between electrodes and a width of 6-7/8 inches, of which 5-7/8 inches could be occupied by the flame sheet. A sketch of the combustion chamber configuration is shown in Figs. 6 and 7.

Above the electrode section of the combustion chamber was a 1½-inch high section of asbestos wall, followed by a one-inch high section into which twelve iron-constantan thermocouples were inserted and spaced over the cross section of the chamber at that height. Above the thermocouple sides was a sheet metal stack which tapered to a two-inch by two-inch cross section five inches in height. In this section a 0.056-inch diameter quartz tube was inserted to withdraw gas samples for composition analysis. Photographs of the chamber and instrumentation are shown in Figs. 8 and 9.

In the experimental program four different flames were studied; in all cases the various gas velocities at the base of the flame were uniform for that flame. The relative amounts of propane and air delivered to the flame are expressed by the equivalence ratio, which is the ratio of the fuel mass rate to the fuel mass rate required for stoichiometric combustion. The portion of the air which flows next to the nitrogen buffer layer is not included in the calculation of the equivalence ratio. The flames studied are listed in Table 2.

Table 2. Flames Used in the Experimental Program

	Equivalence Ratio	Velocity at Base, in/sec	Vol % Propane in Fuel
Flame 1	1.1	2.8	18.5
Flame 2	1.4	2.8	23.6
Flame 3	1.7	2.8	28.5
Flame 4	1.4	4.2	23.6

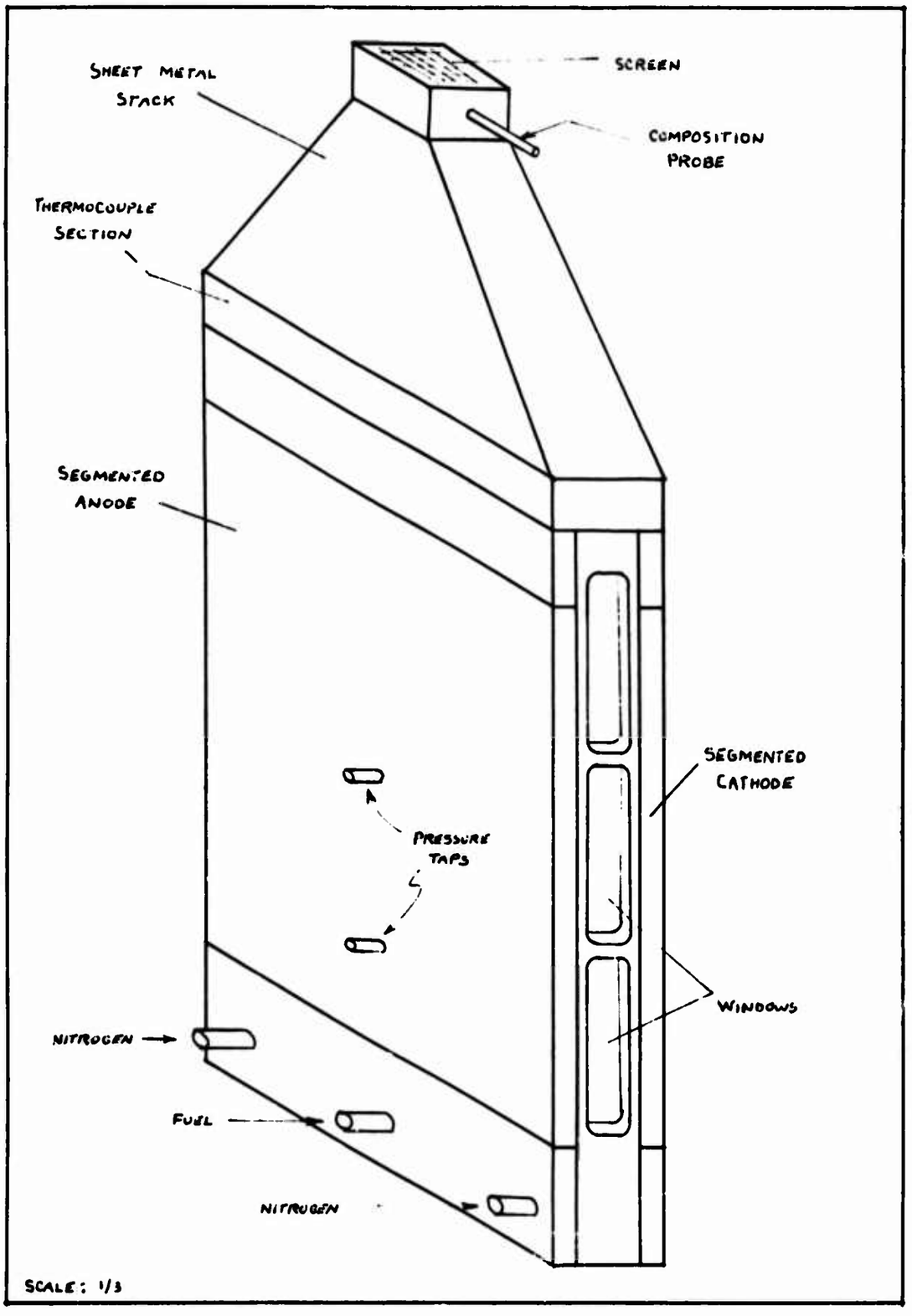

Fig. 6 Diagram of the combustion chamber

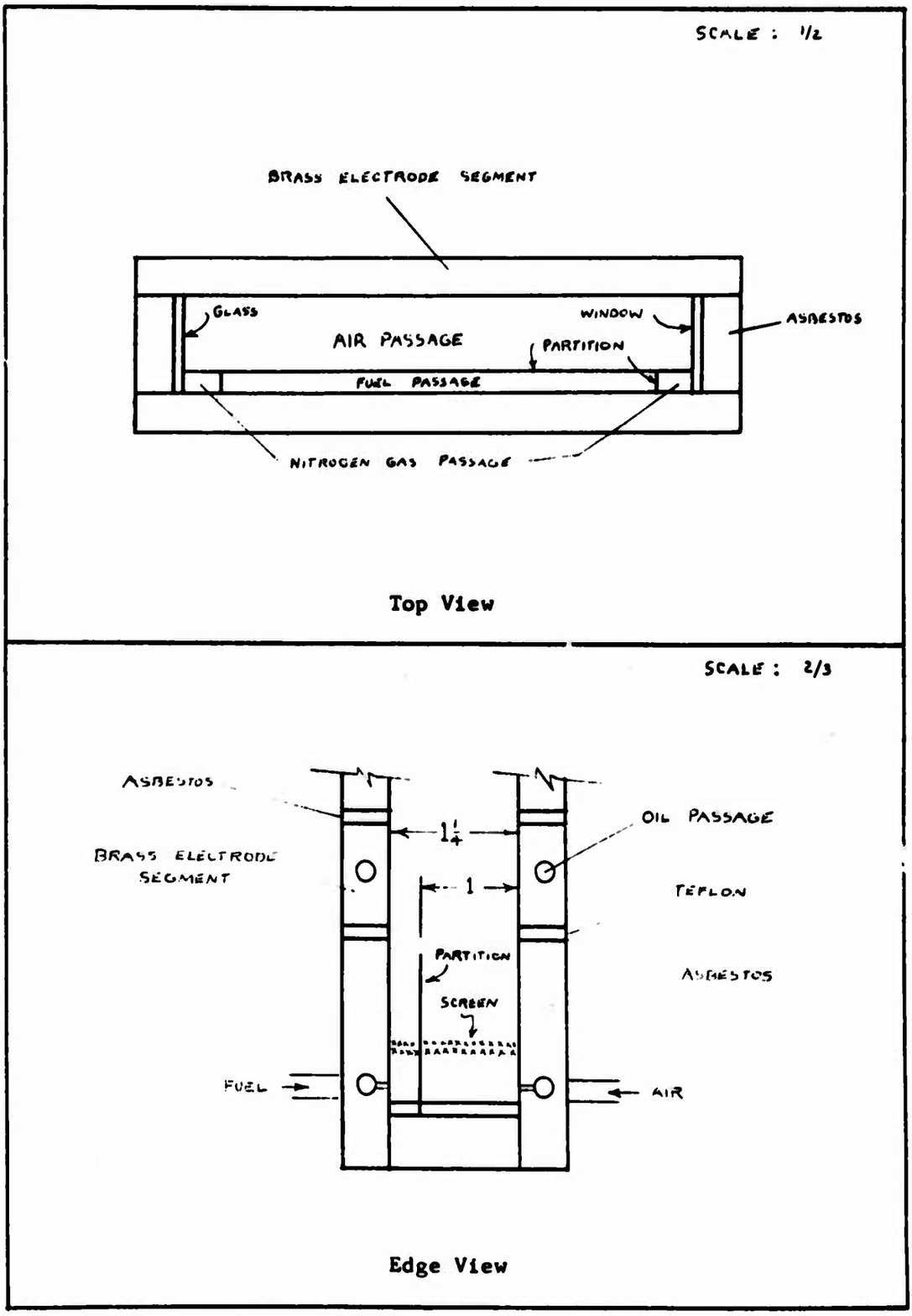

Fig. 7 Cross sectional view of the combustion chamber

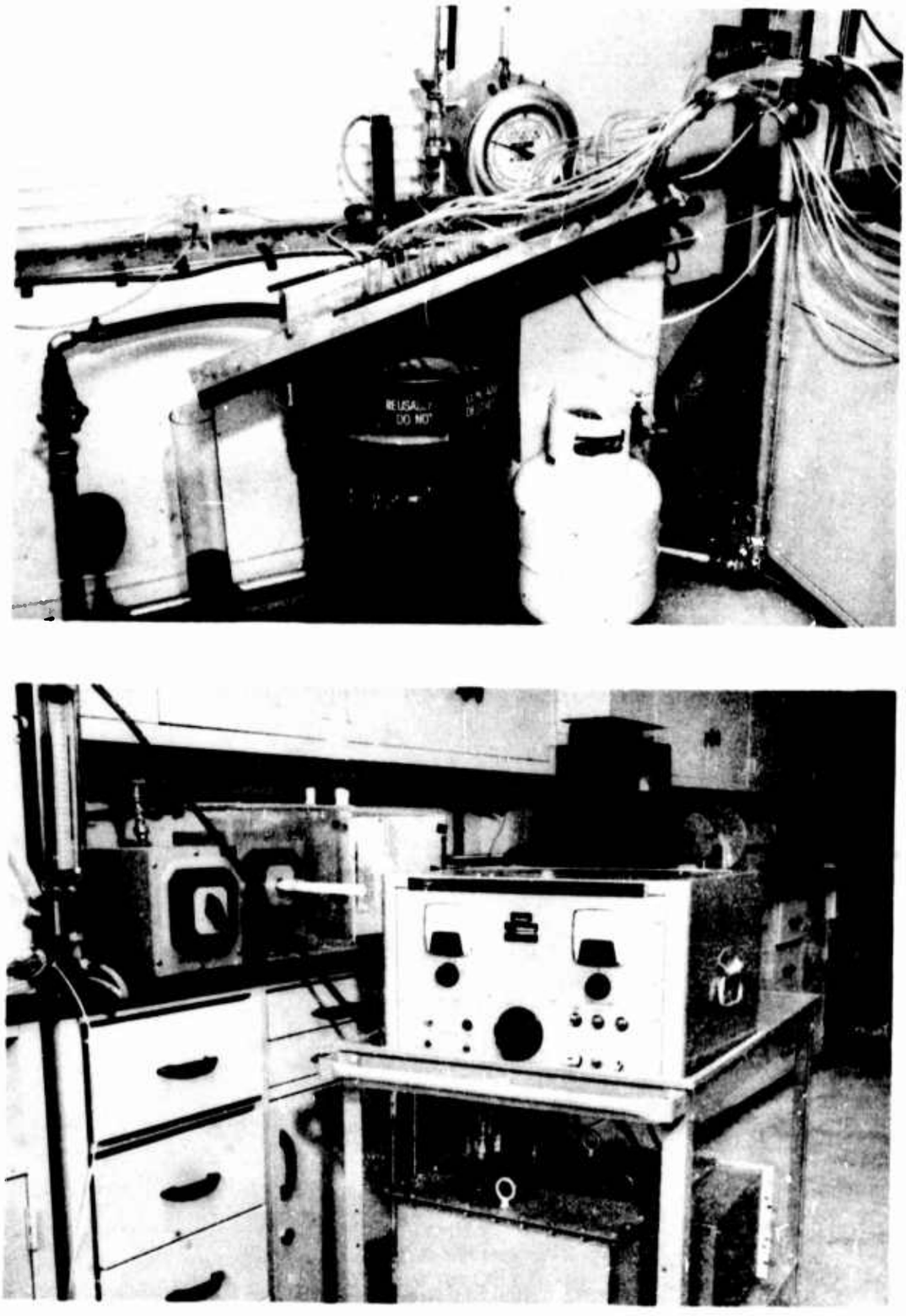

Fig. 8 Photographs of the Experimental Apparatus

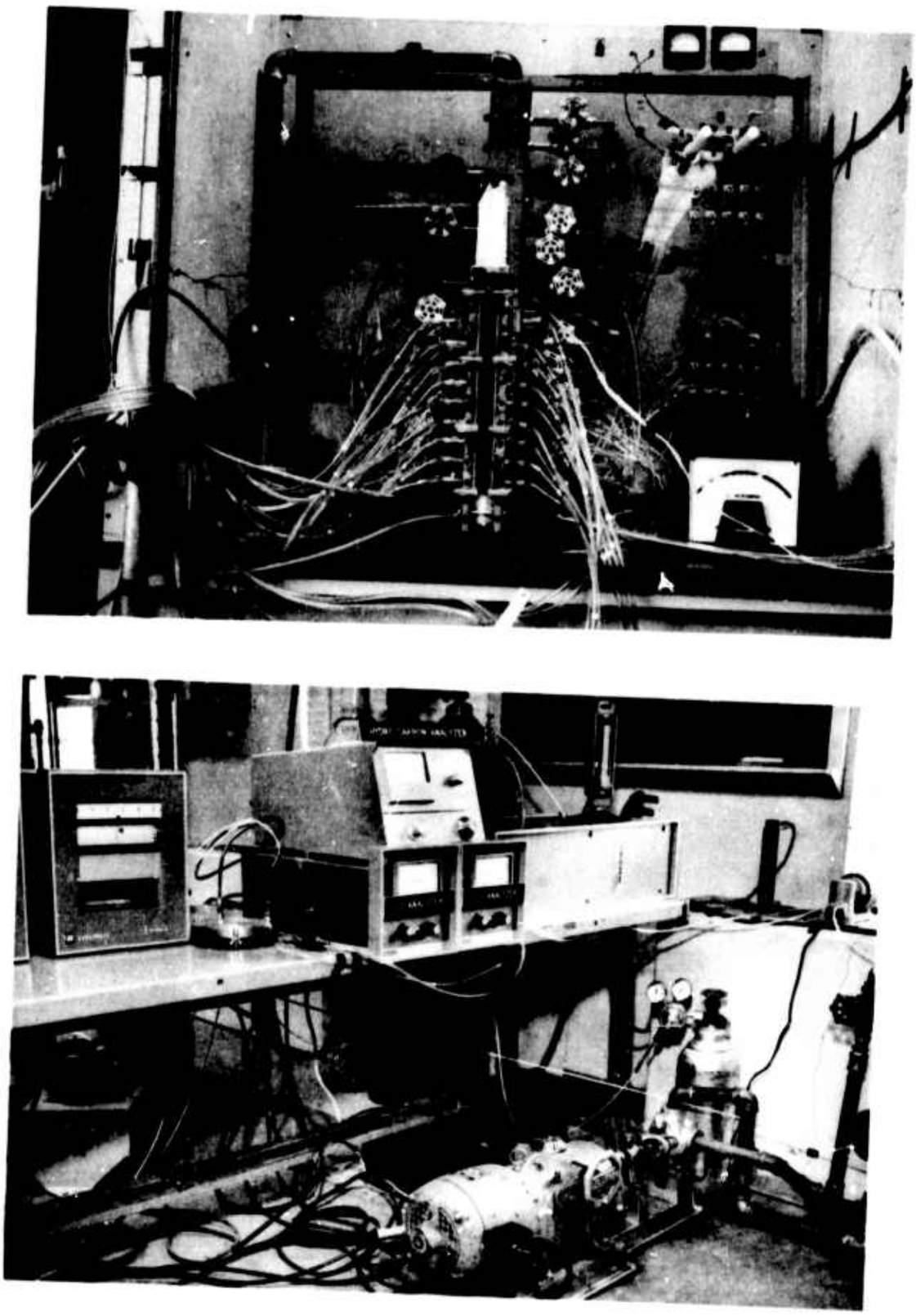

Fig. 9 Photographs of the Experimental Apparatus

CHAPTER 7

EFFECT OF THE FIELD ON THE APPEARANCE OF THE FLAME

The windows in the edge wall of the combustion chamber enabled an observation of the effects on the appearance of the flame to be made. Figures 10-13 show photographs of the flames taken through the window with a Polaroid Model 110A with close-up lenses, ASA 3000 speed film, and no special illumination. Figures 10, 12, and 13 were taken at 1/125 second exposure; Fig. 11 at 1/60 second exposure. Table 3 describes the appearance of the flames for no applied voltage; the trends among the flames are as expected, recalling that flames 1, 2, and 3 are in order of increasing fuel richness, and flame 4 is at a higher velocity.

Table 3. Appearance of the Flames with No Applied Voltage

	Height of Visible Flame, inches	Height of Blue Zone, inches
Flame 1	5	5
Flame 2	7	1½
Flame 3	7	1
Flame 4	8	1½

All the photographs clearly show flame movement toward the cathode as the electrode voltage is increased. At higher voltages, flames 2, 3, and 4 are seen to impinge directly on the cathode a short distance above the base of the flame; flame 1, the leanest flame, is not as stabilized on the dividing partition at the base and is detached from the partition at an electrode voltage of 2400 volts (see Fig. 10, last frame). In this condition flame 1 could be either extinguished by a further increase in voltage or reverted to its former position by a decrease in voltage. At low voltages where the only effect was a slight movement to the right, no change in luminosity was observed; however, at higher voltages, when the flame was considerably shortened, the apparent luminosity was decreased.

Observation of the flame as the electrode voltage was increased revealed a flickering of the flame which was most noticeable above 1600 to 2000 volts. The flame sheet, which previously had a smooth laminar

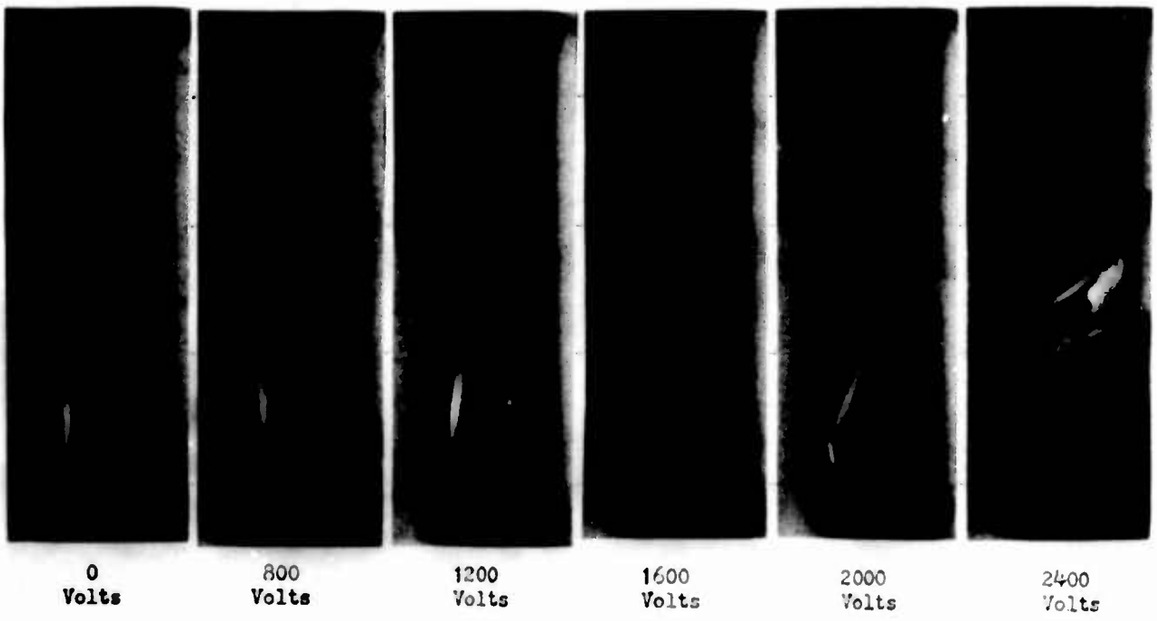

Fig. 10 Photographs of Flame 1 at Several Voltages

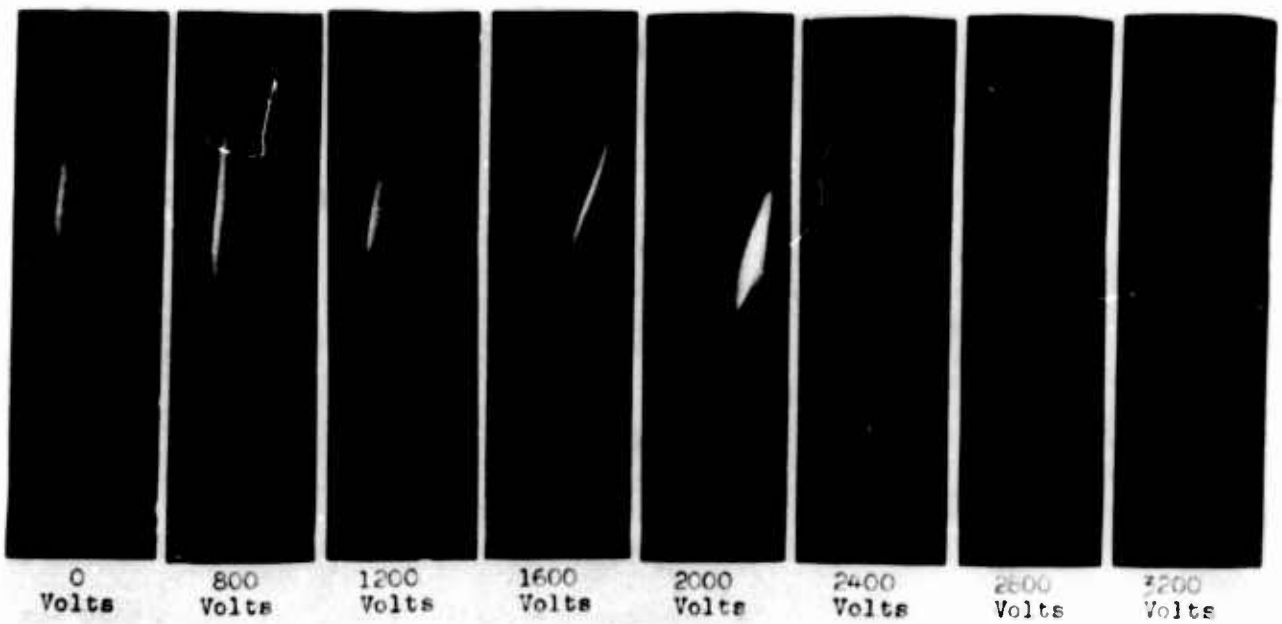

Fig. 11 Photographs of Flame 2 at Several Voltages

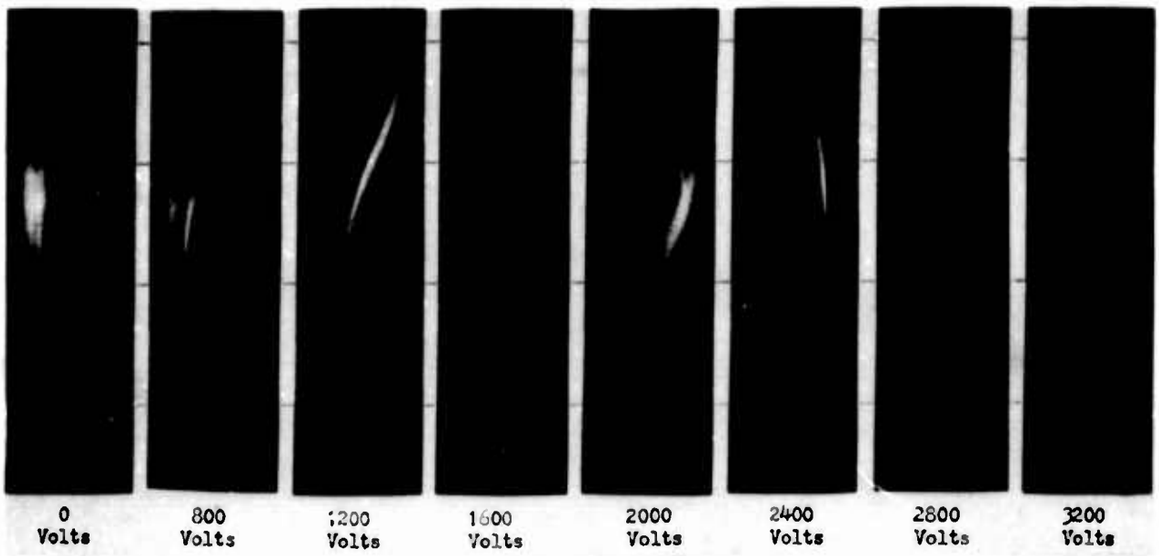

Fig. 12 Photographs of Flame 3 at Several Voltages

Fig. 13 Photographs of Flame 4 at Several Voltages

appearance and was somewhat stationary in space, developed an unsteady appearance. This flickering condition is related to the instability of a flame in a field and is discussed again later in connection with electric measurements on the flame.

It was stated in Chapter 2 that carbon particles in flames may become ionized. Figures 12 and 13 suggest that carbon ionization is active here; frames 5 and 6 show luminous parts of the flames reversing the trend of movement toward the cathode and instead moving toward the anode. This leads one to suspect that electrons are attaching to carbon particles and moving them in the direction of the anode.

CHAPTER 8

ELECTRIC MEASUREMENTS

8.1 CURRENT DENSITY

Both the anode and cathode walls of the combustion chamber consisted of brass segments which were separated from each other by a 1/8-inch thick strip of asbestos. Each segment was, therefore, electrically insulated from adjacent segments, and by proper switching of the electrical circuit, shown in Fig. 14, it was possible to measure the current in each segment on both electrodes within 0.02 microampere. Since only current associated with ion movement out of the flame was desired, the possibility of current leakage along the edge walls of the chamber had to be determined. Current measurements were, therefore, recorded only when, after turning off the fuel supply and extinguishing the flame, the current dropped to a zero value. The coolant loop, which was transformer oil circulating in plastic tubing, was also selected so that no current leakage would flow through the coolant circuit. Only current measurements from the top segments were not obtainable because of leakage, since the upper part of the chamber tended to collect carbon deposits which acted as a current path, and also the top segments did not have a conductor above them at the same potential to act as a "guard ring".

Four different flames corresponding to the gas mixtures and velocities given in Table 2 were formed in the combustion chamber and the currents to each segment of the electrodes were measured as a function of anode voltage. The cathode, on the air side of the flame, was maintained grounded. The current density at the level of a segment was calculated as the current in that segment divided by the area of the segment facing the flame. The current densities thus obtained are presented graphically in Figs. 15-25.

One point to be considered is whether, within the range of voltage applied, the saturation current was obtained. Typically, it can be seen from the current density figures that in the upper parts of the flames, the current density first increased with voltage and then leveled off or decreased, which at first sight appears to indicate current saturation conditions. However, as shown in Chapter 7, the shape and location of the flame is greatly changed at voltages above 1600 volts, and as far as upper parts of the flame are concerned, the leveling off and decrease in current density may be due to the fact that the flame is shortened and combustion is completed at a lower level in the combustion chamber. Because of the loss of the physical integrity of the flames at high voltage, it cannot be determined at what voltage saturation is attained. Figures 15 and 21, which show the current density near the base of the

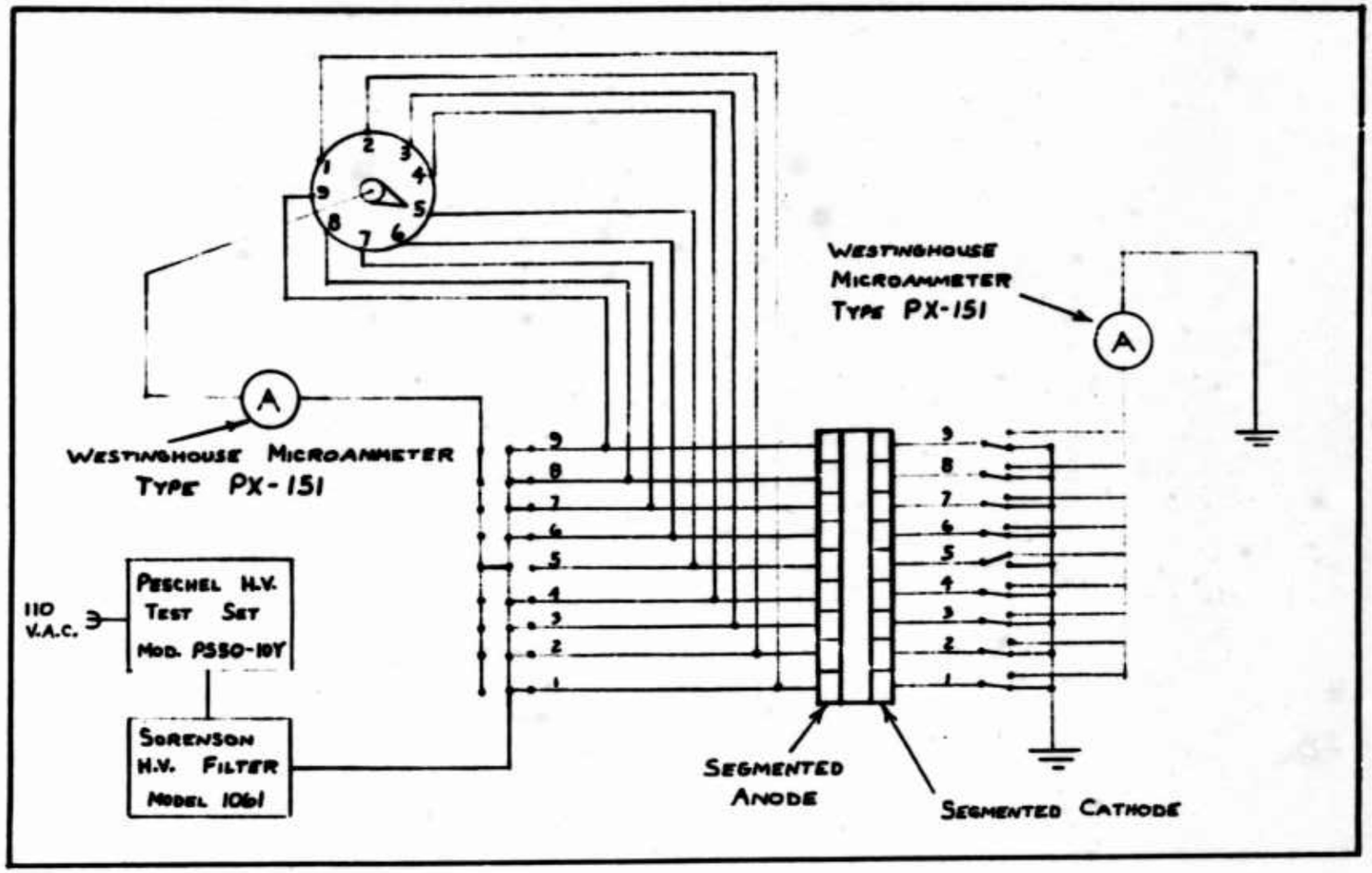

Fig. 14 Electrical circuit

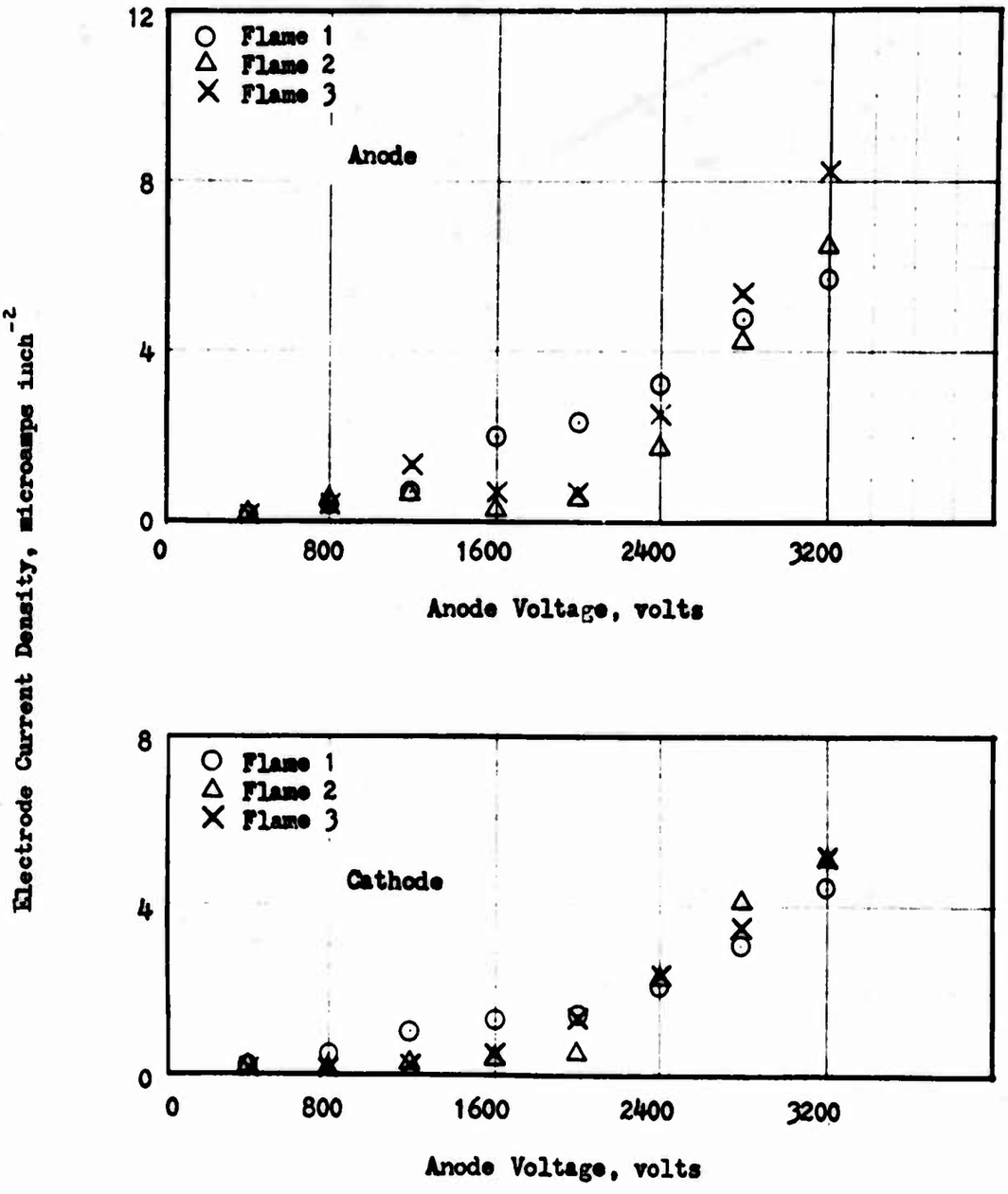

Fig. 15 Current Density Versus Anode Voltage, y = 0.75 inches

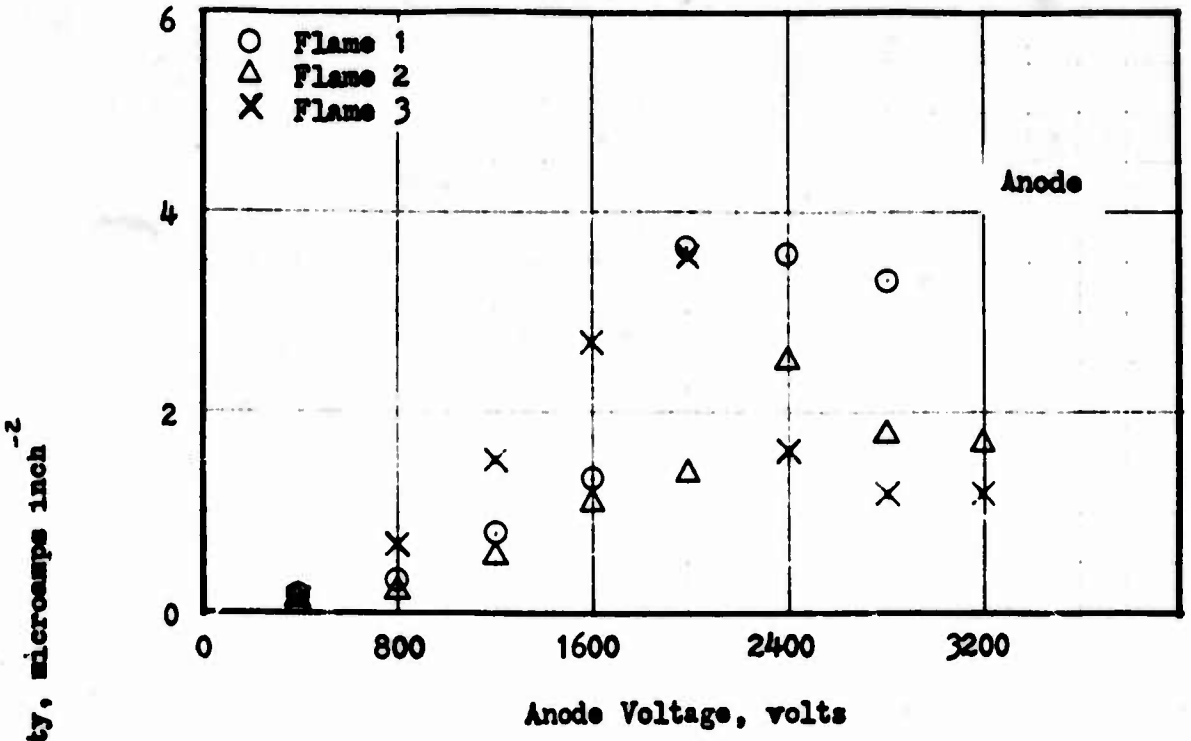

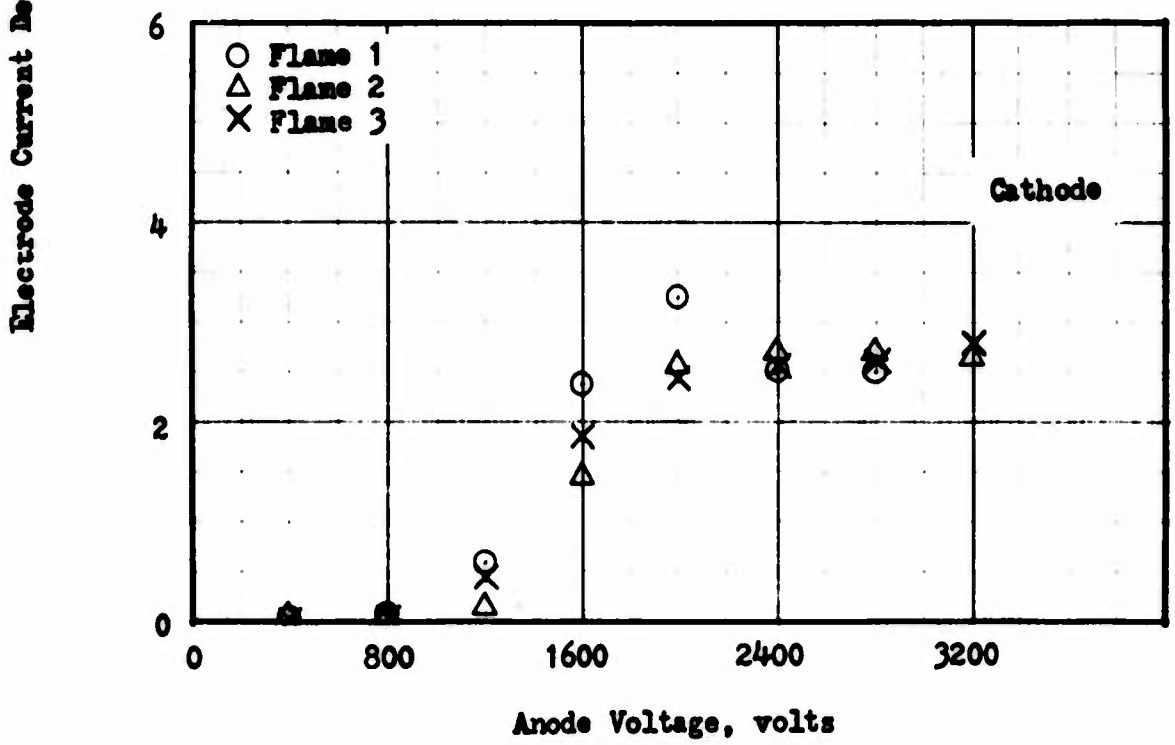

Electrode Current Density, microamps inch^{-2}

Fig. 16 Current Density Versus Anode Voltage, y = 1.875 inches

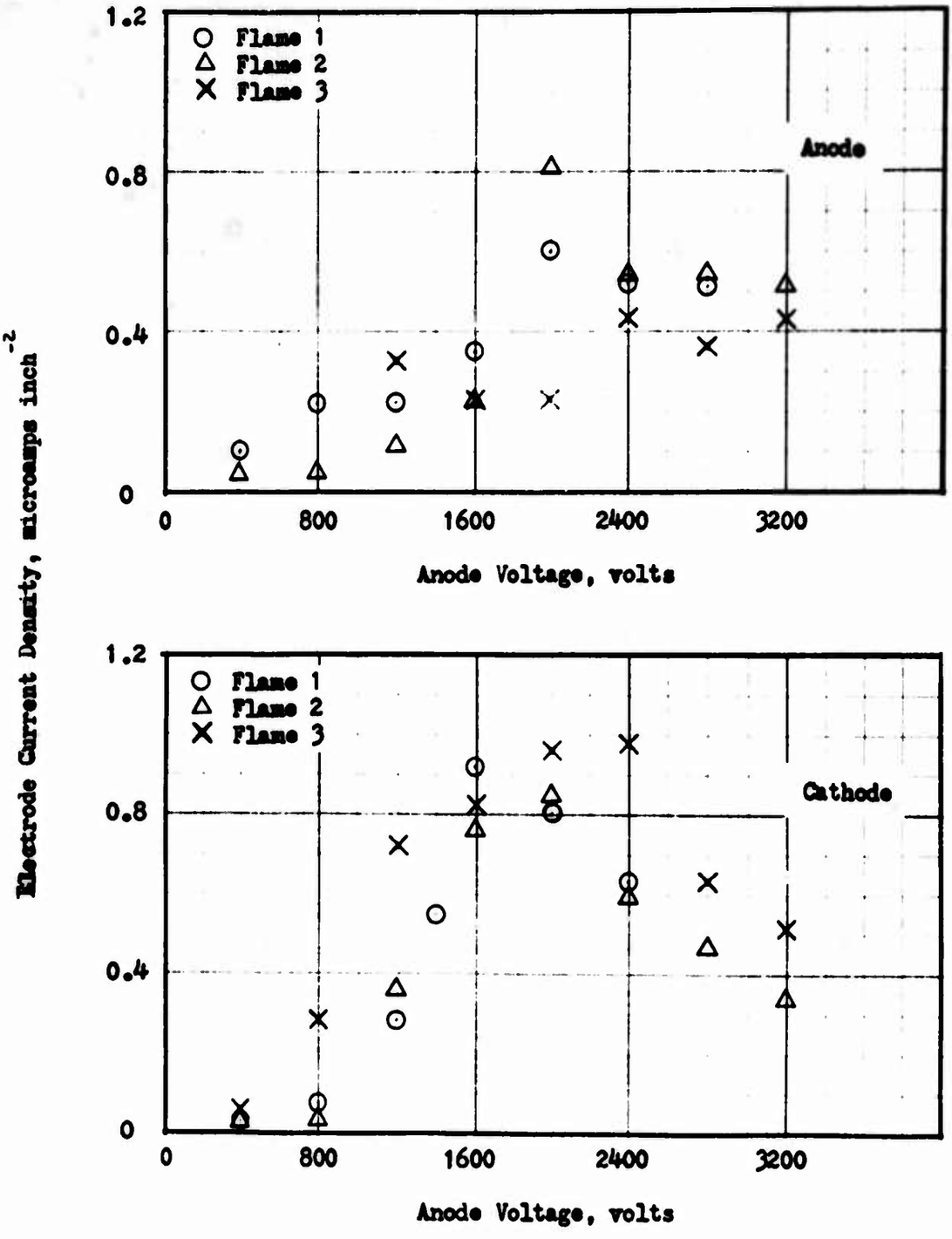

Fig. 17 Current Density Versus Anode Voltage, y = 3.0 inches

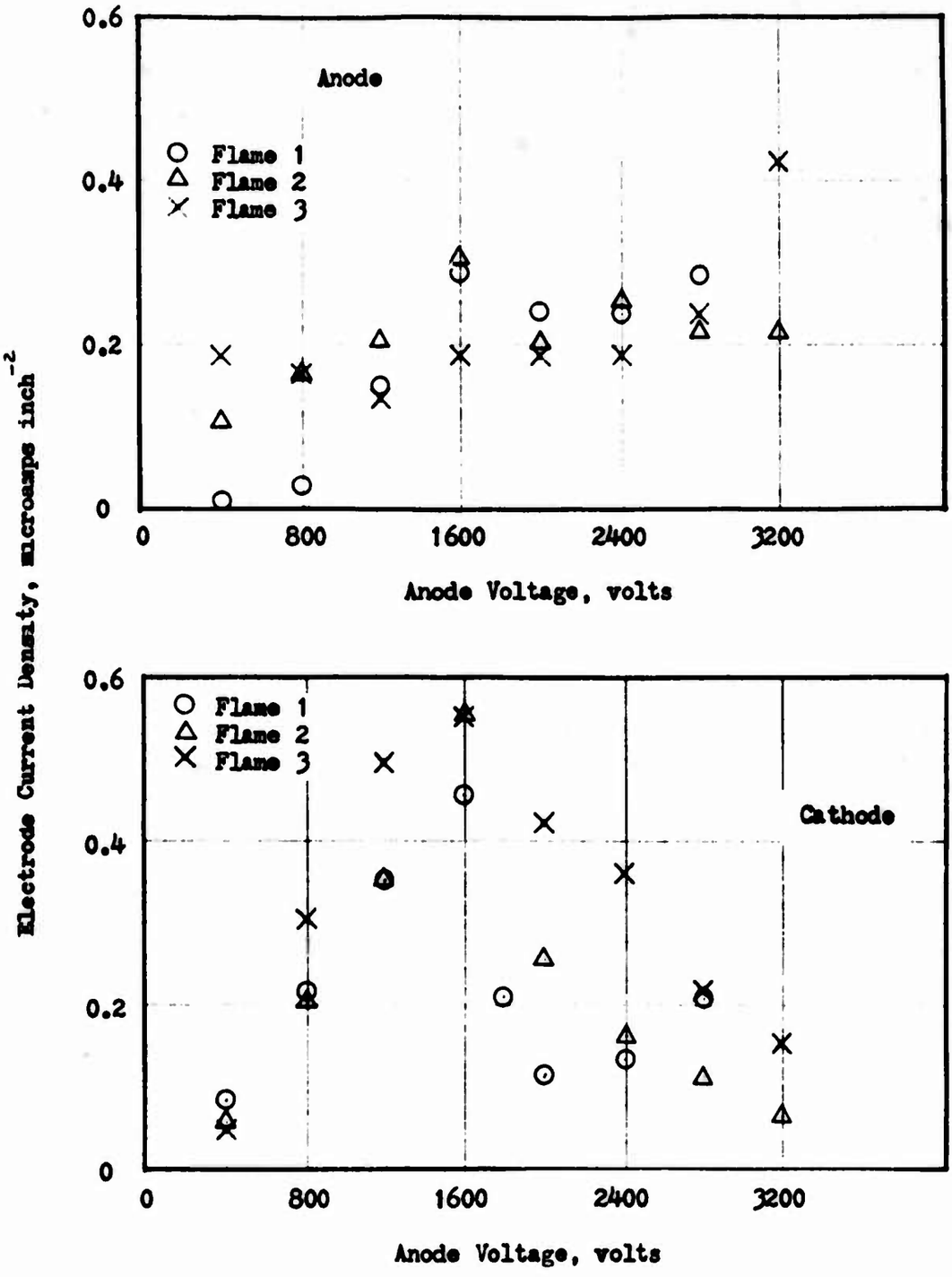

Fig. 18 Current Density Versus Anode Voltage, y = 4.125 inches

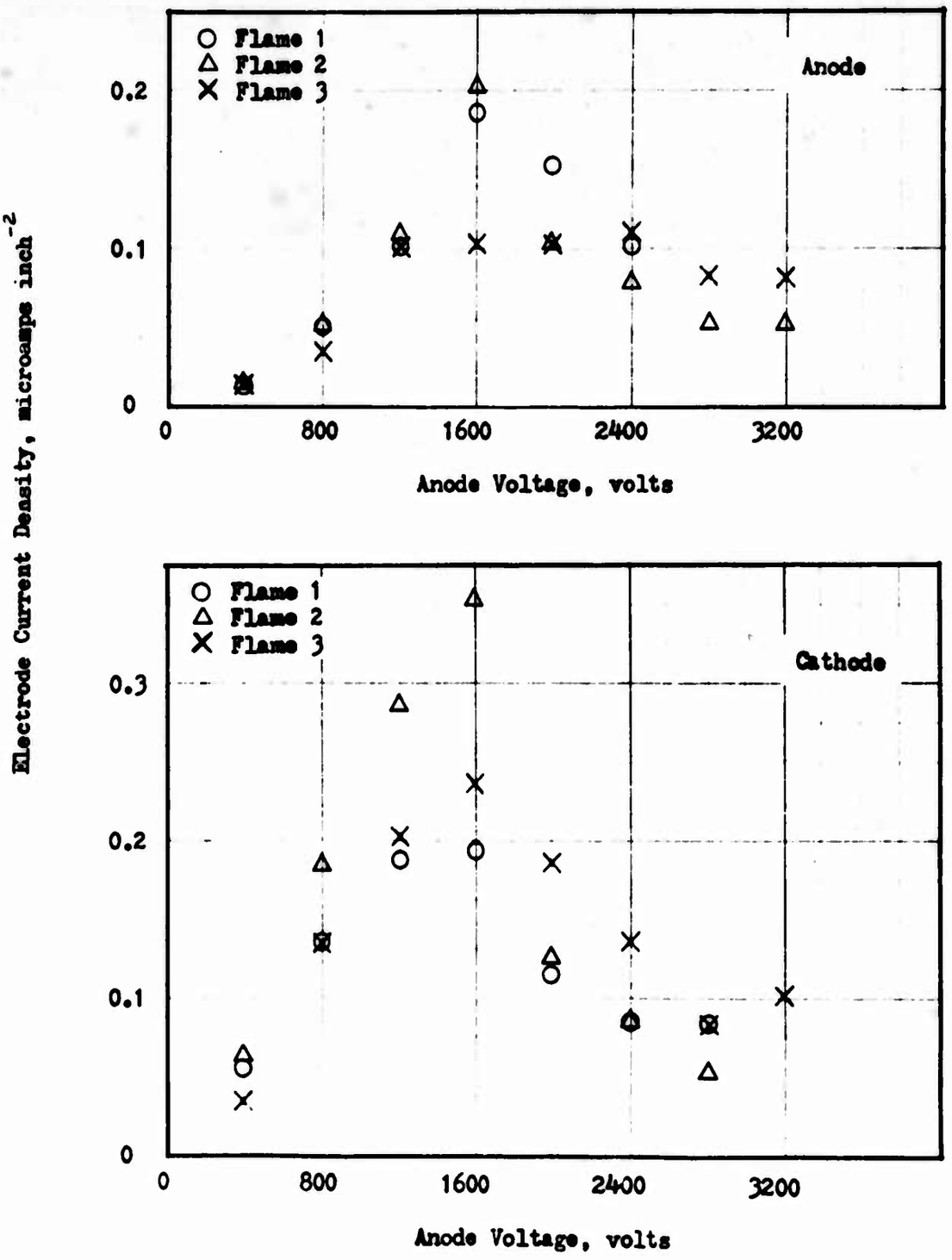

Fig. 19 Current Density Versus Anode Voltage, y = 5.25 inches

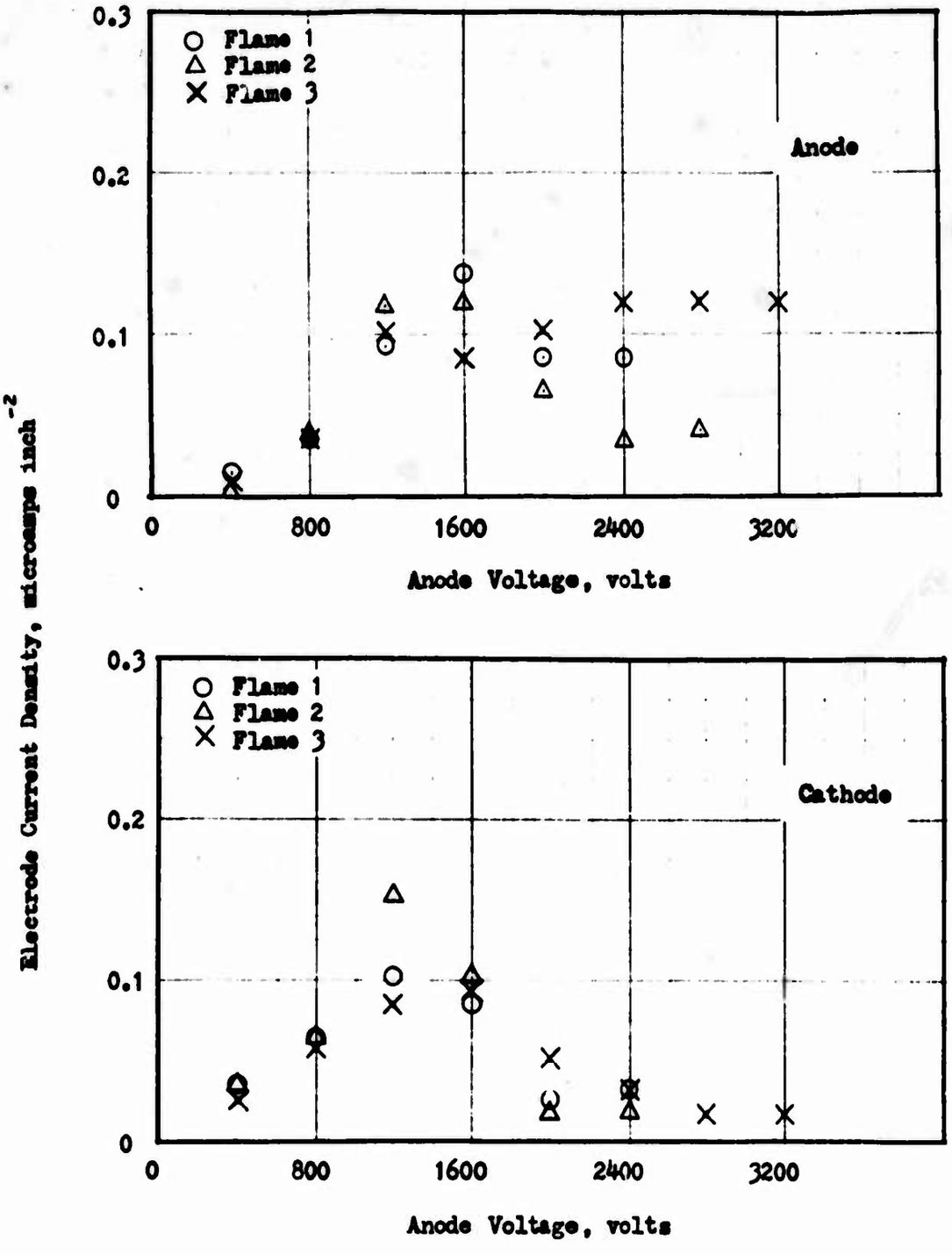

Fig. 20 Current Density Versus Anode Voltage, y = 6.375 inches

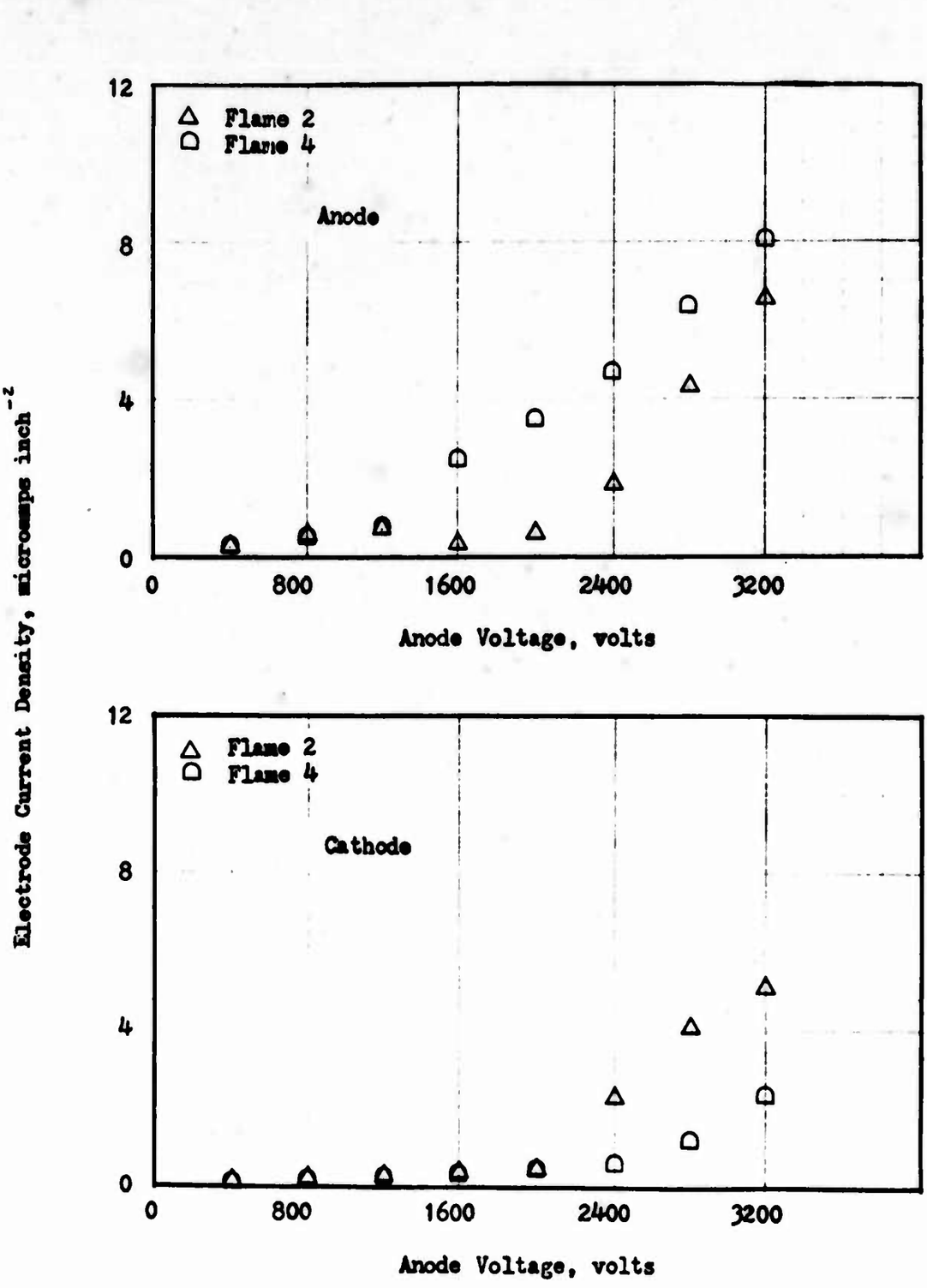

Fig. 21 Current Density Versus Anode Voltage, y = 0.75 inch

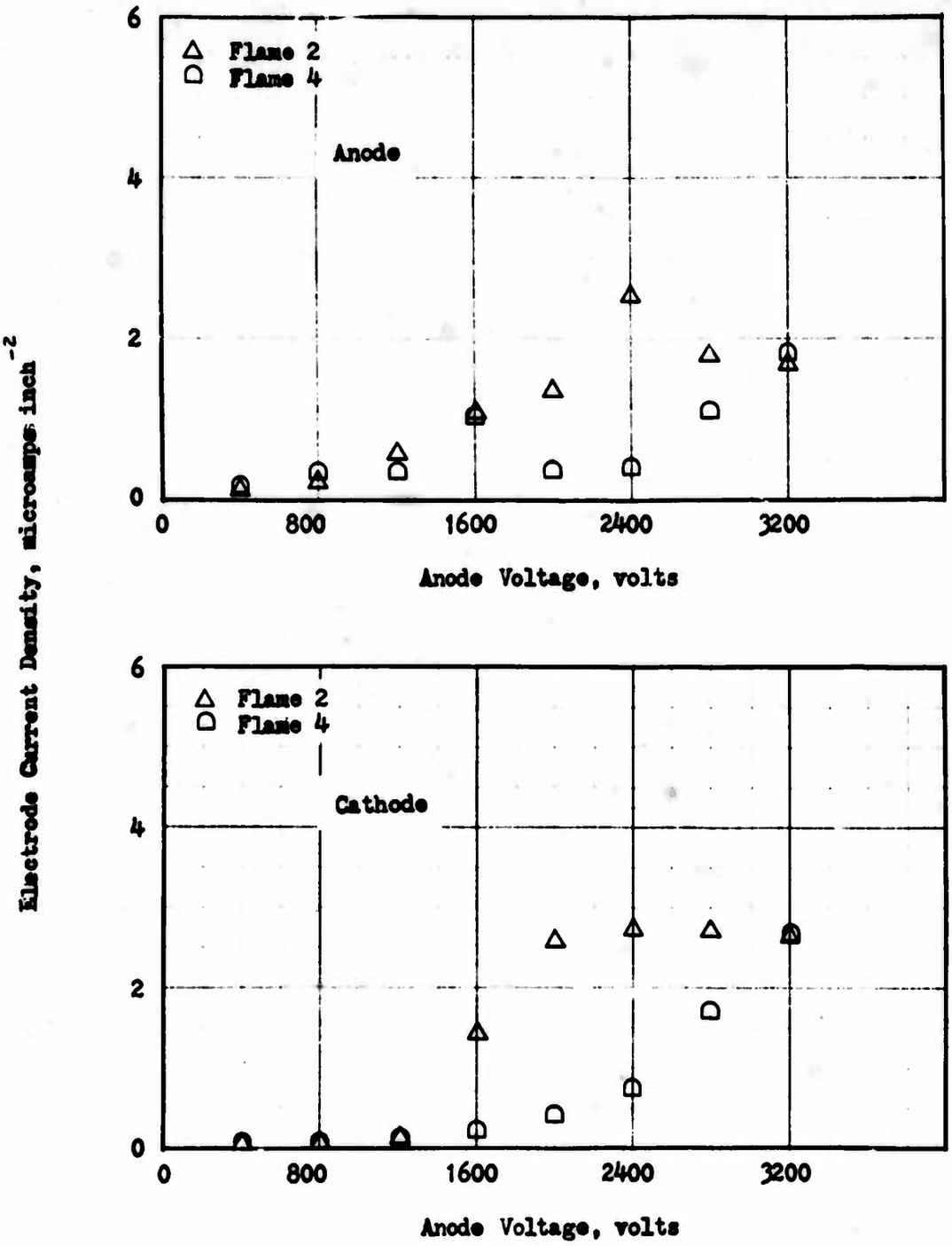

Fig. 22 Current Density Versus Anode Voltage, y = 1.875 inches

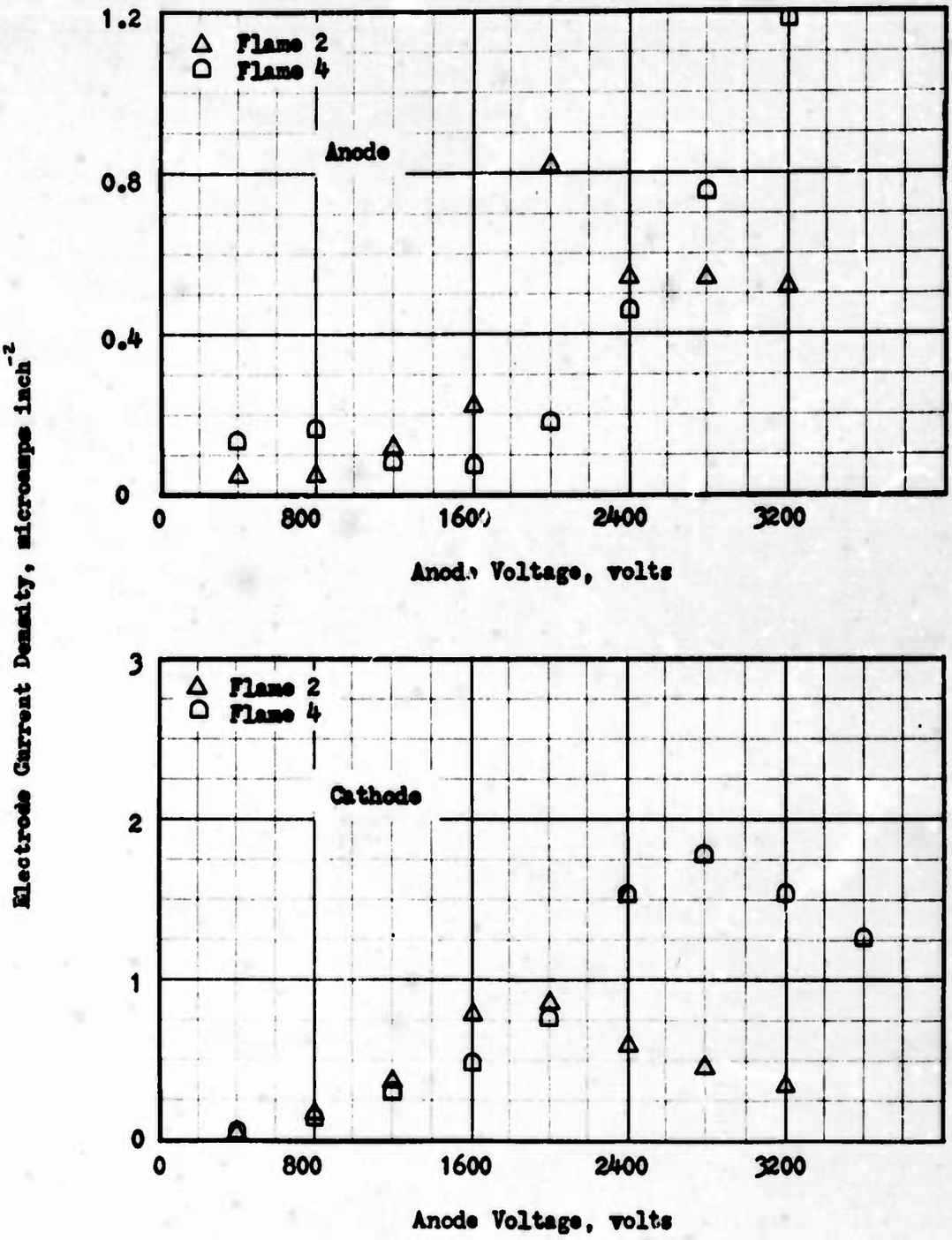

Fig. 23 Current Density Versus Anode Voltage, y = 3.0 inches

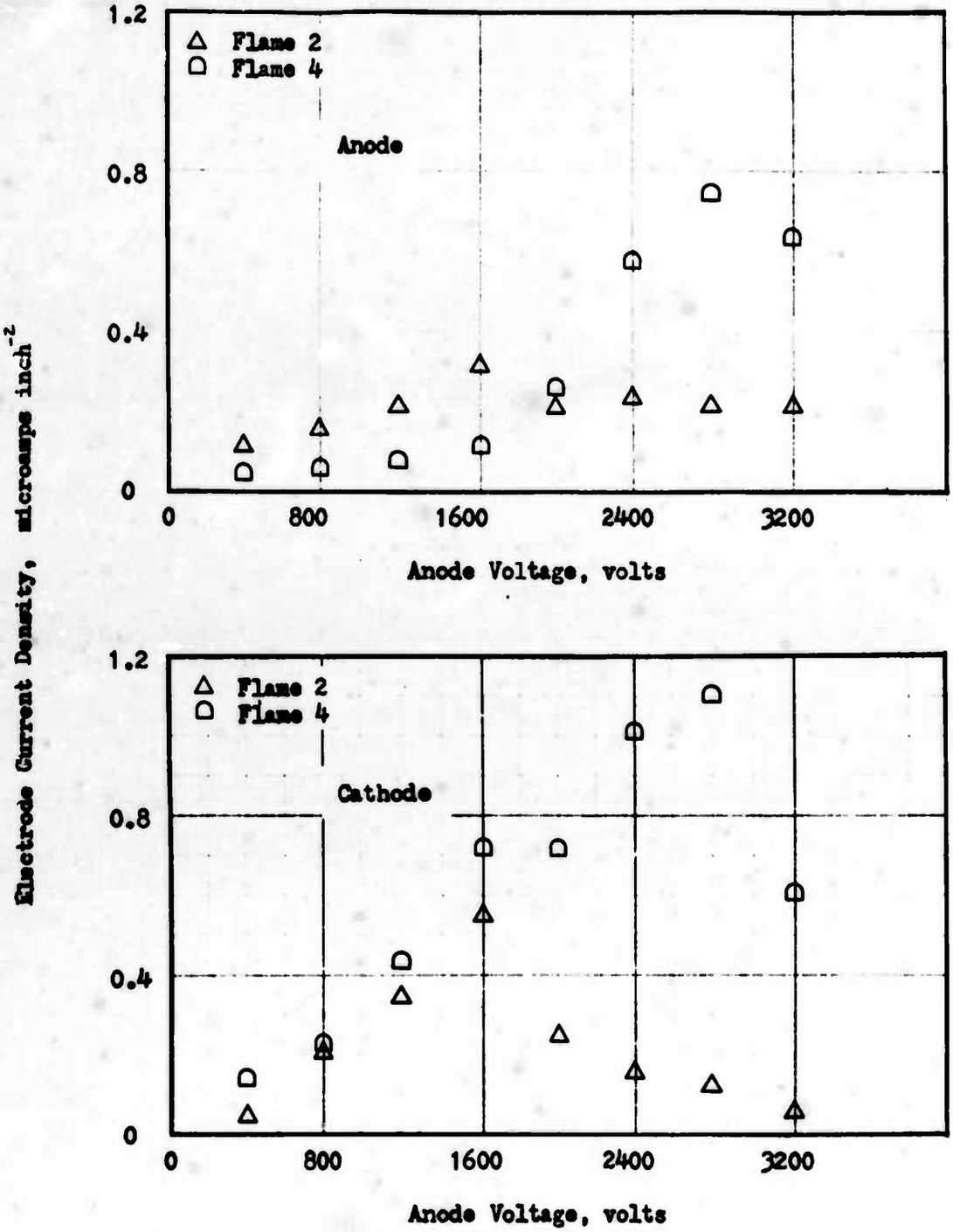

Fig. 24 Current Density Versus Anode Voltage, y = 4.125 inches

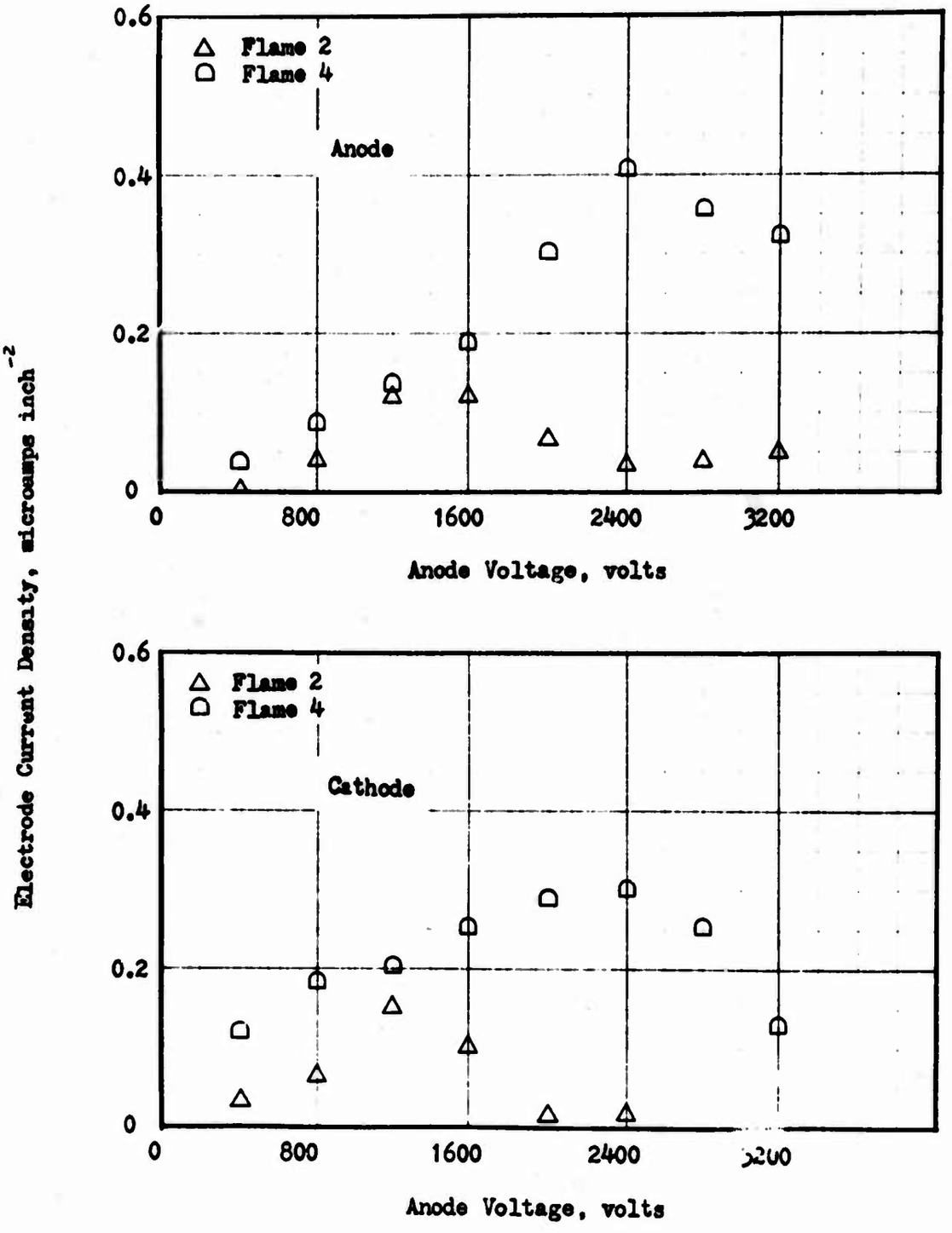

Fig. 25 Current Density Versus Anode Voltage, y = 6.375 inches

flames, show no sign of a saturation condition, as the current is still increasing with voltage at the highest voltage applied. Considering the flame as a whole, it can, therefore, be assumed that the flame is sub-saturated within the limits of the voltages applied.

All of the current density curves, Figs. 15-25, exhibit the same general trends. Near the base of the flame, with increasing voltage, the current increases slowly at first and then shows a more rapid increase. At upper parts of the flame, the current is much lower and at high voltages begins to decrease again as previously mentioned.

The current density figures for flames 1, 2, and 3, which are all at the same velocity, indicate that the current density values and their changes with voltage show essentially the same trends. The gas mixture then is found not to be an important parameter concerning flame current, at least for the range of mixtures and voltages used.

Current density Figs. 21-25 show some interesting results for flames 2 and 4, which are the same gas mixture but at different gas velocities. It is seen that the voltage at which the current begins to increase or decrease more rapidly occurs at different voltages for the two flames. The trend is that the higher velocity flame 4 "lags" in voltage behind flame 2; that is, the voltage where the current shows a more rapid increase or decrease occurs at a higher value for flame 4. A general conclusion is that the flames studied are affected more by hydrodynamic and electric variables than chemical variables, as may be expected since we are dealing with diffusion flames.

The current-voltage characteristics for the segments comprising the cathode can be used to obtain information concerning the mobility of the positive ion. If it is assumed that the negative charge carrier is an electron, and the one-dimensional equations of Chapter 3 are applicable, then Eq. (3.25) applies to the current density and mobility of ions moving toward the cathode. Solving Eq. (3.25) for k, gives

$$k = \frac{4}{9} \frac{\frac{dJ_o}{dV} (R-L)^3}{V\epsilon} \tag{8.1}$$

If the experimental current density curves of Figs. 15-25 are used to determine dJ_o/dV, the mobility at various positions along the flame may be calculated. In this way the mobility was found for each flame at various positions along the flame using the value of dJ_o/dV at 800 volts. The results are shown in Table 4.

Table 4. Positive Ion Mobility Determined from Current Density Data, $inch^2 volt^{-1} sec^{-1}$

Height Above Flame Base, inch	Flame 1	Flame 2	Flame 3	Flame 4
0.75	1.08	0.20	0.27	0.16
1.87	0.68	0.19	0.53	0.09
3.0	0.31	0.47	0.82	0.28
4.12	0.36	0.42	0.58	0.49
5.25	0.16	0.30	0.21	0.31
6.37	0.09	0.16	0.08	0.11
7.5	0.04	0.14	0.20	0.08

Although the mobility values in Table 4 certainly have not been determined with a great deal of accuracy, the results do indicate that the positive ion mobility probably lies in the range of 0.1 to 1 $inch^2 volt^{-1} sec^{-1}$. As a comparison, the mobility values of some singly charged positive ions are (42), in the same units: H_2O^+, 0.17; CO_2^+, 0.13; CO^+, 0.17; N_2^+, 0.20; O_2^+, 0.20. Table 4 does suggest, therefore, that the positive ion is a singly ionized molecule with a molecular weight on the order of magnitude of about 20. On the other hand, the mobility of carbon particles found in Reference 24 would be on the order of 10^{-3}, and the mobility of the electron would be of the order of 10^3 to 10^4, in the same units.

If the current density data presented in Figs. 12-25 are plotted to show the variation in current density along the electrodes at constant voltage, then an important mechanism for an electric effect of the flame comes to light. Figures 26-29 show the current distribution for each flame at 1200 and 2000 volts across the electrodes. For the present, only the distribution along the anode is considered. If the major part of the negative ions are composed of electrons, as was assumed in Chapter 3, then because of the large mobility a negligible coupling would exist between the gas motion and the electron current. It is expected then that the current distribution measured along the anode reflects the current distribution along the flame sheet.

It can be seen from Figs. 26-29 that for all the flames tested the anode current is much greater for the first two inches or so of flame height than for the rest of the flame sheet. As a result, there is a region where the quantity $\partial J/\partial y$ has a relatively high value. A large gradient in current density along the flame, $\partial J/\partial y$, between the regions of high and low current would give rise to induced gas motion as discussed in Chapter 4. In that chapter a typical value of an experimentally determined gradient in current density was used to show that the interaction with the diffusion process was a first order effect.

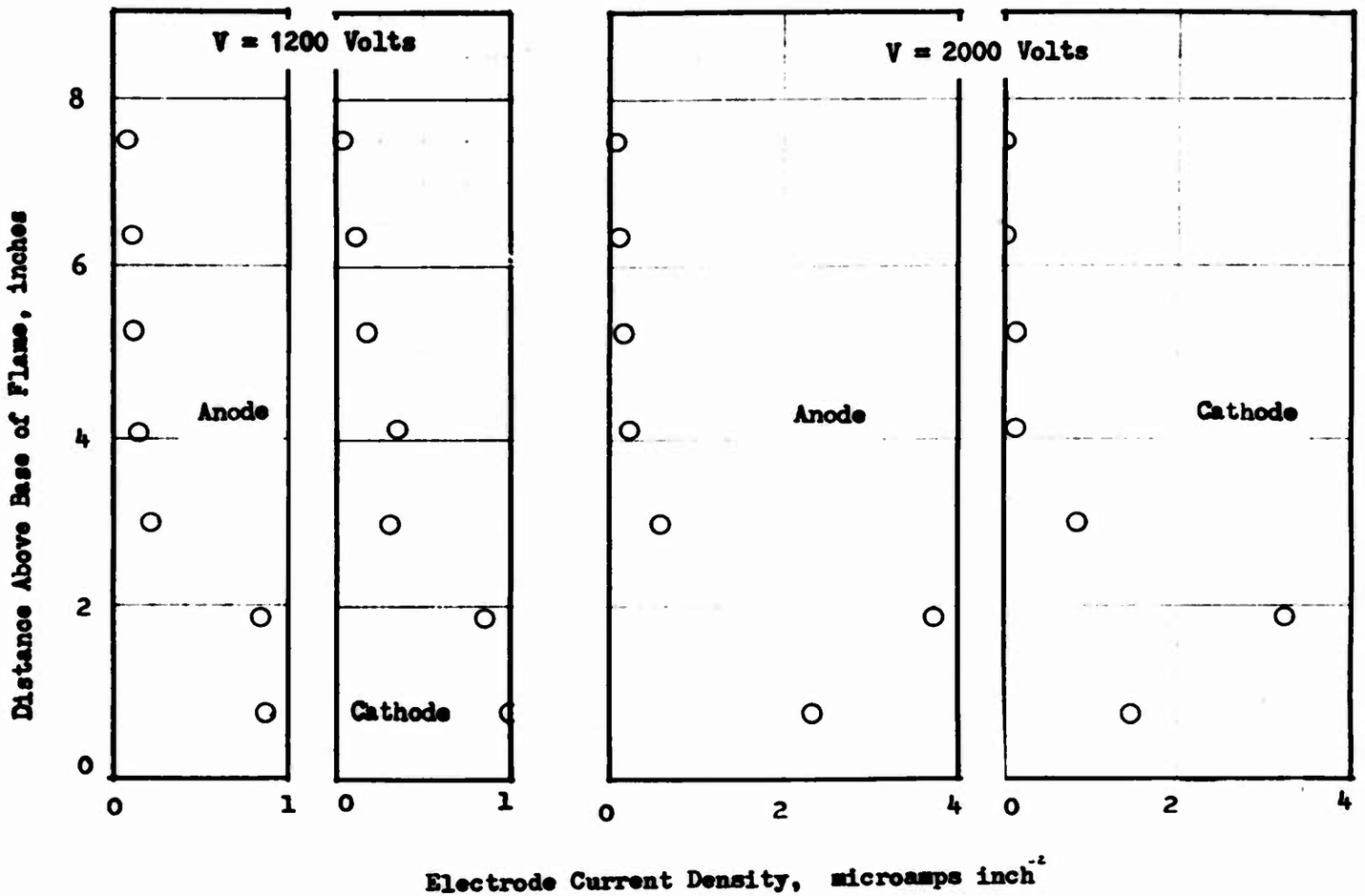

Fig. 26 Current Distribution along Electrodes, Flame 1

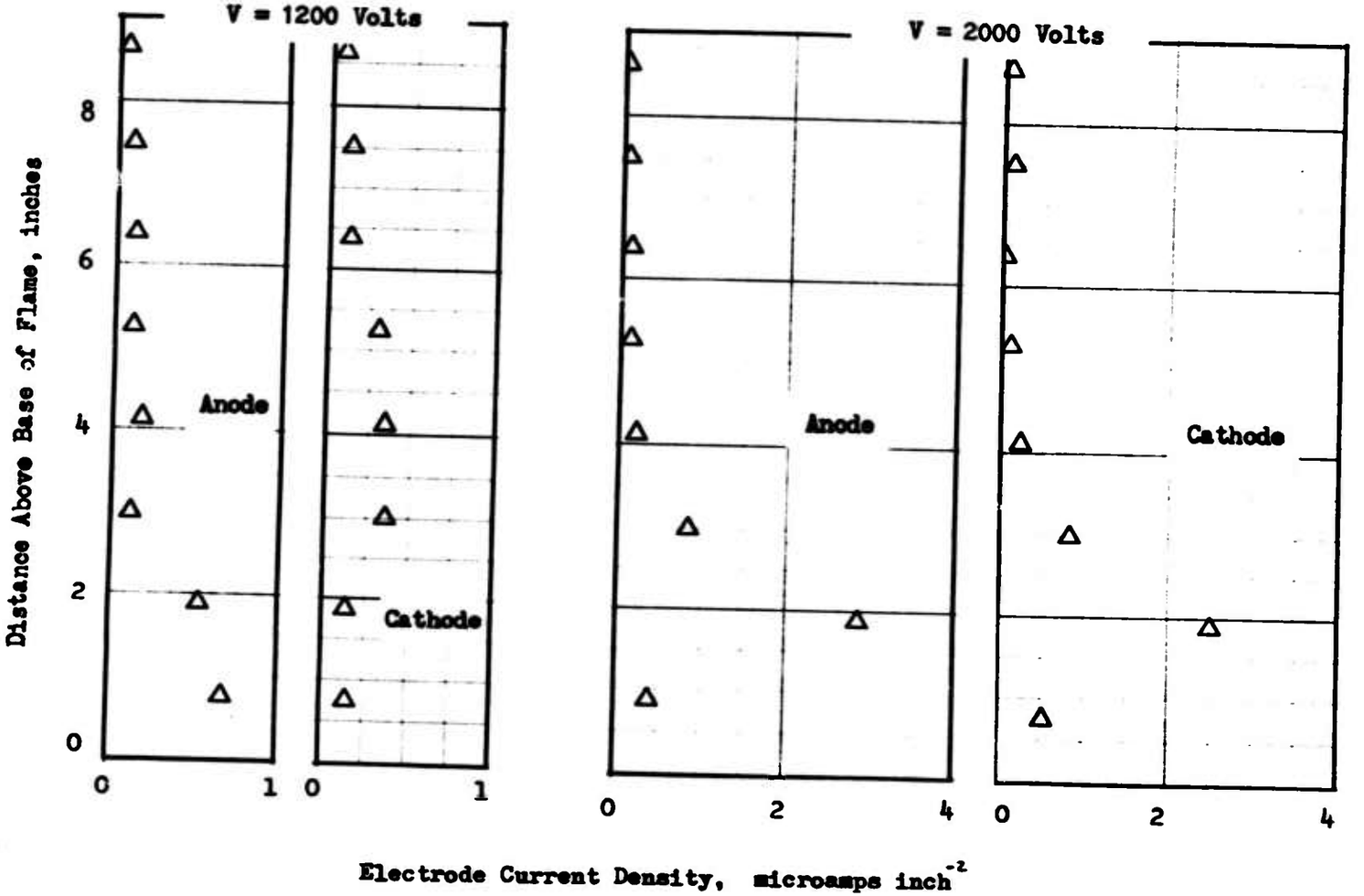

Fig. 27 Current Distribution along Electrodes, Flame 2

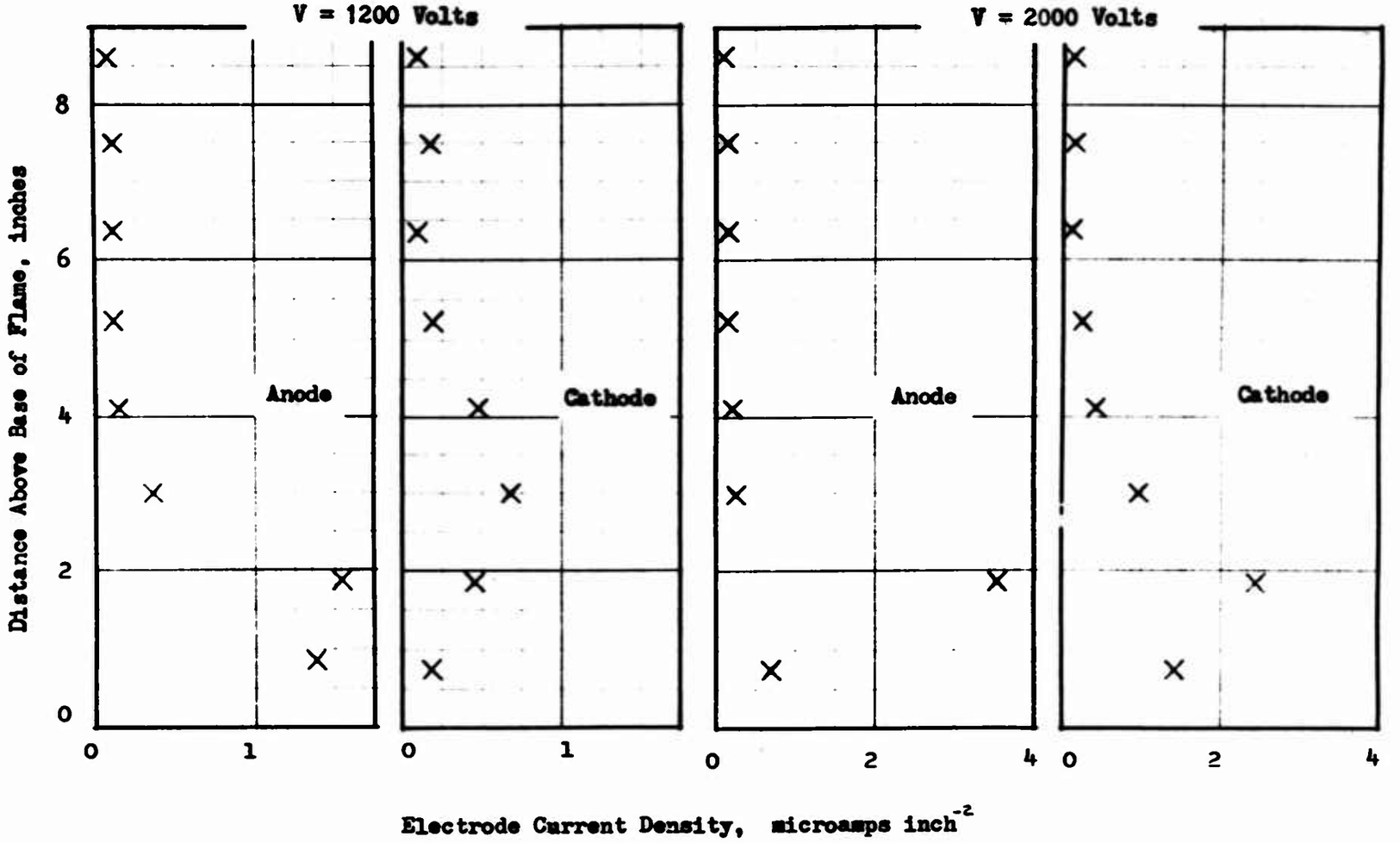

Fig. 28 Current Distribution along Electrodes, Flame 3

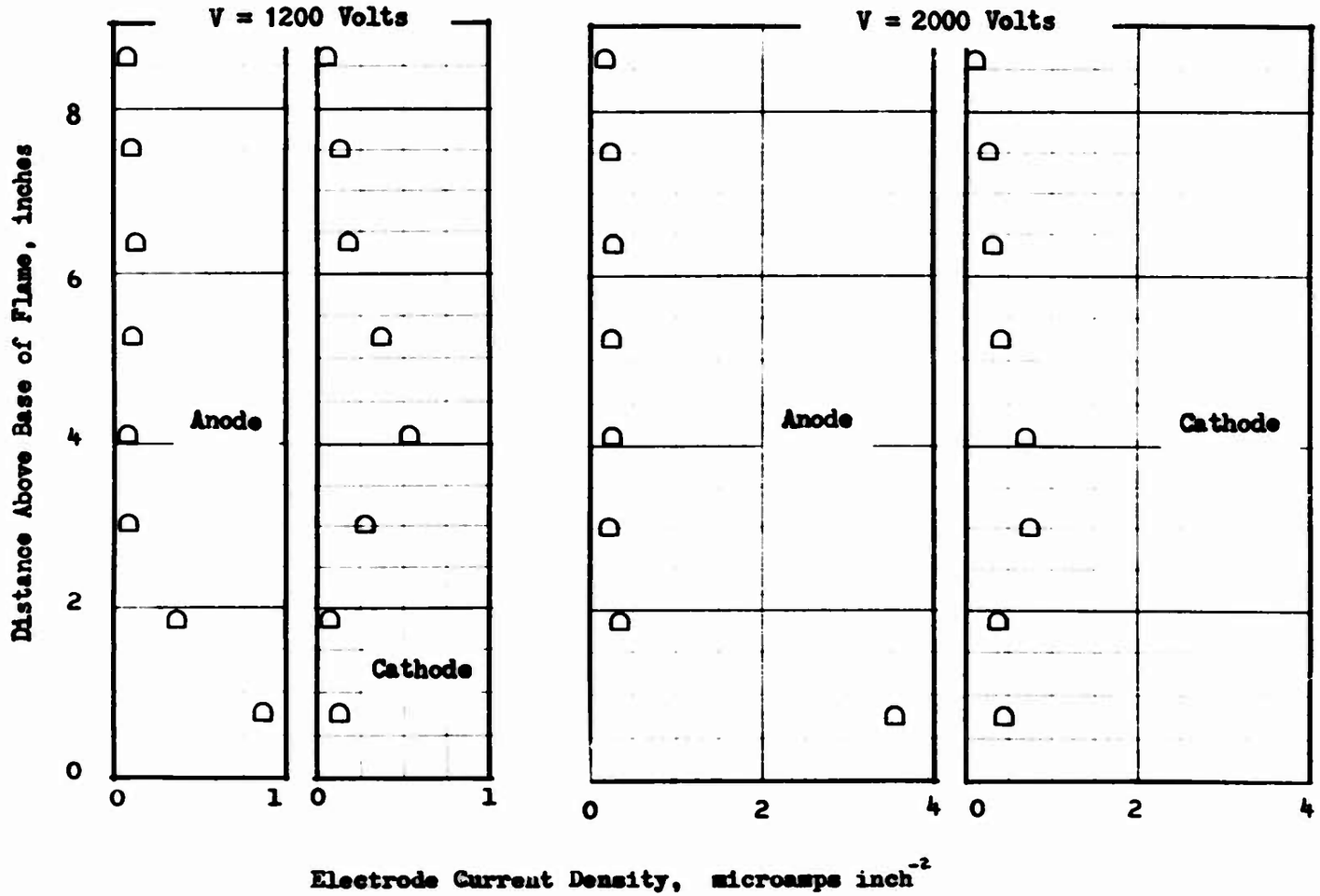

Fig. 29 Current Distribution along Electrodes, Flame 4

Consider now the current distribution along the cathode, which represents positive ion distribution. The most significant observation from Figs. 26-29 is that the distribution of current on the cathode is much flatter than the distribution on the anode. As previously mentioned, if the anode current distribution reflects the distribution at the flame, then these curves indicate that some positive drift downstream after leaving the flame sheet and before reaching the cathode.

Two effects may be responsible. First, the ion drift velocity may be low enough that the gas motion sweeps the ions downstream; and second, the downstream motion of the ions may be caused by an induced electric field in that direction. Considering the first effect, the average transverse electric field strength, E_x, is found by taking the average value of Eq. (3.20), which results in, for A $\ll$ R-L,

$$(E_x)_{avg} = \frac{2}{3}\left[\frac{2J(R-L)}{k\epsilon}\right]^{1/2} \tag{8.2}$$

The average drift velocity is kE_{avg}, and the downstream movement, d, of an average ion would be

$$d = \frac{3U}{2}\left[\frac{\epsilon(R-L)}{2Jk}\right]^{1/2} \tag{8.3}$$

where U is the gas velocity.

Now the induced field will be analyzed as to its effect in displacing the positive ions downstream. The induced field given by Eq. (4.22) can be averaged over the air zone to give

$$(E_y)_{avg} = -\frac{2}{5}\left[\frac{2(R-L)^3}{Jk}\right]^{1/2}\frac{\partial J}{\partial y} \tag{8.4}$$

The downstream movement, d, of an average ion due to this field is

$$d = \frac{(E_y)_{avg}\,(R-L)}{(E_x)_{avg}} = -\frac{3(R-L)^2}{5J}\frac{\partial J}{\partial y} \tag{8.5}$$

A comparison of the values of the downstream movement of the positive ions calculated from Eq. (8.3) (ion drag) and from Eq. (8.5) (induced field) is given in Table 5. The experimental value was determined

from Figs. 26-29 by graphically finding the value of y that satisfies

$$\int_0^y J\,dy = \frac{1}{2}\int J\,dy \qquad (8.6)$$

where the second integral was evaluated over the total length of the flame. The difference in the value of y from Eq. (8.6) for the anode and cathode represents the downstream movement of a ficticious average positive ion. The values in Table 5 were found assuming that the average mobility was 0.2 $inch^2 volt^{-1} sec^{-1}$, (R-L) = 0.75 inch, and the electrode voltage was 1200 volts. The value of $\partial J/\partial y$ was taken as the change in current density between the first and fourth segments of the anode when a voltage of 1200 volts was applied across the chamber.

Table 5. Average Downstream Movement of Positive Ions, Inches

	Experimental	Induced Field	Ion Drag
Flame 1	0.35	0.14	0.004
Flame 2	2.3	0.13	0.004
Flame 3	1.6	0.15	0.003
Flame 4	2.9	0.35	0.007

The results in Table 5 show that the downstream motion of the positive ions because of drag on the flowing gas is much too small to account for the experimental observations. On the other hand, the downstream movement resulting from the calculated induced field is much closer to the experimental value. It is, therefore, concluded that these results lend support to the concept of a field induced gas motion on the air side of the flame.

8.2 ONSET OF FLICKERING

In Chapter 5 we discussed the conditions leading to instability of the flame, and in Chapter 7 we described observations of the flame in an electric field where it was noted that at certain voltages the flame begins to flicker.

A determination of the onset of flickering was performed in the following way. A 2.55-million-ohm resistor was placed in the wires leading from the first and third segments of the cathode to ground.

The current in these segments is then reflected by the voltage drop across the resistor; this voltage drop was placed across the terminals of an oscilloscope. The voltage drop across the resistor was small enough, on the order of ten volts, that it was assumed to not affect the internal electric field in any significant way.

For a stable, steady flame the current would be steady and no fluctuation of voltage would be sensed by the oscilloscope. If flame instability was generated by the field, a fluctuation in current would be expected, and a deflection observed on the oscilloscope. Figures 30-33 show photographs of the oscilloscope traces for two positions of each flame at several values of electrode voltage. It is seen that typically at low voltages a straight line trace is obtained, indicative of stability, and that at higher voltages a definite fluctuation is noted, indicative of flickering. The onset of flickering as indicated on these figures is more definite than observation with the naked eye. Figure 32 also shows oscilloscope traces taken when no flame existed in the chamber, to prove by the absence of fluctuations that the fluctuating current was due in fact to the flame and not associated with current leakage or local breakdown.

A significant observation can be made from the traces showing the onset of flickering. The critical voltage at which current fluctuations appear is lower for the position at y = 3 inches than for the position at y = 0.75 inches along the flame. The approximate critical voltages are shown in Table 6.

Table 6. Voltages for the Onset of Current Fluctuations

	y = 0.75 inch	y = 3.0 inch
Flame 1	2000	400
Flame 2	2000	600
Flame 3	2000	800
Flame 4	2400	1200

It appears, therefore, that at some values of voltage, some lower parts of the flame may be stable and other parts at a higher level destabilized. This agrees with Chapter 5 where it was stated that steep concentration gradients at low levels of the flame tend to render those parts more stable than upper parts of the flame.

Consider now flames 2 and 4, which are the same mixture but at different velocities. Table 6 shows that the onset of flickering at y = 3 inches occurs at 1200 volts for flame 4 and at 600 volts for flame 2. A reason for this difference is revealed by comparing the values of the stabilizing parameter for the two flames. The stabilizing parameter is plotted in Fig. 4 for flame 2 and has a value of 3.2 at

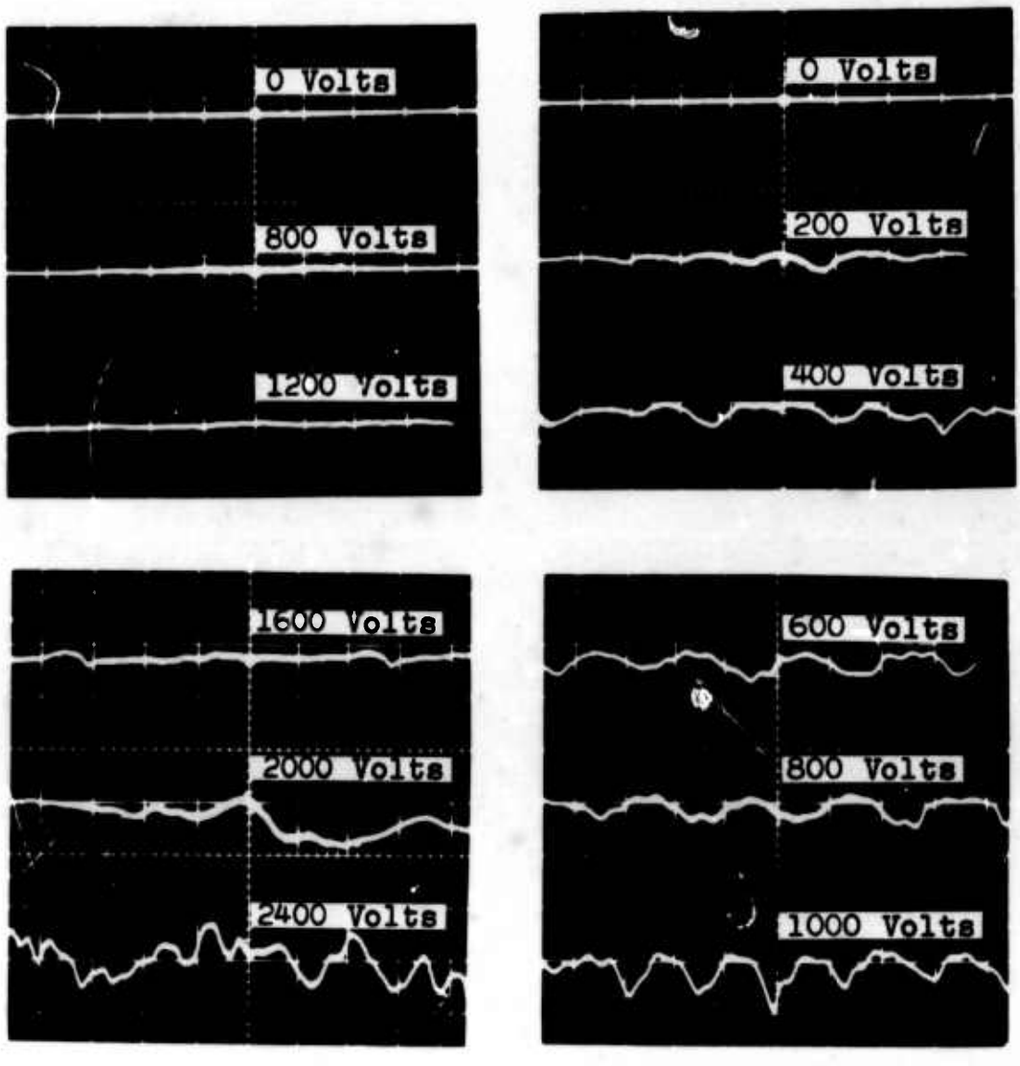

y= 0.75 inch
Flame 1

y= 3.0 inch
Flame 1

Fig. 30 Onset of current fluctuations in flame 1

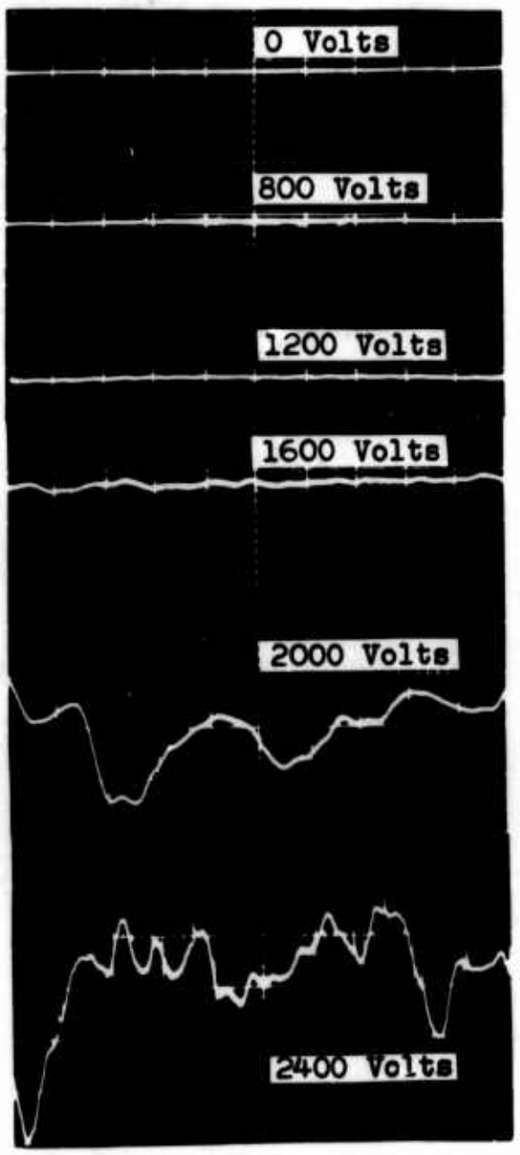

y= 0.75 inch
Flame 2

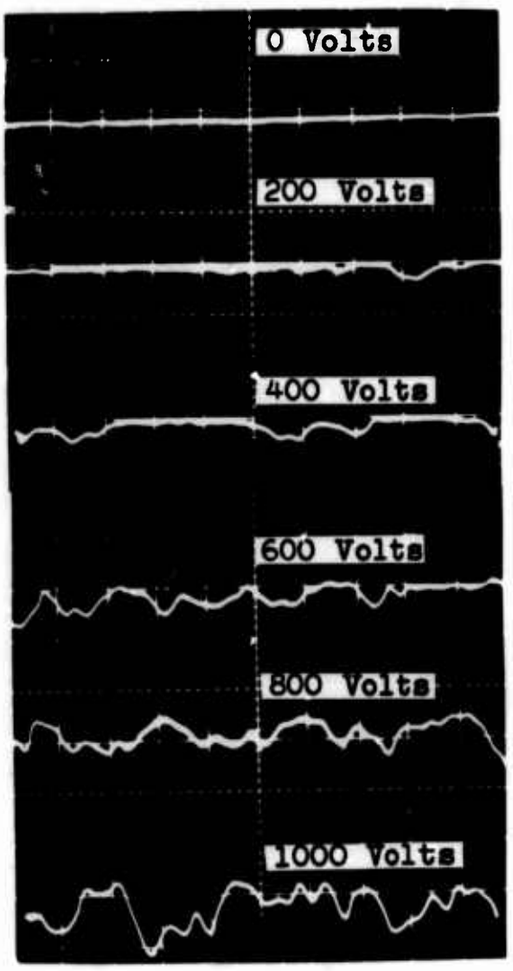

y= 3.0 inch
Flame 2

Fig. 31 Onset of current fluctuations in flame 2

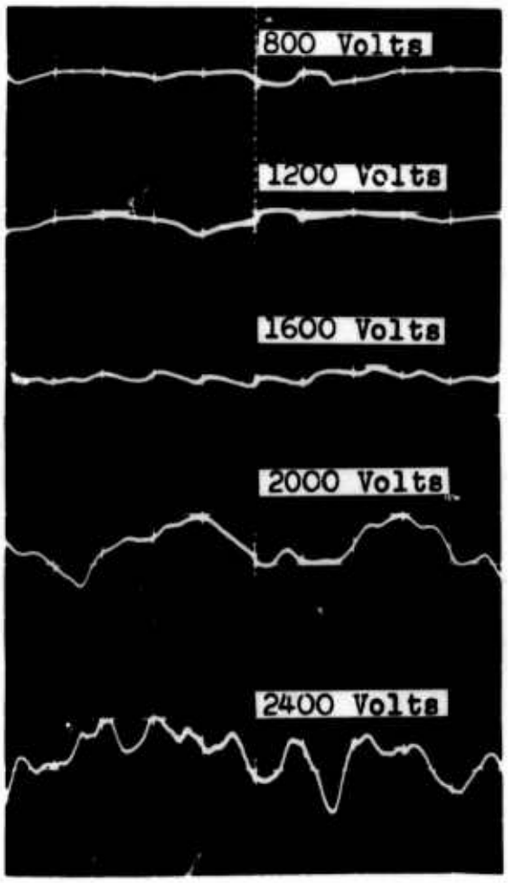

y= 0.75 inch
Flame 3

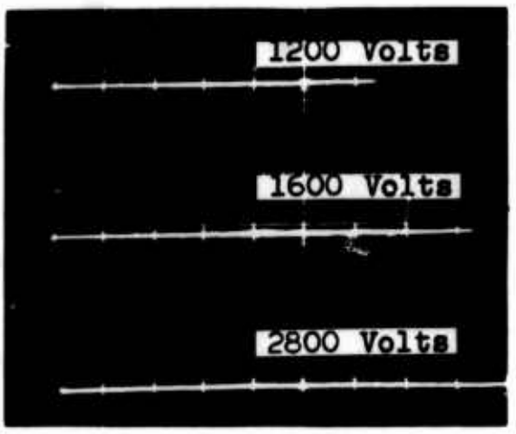

y= 3.0 inch
No Flame

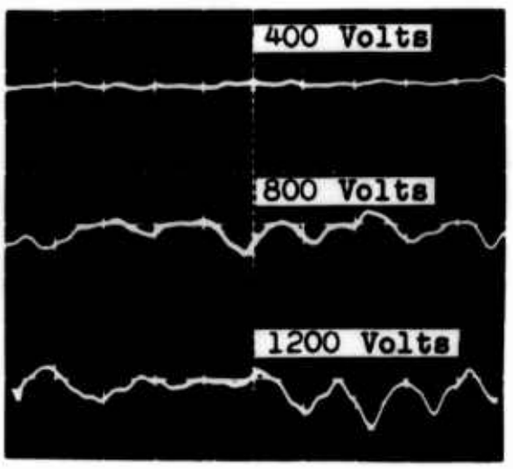

y= 3.0 inch
Flame 3

Fig. 32 Onset of current fluctuations in flame 3

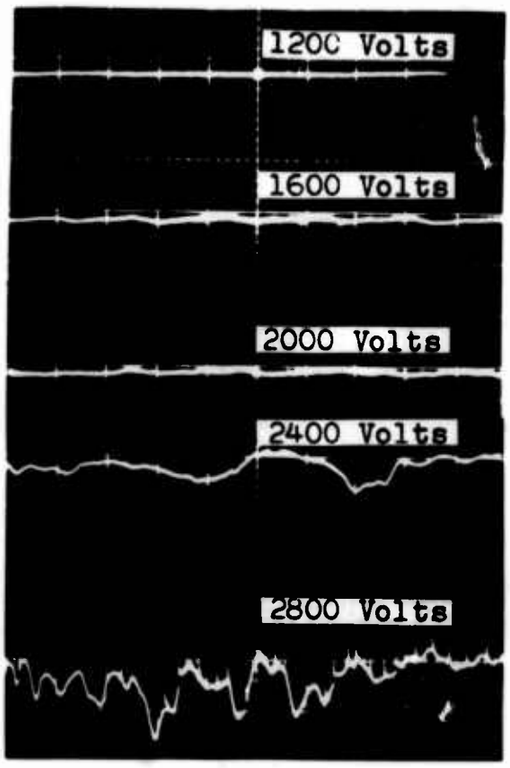

y= 0.75 inch
Flame 4

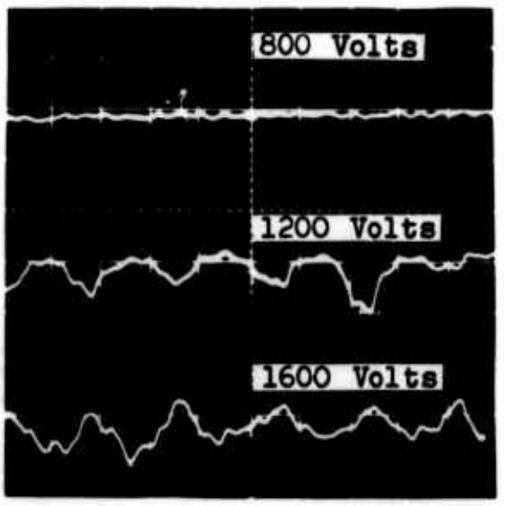

y= 2.0 inch
Flame 4

Fig. 33 Onset of current fluctuations in flame 4

y = 3 inches. Flame 4 has the same gas mixture so its curve corresponding to Fig. 4 is similar; in fact, from Eqs. (4.4) and (4.5) we see that the concentration depends on the group Dy/UR^2. Since the velocity for flame 4 is 1.5 times the velocity for flame 2, a height of three inches on flame 2 is equivalent to a height of two inches on flame 4 when the curve of Fig. 4 is used. The stabilizing parameter of flame 4 is then found to be about 10% greater than for flame 2 at the same level. If the electric properties were the same, flame 4 would consequently be expected to require a higher voltage to induce flickering, which was the observed trend.

A characteristic of the current-voltage curves of Chapter 8 can now be explained. As the electrode voltage is increased, upper levels of the flame begin to flicker first as a result of lower stabilization. Accompanying the onset of flickering is a more rapid increase in current. As the voltage is further increased, lower parts of the flame flicker and cause a more rapid increase in current there. High current density gradients then cause induced gas motion which results in combustion being completed at a lower level of the combustion chamber; as a result the currents in the upper parts of the chamber decrease.

8.3 ELECTRIC PRESSURE

Holes of 0.05-inch diameter were drilled through the walls comprising the anode and cathode at a position midway along the width of the combustion chamber and at a level of 2.19 and 5.56 inches above the base of the flame. The holes in the anode and cathode at the same level were directly opposite each other, and served as static pressure taps to measure the difference in pressure across the flame as a function of electrode voltage. The pressure measuring instrument was a Flow Corporation micromanometer fitted with a special traversing microscope capable of reading relative pressures to within 1.4×10^{-5} inches of water. Because of zero shift, the pressures are only accurate to about 3×10^{-5} inches of water.

Considering first a region between the flame and the cathode, in the presence of an electric field there is a body force

$$F = \frac{J}{k} \tag{8.6}$$

existing on the gas. The body force appears in the equation of motion in the x direction to yield

$$\rho \; w\left[\frac{\partial w}{\partial x} + u \frac{\partial w}{\partial y}\right] = - \frac{\partial p}{\partial x} + \frac{J}{k} \tag{8.7}$$

where w is the induced transverse velocity, u is the velocity parallel to the electrodes, and incompressible, inviscid flow is considered. The

terms on the left side of Eq. (8.7) are several orders of magnitude less than the terms on the right side for the induced velocities considered, so Eq. (8.7) is rewritten as

$$\frac{\partial p}{\partial x} = \frac{J}{k} \tag{8.8}$$

Since the pressure and current density are measured quantities, Eq. (8.8) serves as a method to determine the mobility. Figure 34 shows a plot of the cathode pressure minus the anode pressure versus voltage for the position of 2.19 inches above the base of the flame. These curves show only the electric pressure and therefore indicate zero pressure difference at zero electrode voltage. Actually, there was a small measured difference between the electrode pressures at zero voltage equal to 1.55 for flame 1, 0.28 for flame 2, 2.4 for flame 3, and 1.0 for flame 4 where the value represents cathode pressure in excess of anode pressure in inches of water times 10^{-4}.

Since it is assumed a priori that the negative ion at this level is an electron, the pressure gradient between the anode and the flame is very small. The positive ion mobility from Eq. (8.8) is then

$$k = \frac{(R-L)\ J}{P} \tag{8.9}$$

where P is the cathode pressure in excess of the anode pressure from Fig. 34. The distance (R-L) was not directly measured, but from visual observations, the following are taken as approximate values: for 400 volts, 1 inch; for 800 volts, 7/8 inch; for 1200 volts, 3/4 inch; for 1600 volts, 1/2 inch; for 2000 volts, 1/4 inch. Using the measured values of electric pressure from Fig. 34 and measured value of current density, the mobility was calculated using Eq. (8.9) and is listed in Table 7 below.

Table 7. Positive Ion Mobility at y = 2.19 Inches Determined From Electric Pressure Measurements, $inch^2 volt^{-1} sec^{-1}$

Electrode Voltage	Flame 1	Flame 2	Flame 3	Flame 4
400		0.80	0.30	
800	0.39	0.27	0.07	0.64
1200	0.56	0.22	0.36	0.65
1600	0.65	0.32	0.34	0.87
2000	0.67	0.41	0.23	0.21

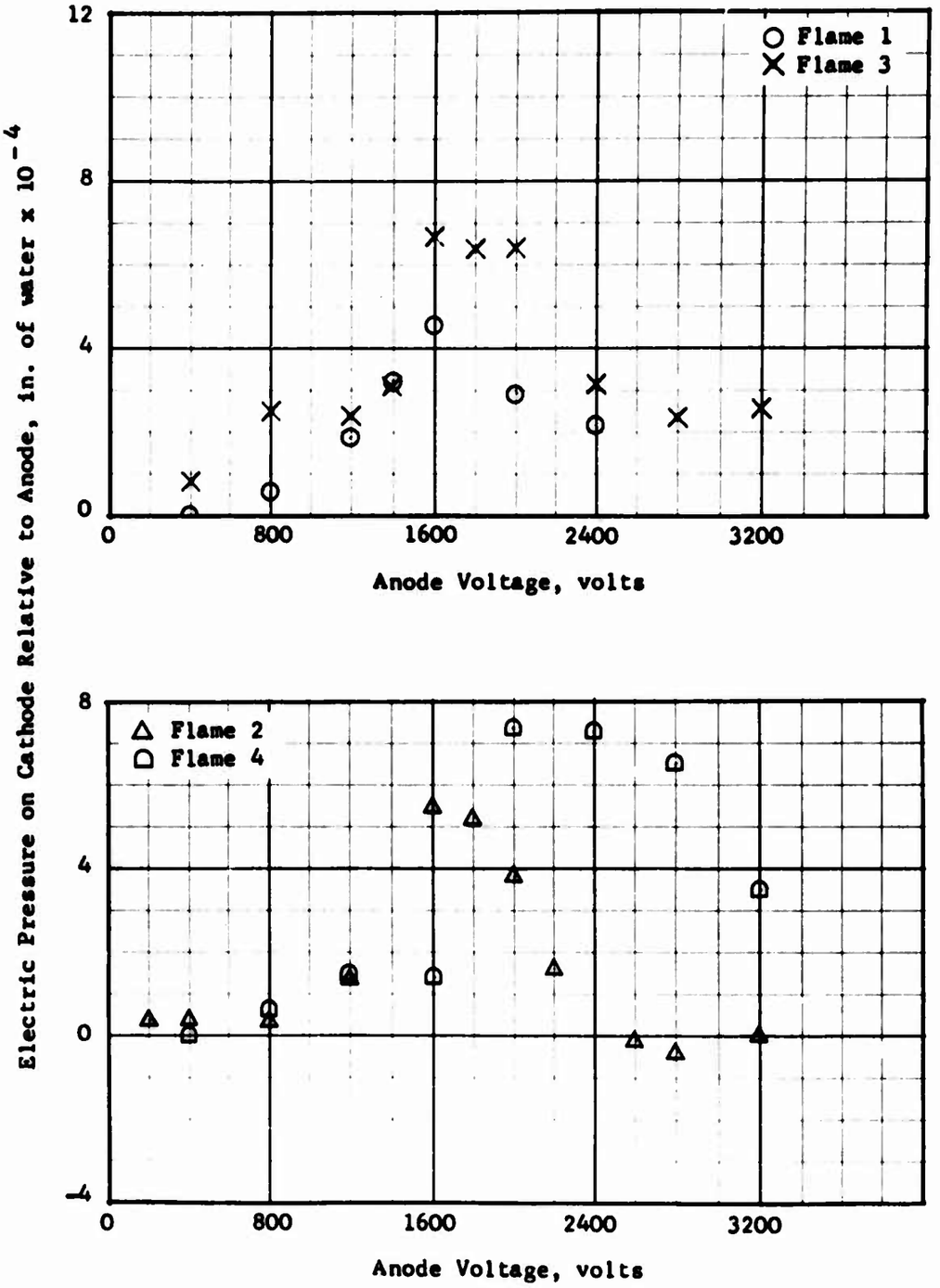

Fig. 34 Electric pressure at y = 2.187 inches above the flame base

The values in Table 7 are in the same range as the values of mobility found earlier and listed in Table 4. There is a strong indication, therefore, that the assumption of a positive ion with an atomic weight on the order of about 20 and a negative ion being an electron is justified for the portion of the flame 2.19 inches above the base.

Attention is now turned to the pressure measurements at a level of 5.56 inches above the base of the flame, which are shown in Fig. 35. It is readily apparent that conditions have changed, for at this level the electric pressure on the anode is greater than on the cathode--a reversal of the effect observed at the lower level of the flame. Apparently the average negative ion at this level is not an electron but is an ion with a mobility even lower than the positive ion. By writing the pressure rise across the air and fuel zones we get

$$k_- = \frac{LJ_-}{(P_{anode} - P_{cathode}) + \frac{(R-L)J_+}{k_+}} \qquad (8.10)$$

If the positive ion mobility is assumed to be unchanged, Eq. (8.10) leads to values of negative ion mobility of around 0.1 $inch^2 volt^{-1} sec^{-1}$, or on the order of the value of the positive ion mobility. Of course, since only average mobilities are detected, some negative ions may have a mobility larger than this, and others may have a mobility lower.

Two mechanisms for the increase in negative ion mobility along the flame may be active. One case is electron attachment to neutral molecules. Near the base of the flame the gas between the anode and the flame is mostly nitrogen with some propane, and small amounts of combustion products. Nitrogen has a very low probability of attachment and does not act as a charge carrier. The products of combustion, notably water vapor, however, readily attach to electrons and can act as an electron carrier. As more combustion products are present at higher levels in the chamber, an increasing percentage of the negative ions would have a mobility corresponding to ionized molecules.

Another process for decreasing the mobility is the attachment of electrons to carbon particles. Carbon particles would be formed in the combustion chamber by pyrolysis of fuel in the region near the flame. The particles would be in a region of electron flux. Weinberg and Place (24) have shown in a discussion of electrical control of flame carbon that under the above conditions thermal ionization of carbon particles and electron attachment to carbon particles are both active processes which produce charged particles of opposite sign. Honda (42) has also shown that in a soot-producing flame, the soot had an electric charge. Since a net electric pressure was measured on the anode at this level of the chamber, it is thought that the electron attachment is predominant.

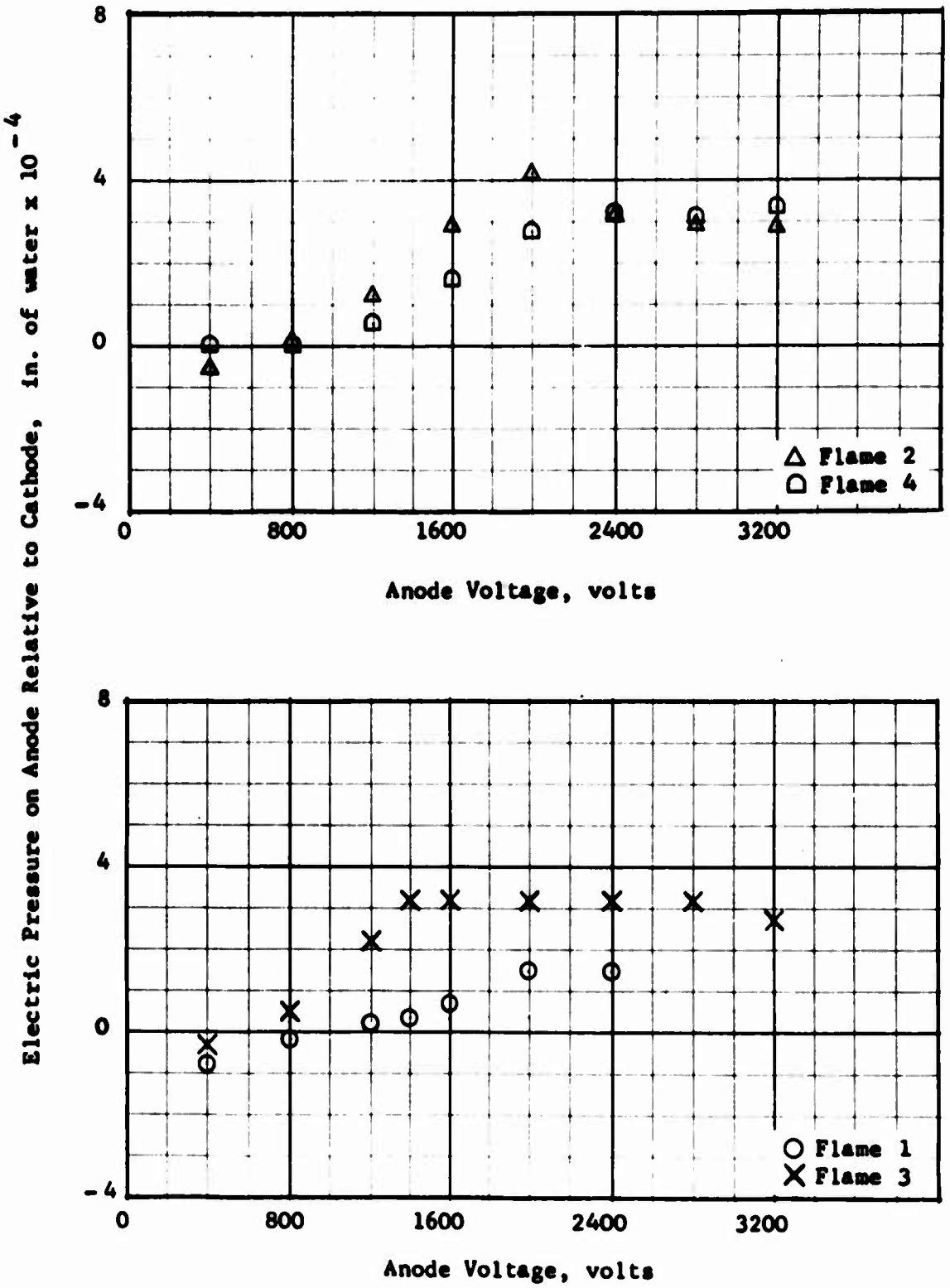

Fig. 35 Electric pressure at y = 5.562 inches above the flame base

This increase of pressure on the anode agrees qualitatively with observations of the flames discussed in Chapter 7. It was observed that movement of luminous gases toward the anode took place, reversing the general trend of movement toward the cathode.

The possibility that pressure differences on the electrodes may be due to an unsymmetric heating of the flowing gases has not been established, although this effect may be present. However, since the mobility values calculated from the pressure differences at y = 2.19 inches gave expected values, it seems that the pressure difference is caused by current, at least for that location.

8.4 ELECTROSTATIC PROBE MEASUREMENTS

A probe technique was used to measure the local ion density at a point within the combustion chamber in the air zone between the flame and the cathode. A steel wire, 0.008-inch in diameter, was stretched horizontally at a level of 2.19 inches above the base of the flame and parallel to the cathode wall at a distance of 3/8 inch from the cathode. The wire was supported at each end by a piece of quartz tubing projecting through holes drilled in the cathode wall, and cemented in place. The wire supports were 5-1/8 inches apart and hence the wire stretched along practically the entire width of the flame sheet.

The wire probe was connected to a probe measuring circuit, Fig. 36, which the current to the probe could be measured as a function of the voltage impressed on the wire. From simplified probe theory, (43), the ion density and space potential at the position of the probe can be determined by the probe curren-voltage characteristic. For the case of positive ions and neutrals only, the current-voltage characteristic plotted on a semi-log graph is typically as shown in Figs. 37-40. The significant point on such curves is the point where the theoretically linear portion of the curve at high positive voltage breaks off to a flatter curve at high negative voltages. At the point corresponding to the knee of the curves, the voltage is equal to the space potential at the point of the probe, and the probe neither attracts nor repels ions electrically. The probe current at this condition is then a measure of the local ion density. If J_p is the probe current density at the knee of the curve, K is Boltzmann's constant, and T is the temperature, the positive ion density is given by

$$n_+ = 4J_p\left[\frac{\pi\, m}{8KT}\right]^{1/2} \qquad (8.11)$$

The current-voltage characteristic for the probe for each flame at a voltage of 800 volts across the combustion chamber is shown in Figs. 37-40. The probe currents fluctuated during the measurement, and the range of fluctuation was recorded and plotted as a vertical line. As

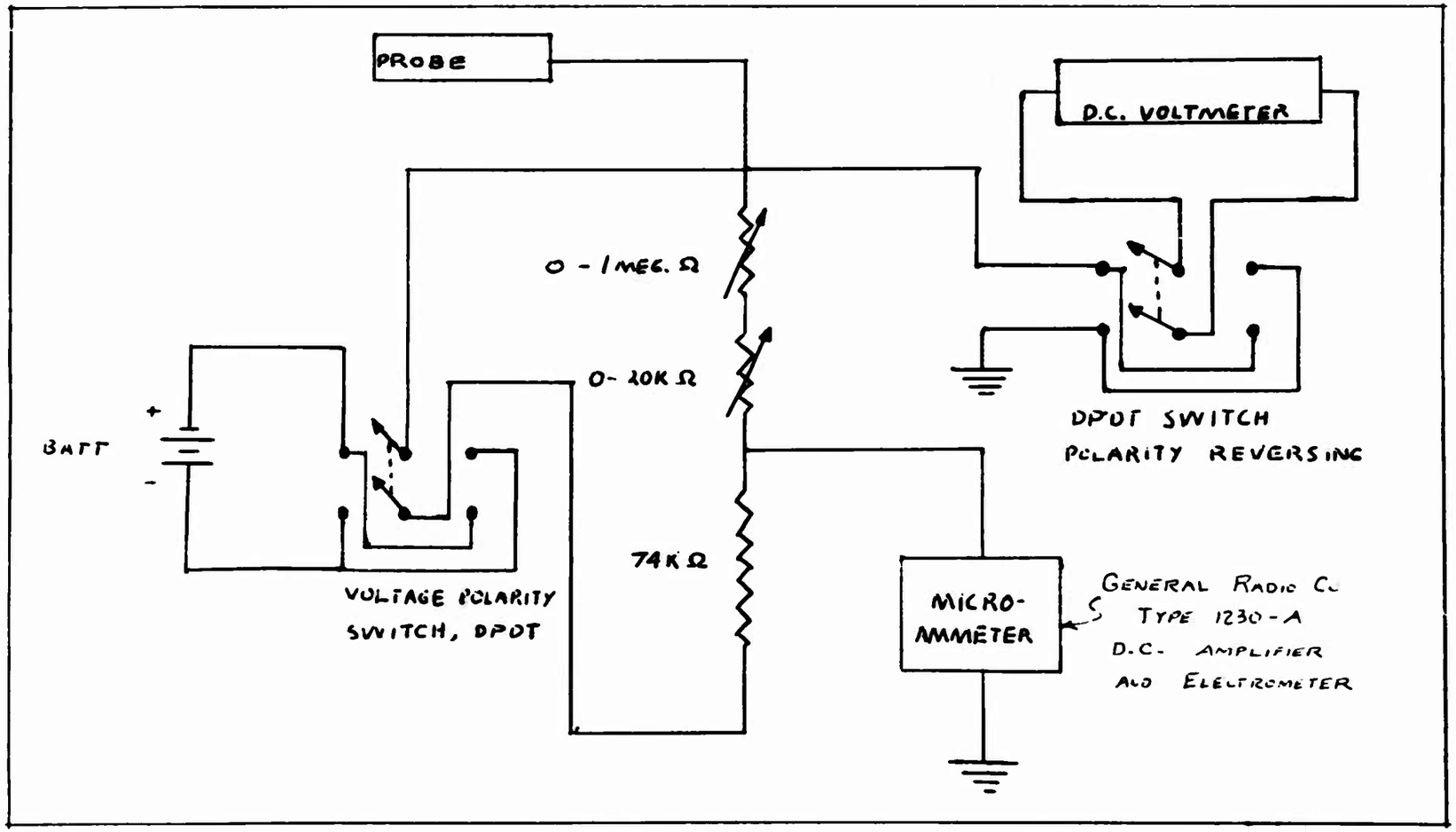

Fig. 36 Electrostatic probe circuit

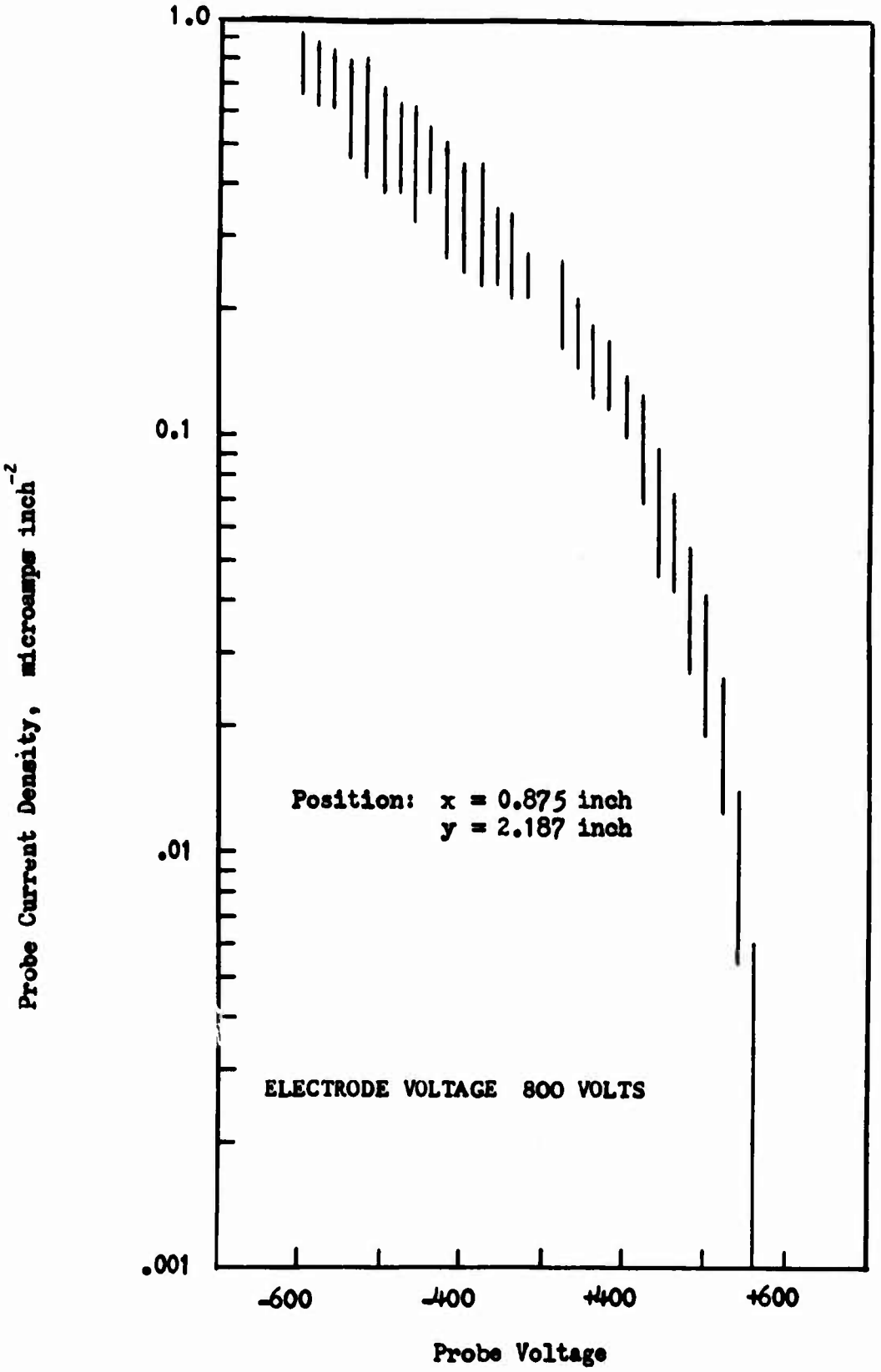

Fig. 37 Electrostatic Probe Characteristic for Flame 1

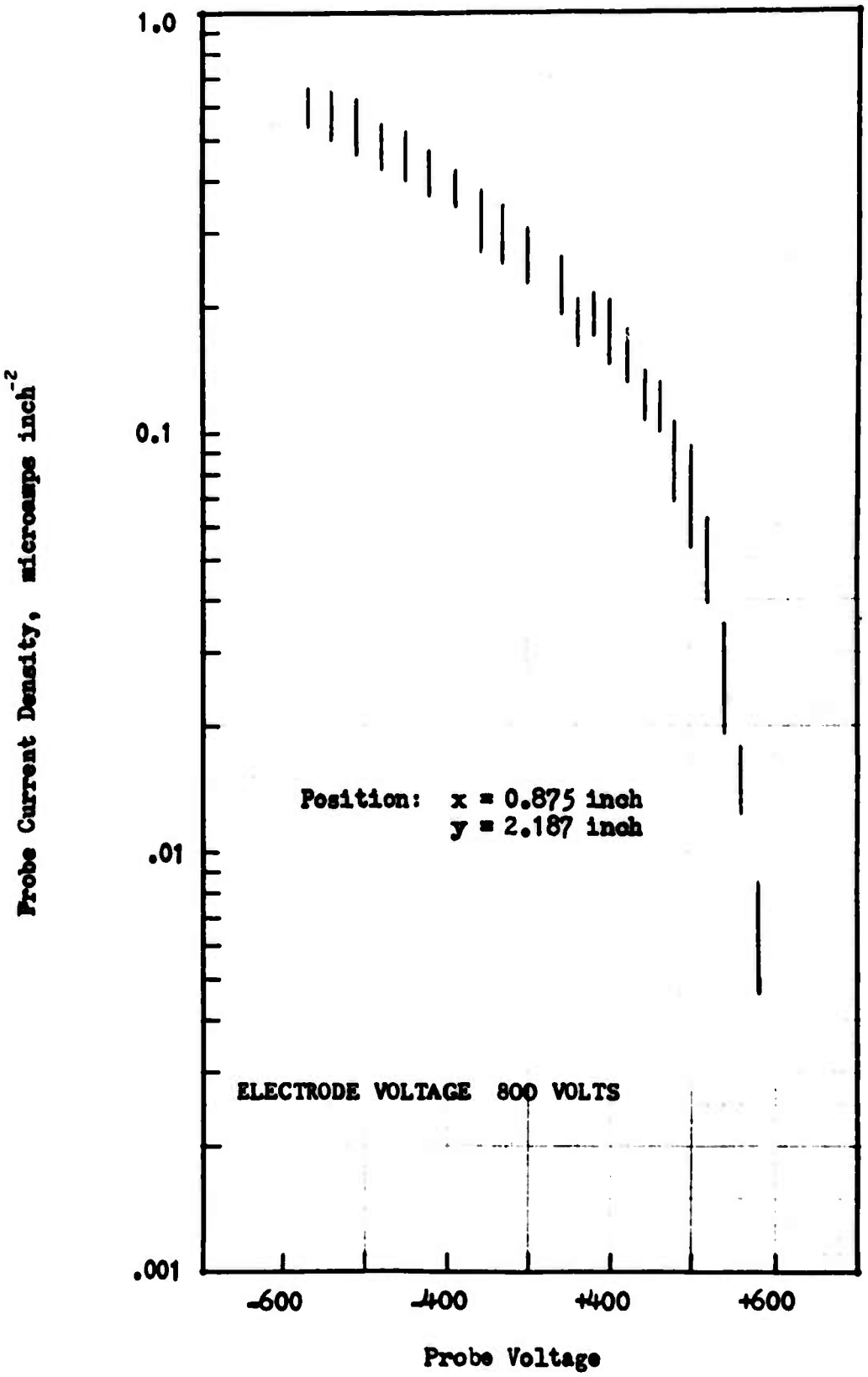

Fig. 38 Electrostatic Probe Characteristic for Flame 2

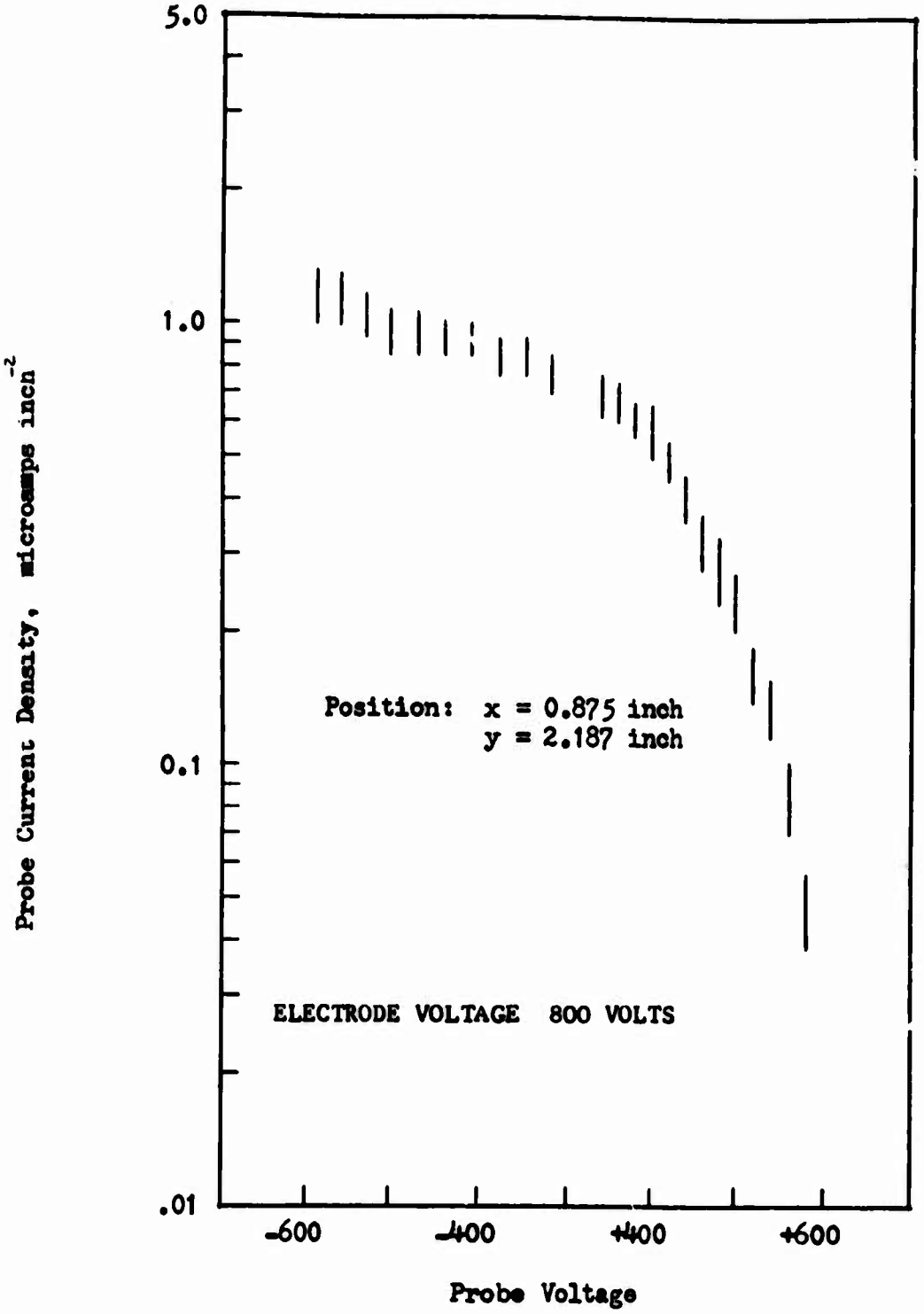

Fig. 39 Electrostatic Probe Characteristic for Flame 3

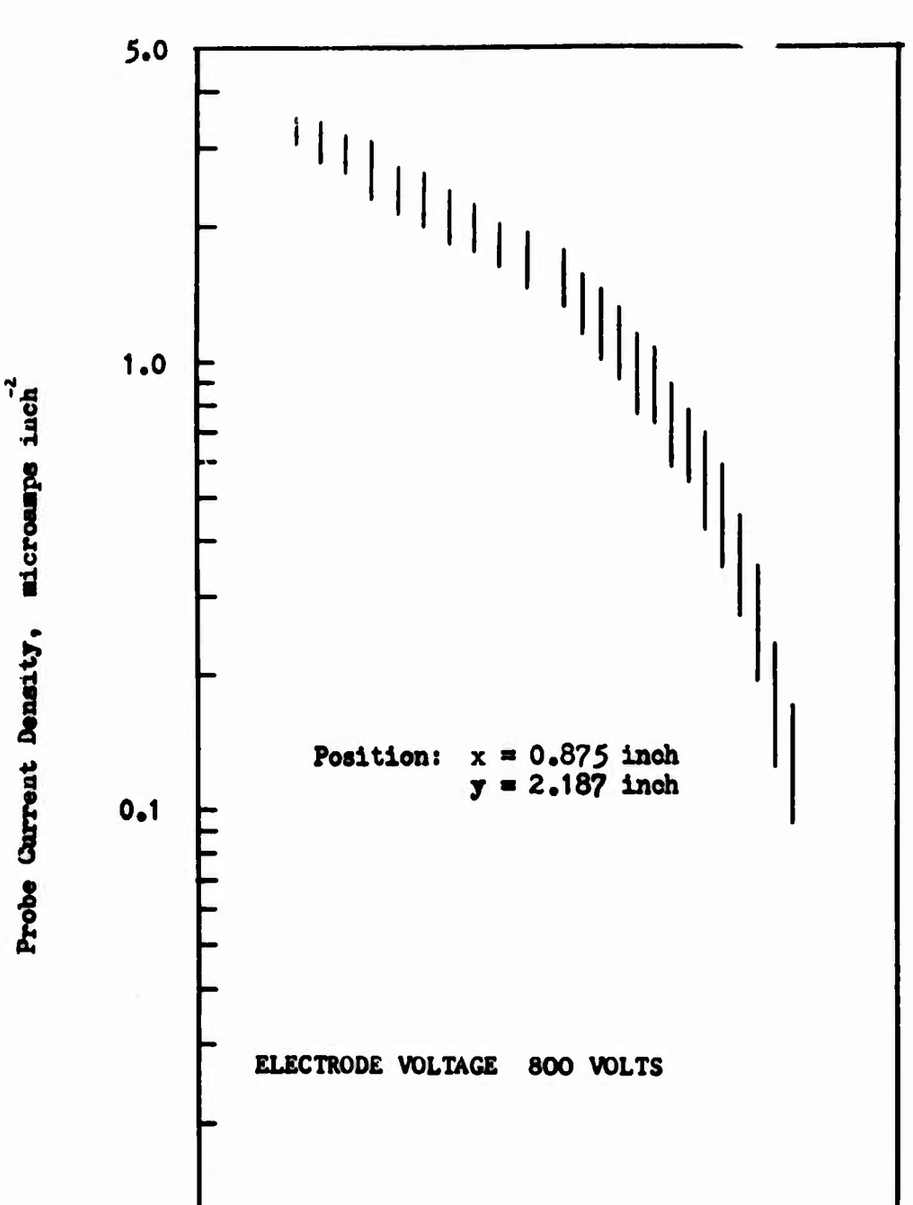

Fig. 40 Electrostatic Probe Characteristic for Flame 4

usual, the knees of the probe characteristics are not clearly defined, but a representative point can be chosen such that the value is correct within about an order of magnitude at most. The ion density was thus determined from the curves in Figs. 37-40 and the results shown in Table 8. An atomic weight of 20 and a temperature of 200°F was used to evaluate Eq. (8.11).

Table 8. Positive Ion Density, Ions $Inch^{-3}$

	Probe Measurement	Equation 8.12
Flame 1	0.09×10^9	1.7×10^9
Flame 2	0.1×10^9	3.0×10^9
Flame 3	0.31×10^9	4.5×10^9
Flame 4	0.61×10^9	5.4×10^9

The ion density can also be calculated using the one-dimensional electric equations of Chapter 3. Equation (3.20) for $A << L$ leads to

$$n_+ = \left[\frac{J_o \epsilon}{2k(x-L)}\right]^{1/2} \qquad (8.12)$$

Using a mobility value of 0.2 $inch^2 volt^{-1} sec^{-1}$ and $(x-L) = 1/2$ inch, and measured values of current density, the ion density was calculated from Eq. (8.12) and listed in Table 8. The probe data is seen to indicate a lower ion density than Eq. (8.12) by about one order of magnitude. In dealing with experimental measurement of number densities of ions however, agreement within a factor of 10 is occasionally accepted as satisfactory.

CHAPTER 9

EFFECT OF THE FIELD ON THE PRODUCTS OF COMBUSTION

The question arises when dealing with electric field effects on flames whether the field alters the combustion process itself, therby possibly changing the heat release, composition of products, or temperature.

The mechanisms by which the applied field can affect the combustion process can be categorized into two types. In one type we can list hydrodynamic and mechanical effects caused by electric forces on the gases or particles, as,for example, the induced gas motion discussed in Chapter 4. It can be expected that hydrocarbon diffusion flames of the type under investigation would exhibit a particularly strong influence by mechanical effects because of the existence of a pyrolysis zone near the flame sheet where fuel is heated and chemically changed. Induced gas motion would conceivably affect the transfer of heat into the pyrolysis zone, thereby directly changing the amount of fuel pyrolyzed, or carbon particles could become charged and consequently move through the combustion chamber under the influence of electric forces. The subsequent growth or combustion of the particle would then be determined by electrical as well as chemical and thermal conditions. This was demonstrated in Reference 24 where the field strength was adjusted to hold a carbon particle stationary within the pyrolysis zone, resulting in large visible growth of the particle.

The other type of interaction with the combustion process is the effect on chemical kinetics during combustion. Ionized intermediates and radicals formed during the complex chain reactions could be displaced in such a way as to alter the final reaction. Unstable reaction species could be moved to lower temperature regions where nonequilibrium is frozen. Nakamura (10) found a shift in the distribution of some radicals in a hydrocarbon diffusion flame with an applied electric field; Place and Weinberg (24) found in a hydrocarbon diffusion flame that the radiation intensity of OH increased with the application of a field while the radiation intensity of CH decreased.

In the present investigation it cannot be determined if chemical kinetics are being altered by the field because the strong action of induced gas motion tends to overshadow changes in kinetics. Diffusion flames, however, are generally considered to be reaction independent and diffusion controlled, and, therefore, it is suspected that mechanical effects on the flame are more important than changes in kinetics.

The overall effect of the field on the combustion process can be determined by an analysis of the combustion products. Figure 41 shows the flow diagram by which a sample of exhaust gas was analyzed for CO, CO_2, and unburnt hydrocarbon content. The sample was withdrawn from the 2-inch x 2-inch cross section at the top of the combustion chamber (see Fig. 6). The tip of the sample probe, which was a quartz tube, 0.057-inch O.D. and 0.025-inch I.D., was positioned in the center of the cross section. The gases were sufficiently mixed at this level that the position of the probe was not important.

The CO and CO_2 concentrations were measured by infrared absorption analyzers calibrated with a sample of known concentration with nitrogen as a background gas. The sample withdrawal rate was less than 5% of the total flow. Figure 42 shows that the CO_2 concentration for all the flames is practically independent of the electrode voltage. The CO concentration, Fig. 43, however, is seen to decrease above voltages of around 800 to 1600 volts, depending on the flame, and then increase again at voltages above 2400 volts. At the voltages of minimum CO concentration, the CO experiences a 25% to 40% reduction from its no-voltage concentration. The level of concentration is so low compared to the CO_2 that it cannot be established whether the changes in CO are reflected in changes in the amount of CO_2.

The unburnt hydrocarbon content of the exhaust was measured by the flame ionization method. The measuring instrument was supplied with a hydrocarbon free mixture of hydrogen and nitrogen and air which reacted in a burner assembly. The sample was injected into the burner, and if hydrocarbons were present in the sample, an electric current was measured in an electrode system near the burner. The instrument could not determine which hydrocarbon was present, since it is sensitive to both concentration and number of carbon atoms per molecule. For example, a given reading may correspond to a certain volume percent propane, or to three times as much methane. In the present case, the unburnt hydrocarbon was assumed to be propane, although it is realized that lighter hydrocarbons could be present from the products of fuel pyrolysis. To remain within the range of the instrument, the sample rate was set at around 0.02% of the total exhaust flow.

Since all the flames were richer than stoichiometric, it is not surprising that unburnt hydrocarbon was present in the exhaust. Figure 44 shows the measured concentrations for the flames investigated. The trends with increasing electrode voltage are similar to the trends with CO concentration. A decrease is noted above intermediate values of voltage; at high voltage, flames 1 and 4 show a rise in unburnt hydrocarbon following the decrease at intermediate voltages.

The measured amounts of input propane and exhaust products enable a carbon balance to be made on the combustion chamber. Carbon, which is not accounted for in the CO, CO_2, and unburnt hydrocarbon, is assumed to be solid carbon formation and is shown plotted in Fig. 45 as a function

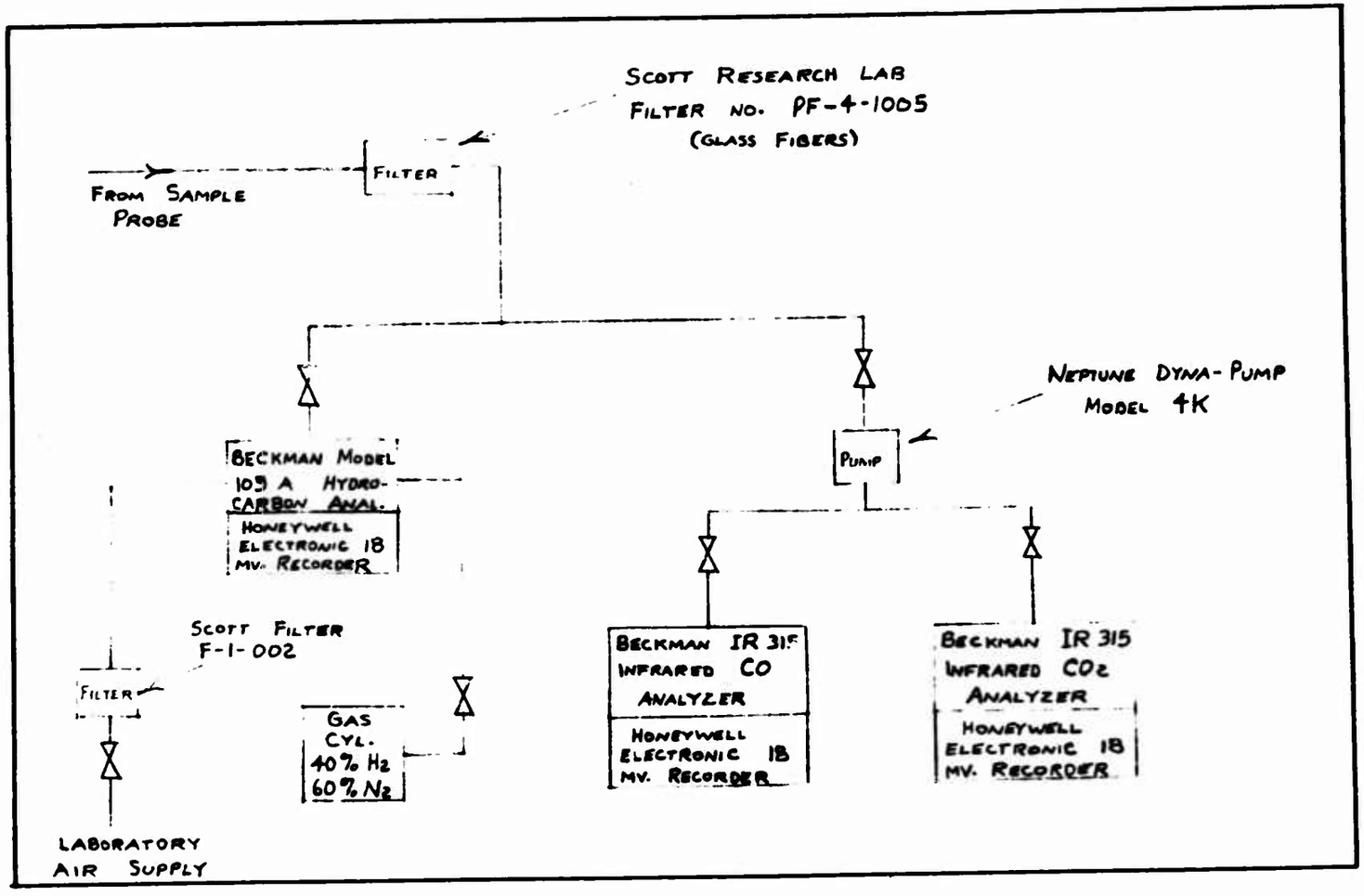

Fig. 41 Gas analysis flow diagram

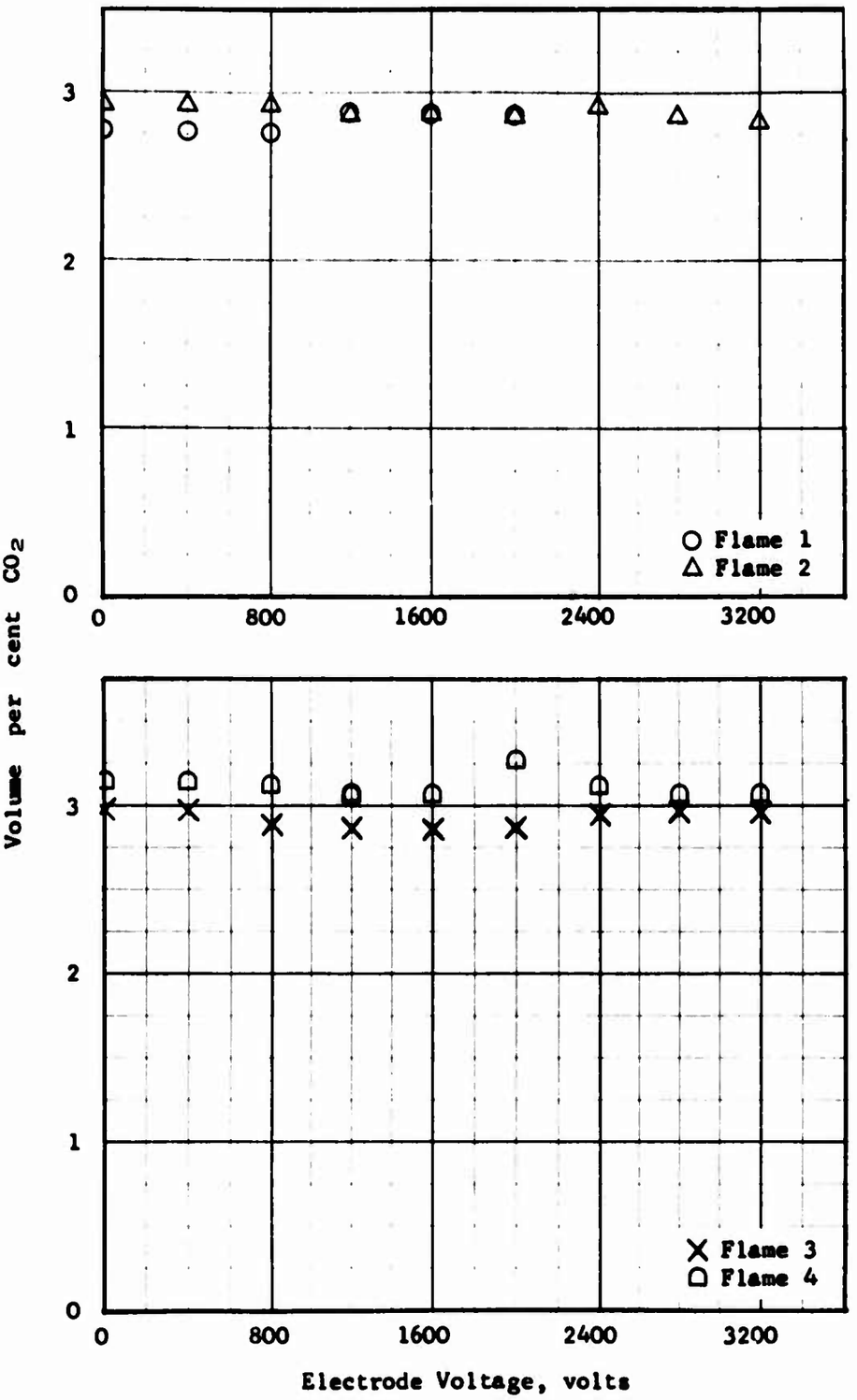

Fig. 42 Volume per cent CO_2 in the exhaust gases

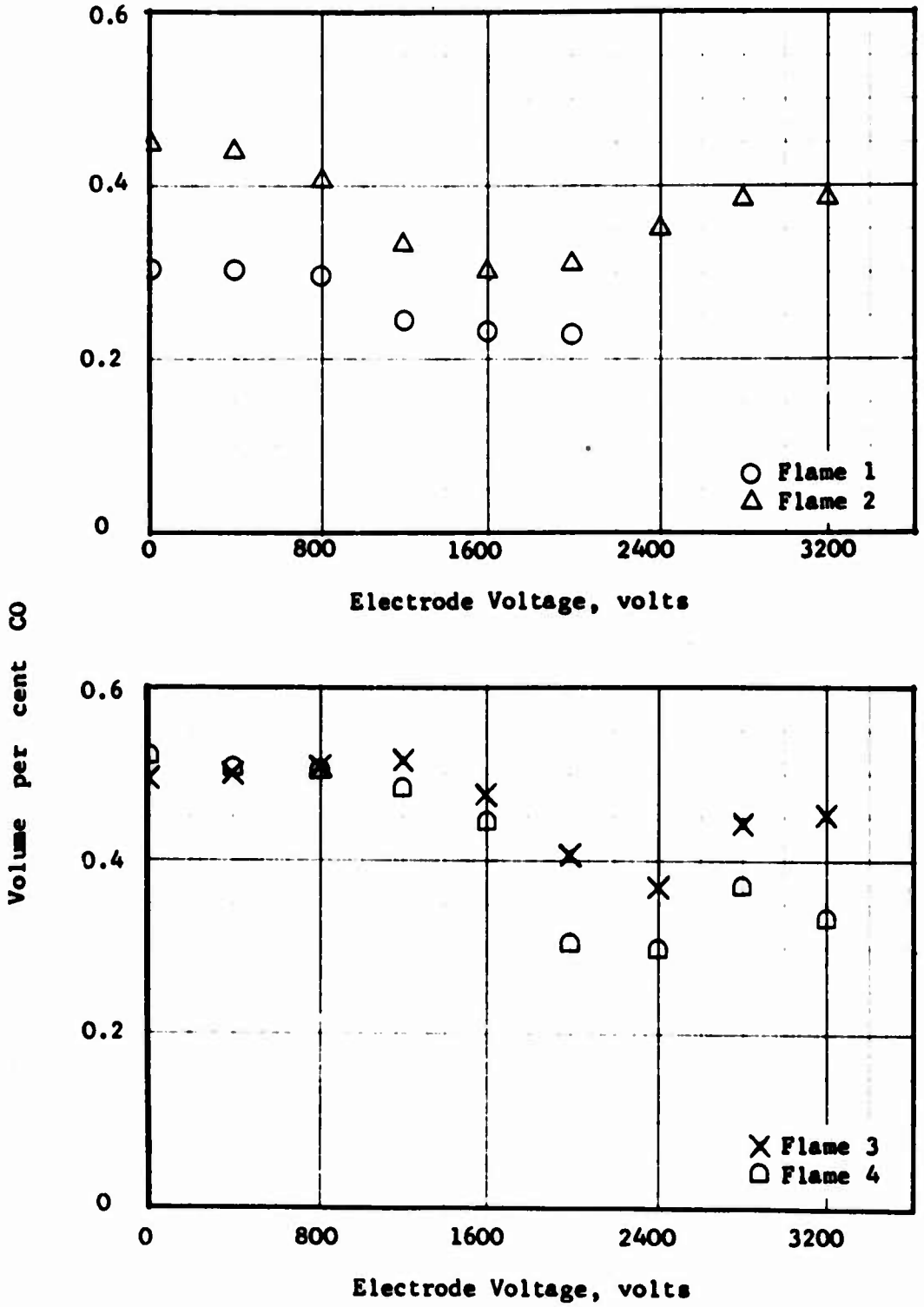

Fig. 43 Volume per cent CO in the exhaust gases

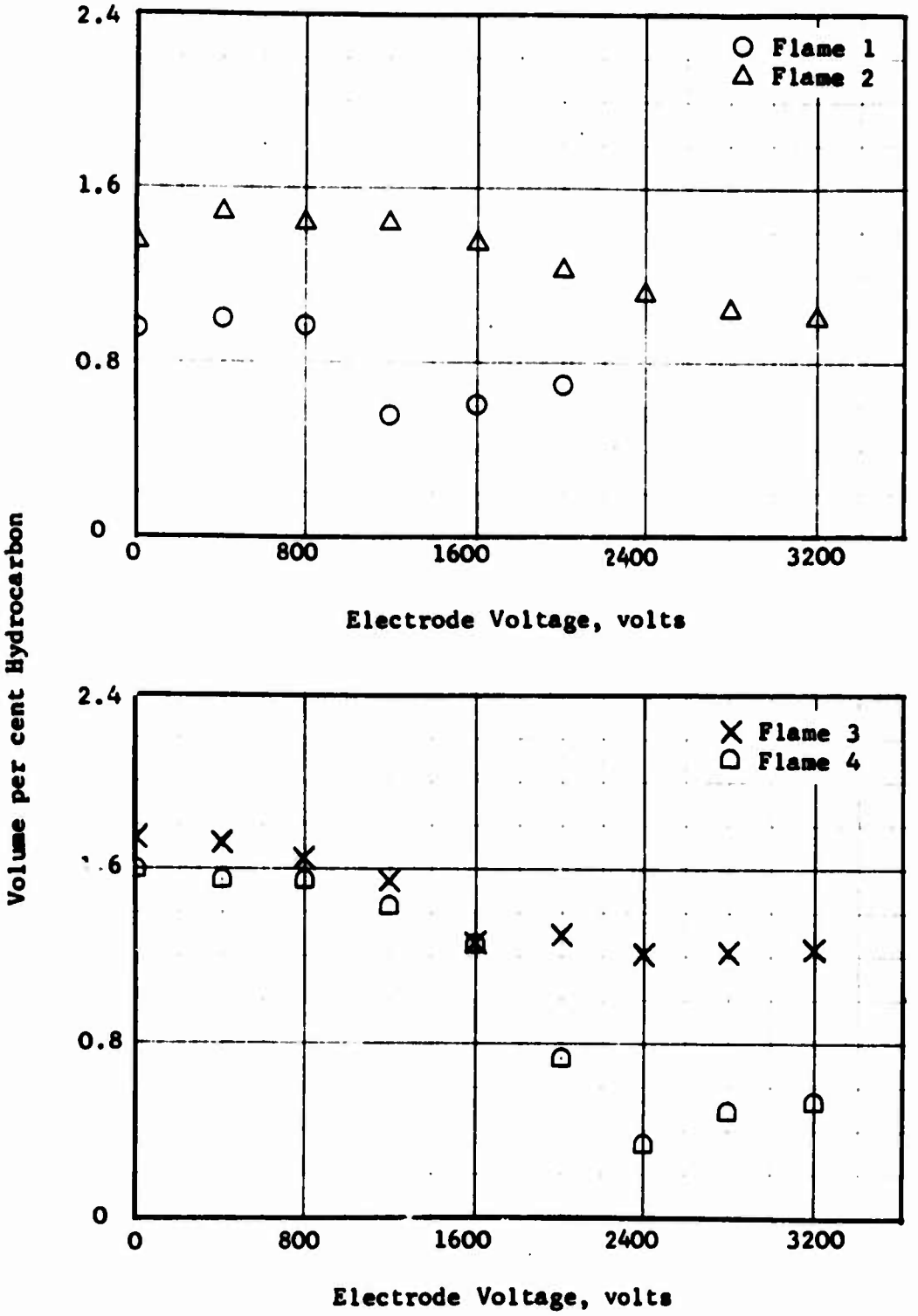

Fig. 44 Volume per cent hydrocarbon in the exhaust gases

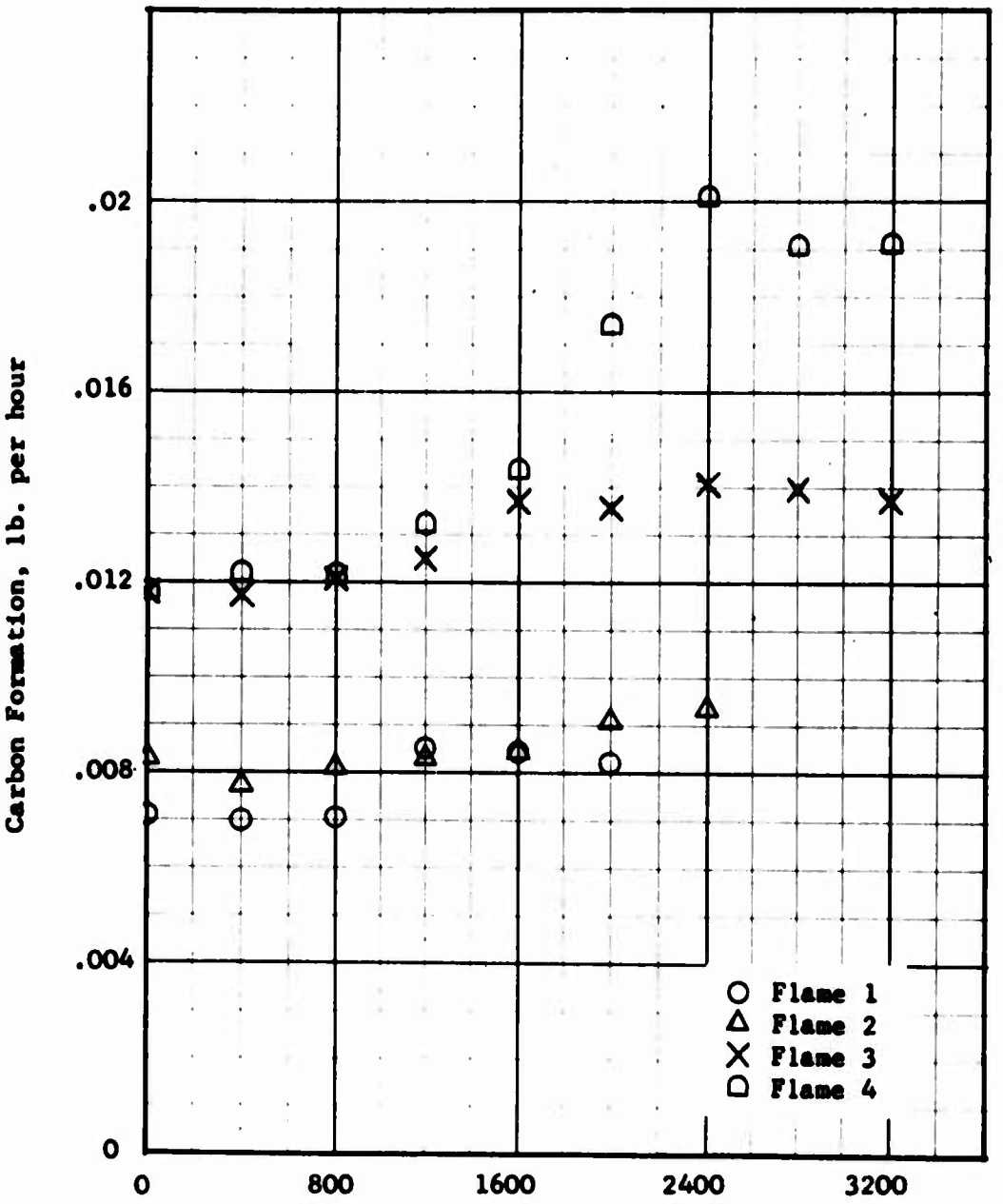

Fig. 45 Carbon formation versus electrode voltage

of electrode voltage. The carbon balance indicates that solid carbon is formed at zero voltage, and that the amount increases with increasing voltage. The fact that there is gas borne solid carbon is also supported by experimental observations; both the gas sample filter and the screen at the exit plane of the chamber were found to collect carbon. The interior walls of the chamber, although becoming black after a time of operation, did not cintinually build up a deposit of carbon. It appears that the following events take place: propane, which normally at zero voltage would escape unburnt from the chamber, is caused to pyrolyse and form free carbon as a result of electrically induced mixing within the chamber. This free carbon then mostly escapes from the chamber, because neither the CO nor the CO_2 concentration shows an increase with voltage.

CHAPTER 10

EFFECT OF THE FIELD ON THE HEAT TRANSFER RATE

10.1 EXPERIMENTAL PROCEDURE

Although the great majority of flames used in industry have as their purpose the supply of heat to be beneficially used in some process, the general subject of flame heat transfer historically has not received a great deal of emphasis from either flame researchers or engineers. The organization of the International Flame Research Foundation (44) and such works as Thring's (45) were therefore welcomed by workers in the subject. More recently other works (e.g., 46, 47, 48) concerned with heat transfer between flames and enclosing or adjacent surfaces have appeared. In the area of special effects on flame heat transfer, sound waves have been investigated and found to be capable of significantly increasing heat transfer rates. Also, Payne and Weinberg (2) with premixed flames in a round tube showed that a radial electric field could increase the heat transfer rate up to a factor of two.

In the present investigation, heat transfer rates were determined by measuring the temperature rise and flow rate of coolant to the electrodes. The measurement system is shown in Fig. 46 and the photographs in Figs. 8 and 9. Each electrode segment, a one-inch-wide by one-half-inch thick by eight-inch-long brass bar, was drilled through longitudinally to form a 1/4-inch diameter oil passage; a twisted ribbon of aluminum was inserted into the hole to promote mixing and the ends were plugged. Access holes for the inlet and outlet flow of oil were drilled through the side of the segment into which were cemented short nylon tubes which served as thermocouple sections and tubing fittings. The oil to each segment was supplied from a manifold containing a valve for each segment by which the flow rate could be regulated. After passing through the electrodes, the oil streams flowed in plastic tubing to a trough down which the oil flowed into a sump. When it was desired to measure the flow rate in any particular segment, the oil tube from that segment was manually diverted from the main oil trough into a trough that emptied into a 2000 ml graduated cylinder. The flow rate was then measured by a stopwatch.

The electrode segments when stacked up to form the anode and cathode were separated by a 1/8-inch-thick strip of asbestos which isolated each segment thermally. The stack of segments constituting either electrode were held in place by two threaded tension rods 1/8-inch in diameter encased in a 3/16-inch O.D. nylon tube, passing through a hole near each end of each segment. The segments were pulled together by tightening nuts on the ends of the tension rods. The anode and cathode assembly

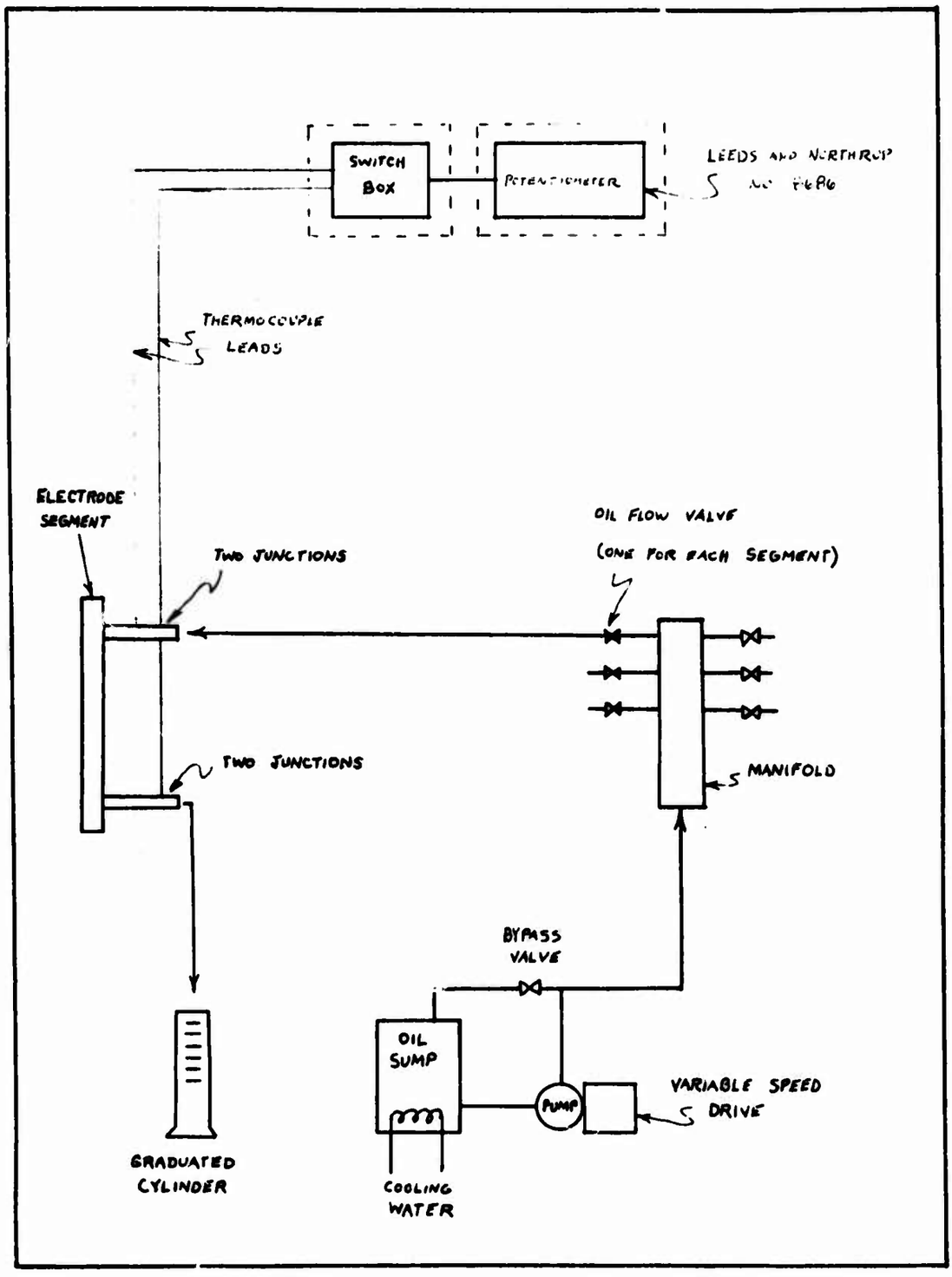

Fig. 46 Diagram of the heat transfer measurement system

were then squeezed together against the edge walls of the combustion chamber by four plastic clamps on each side.

Two junctions of copper-constantan thermocouples were placed directly in the inlet oil stream and two junctions in the outlet oil stream; the thermal EMF which was measured represented the temperature rise of the oil stream as it passed through the electrode. Each segment also had a thermocouple bead imbedded 1/4-inch deep into itself and cemented in place. All thermocouple leads went to two switch boxes which were connected to the measuring potentiometer capable of reading to within 0.0025 millivolts, or about 0.06 degrees F of the oil temperature rise. Thermocouple wires from the anode were at high voltage and so were encased in polyethylene tubing; the anode thermocouple switch box and the potentiometer were electrically insulated and provided with insulating extended stems for switching.

The experimental procedure for measuring the heat transfer rates was as follows: When the desired flame was obtained in the chamber, with no voltage, the temperature of each electrode segment was read. It was desired to have the temperature of each segment differ from its neighbor by less than about 10°F to keep the heat transfer between segments below a small value. The temperatures of the segments were regulated by adjusting the oil flow to the individual segments. It was also desired to maintain the temperature level of the electrodes at less than about 50°F above ambient to keep the external heat loss from becoming appreciable. The oil pump speed, bypass valve, or individual oil flow rates were adjusted to satisfy this temperature condition. When the observed temperatures no longer varied with time, steady state was assumed, and temperatures were recorded for each electrode segment. A voltage was then applied to the anode, and the temperatures were measured again, etc.

The heat transfer to each segment was determined by the equation

$$Q = \rho(0.F.)\Delta TC_p \qquad (10.1)$$

where ΔT is the measured oil temperature rise in the segment, (0.F.) is the measured volumetric oil flow rate, and ρ and C_p are the density and specific heat of the General Electric 10C transformer oil coolant obtained from Table 9 below.

Table 9. Properties of Oil Coolant

Temperature, °F	Specific Gravity	Specific Heat BTU lbm^{-1} F^{-1}
70	0.884	0.443
100	--	0.459
120	0.866	--
140	--	0.481

The local heat transfer rate per unit area was found from

$$q = \frac{Q}{\text{area}} \qquad (10.2)$$

where the area is calculated from a segment height of one inch and a flame width of 5-7/8 inches and represents the area of a segment exposed to the flame. The flames were found not to extend completely across the ideal width at all levels, but since the main study is relative effects of fields, the use of a constant width is not significant.

10.2 DISCUSSION OF DATA

The first task was a determination of the heat transfer distribution along the anode and cathode for no applied voltage, the results of which are shown in Figs. 47 and 48 for the four flames. Several statements can be made regarding the results; first, the general trend of the heat transfer distribution is similar for all the flames. Second, the heat transfer to the anode experiences a maximum at or near the base of the flame and decreases upward. This is a consequence of the flame being nearer the anode at the base and moving to a more central position in the chamber at higher levels of the flame. The trends also indicate that radiation is secondary to convection. Flame 1 which is nonluminous and therefore would have a relatively low emissivity has nearly the same heat transfer rates and distribution as flames 2 and 3 which are luminous. Also, the anode is seen to have a much higher heat transfer rate at lower parts of the flame than the cathode. This would not be the case if the idealized flame sheet had a significant radiation, since only a small fraction of the radiation would be absorbed by the gas layers.

The electric field effect on the heat transfer is presented as a deviation from the heat transfer at no voltage and is a more accurate measurement since systematic experimental errors are cancelled out. Figures 49-60 show the ratio of q with voltage applied to q at no voltage, as a function of electrode voltage and for several positions above the base of the flame. The measured points correspond to the center of the electrode segments. Flame 3, the richest flame, yielded heat transfer measurements which frequently did not show the same trends as the other flames. It is thought that because of the greater carbon formation in this flame the effects of both electron attachment and deposition of carbon on the electrode surfaces could be influencing the heat transfer.

Since the electrically induced gas motion is such as to relocate the flame closer to the cathode and further from the anode, the expected effect is to decrease the anode heat transfer and increase the cathode heat transfer. Figures 49 and 55 show that near the base of the flame the anode heat transfer rate can be decreased up to an 85% reduction of the heat transfer at no voltage; and the cathode heat transfer can be

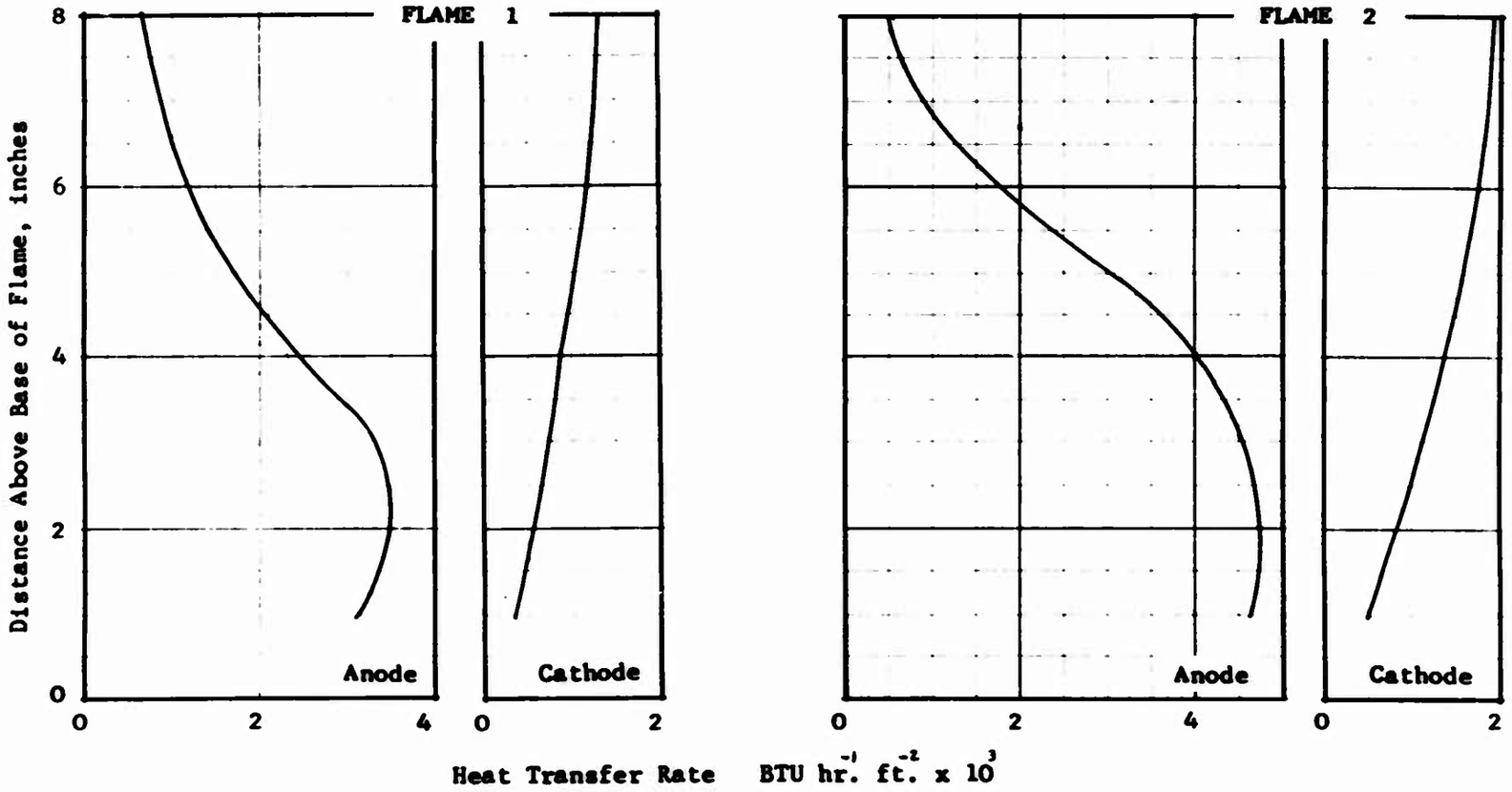

Fig. 47 Heat Transfer Distribution along Electrodes for No Field, Flames 1 and 2

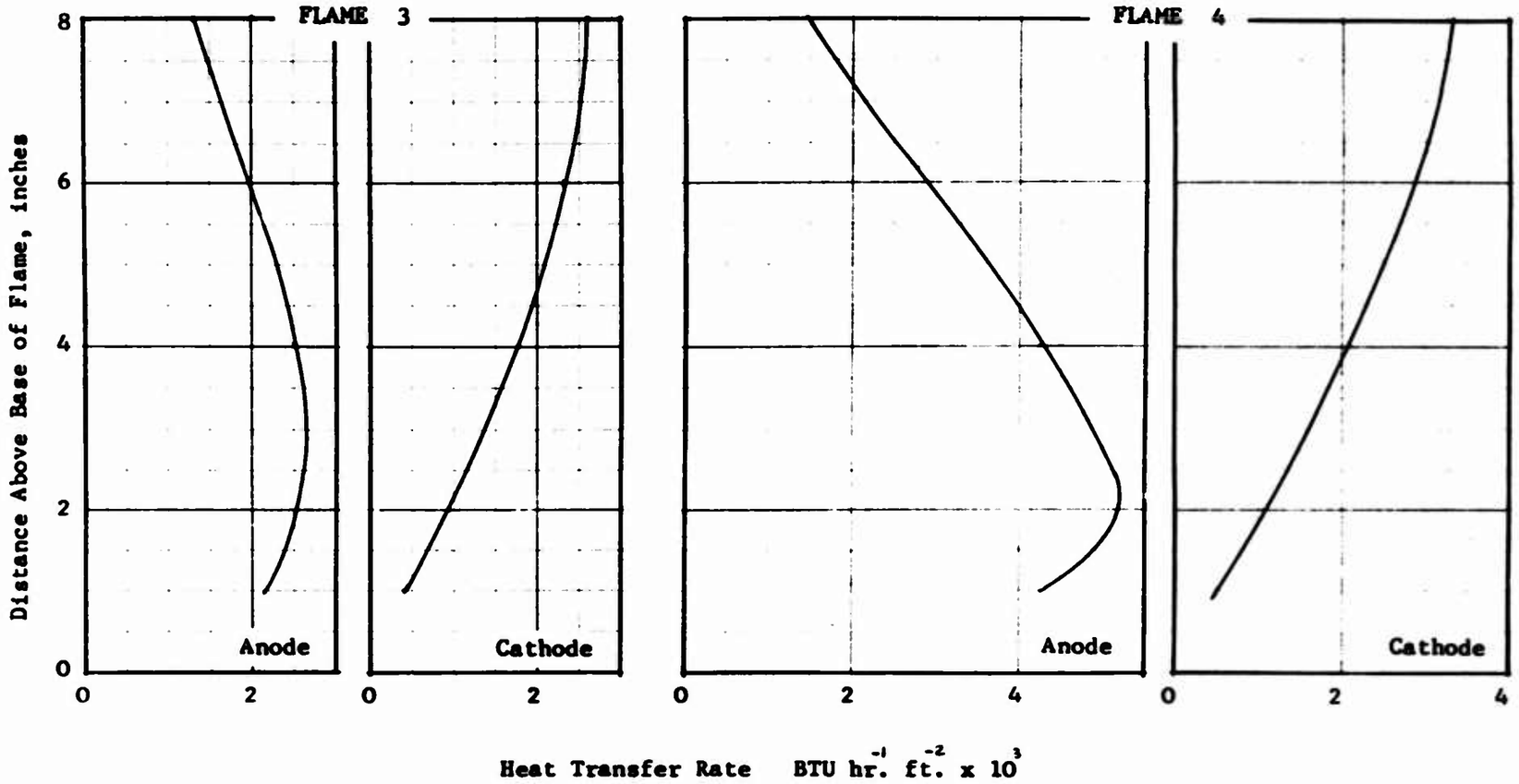

Fig. 48 Heat Transfer Distribution along Electrodes for No Field, Flames 3 and 4

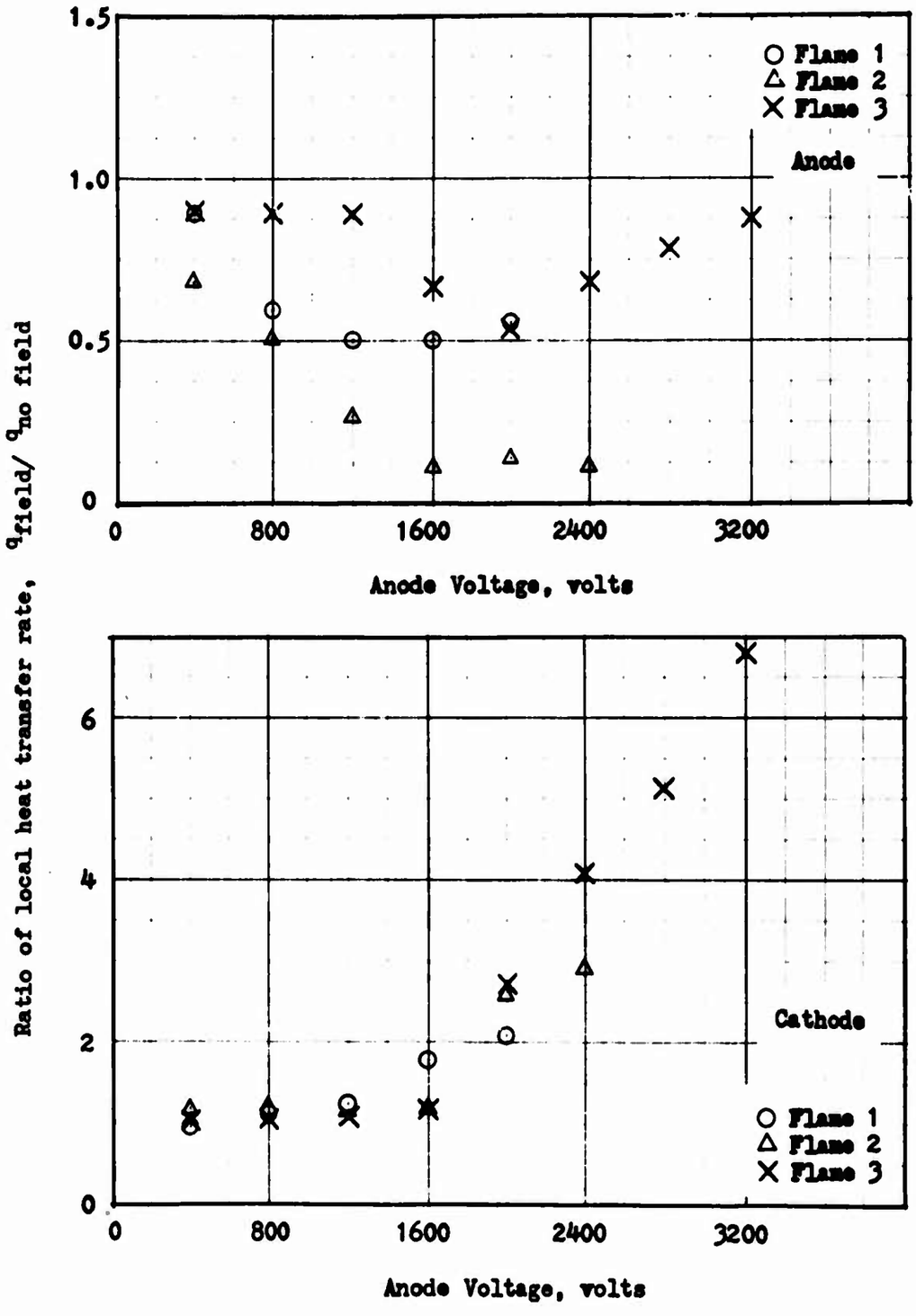

Fig. 49 The effect of the electric field on the heat transfer rate, y = 0.75 inch

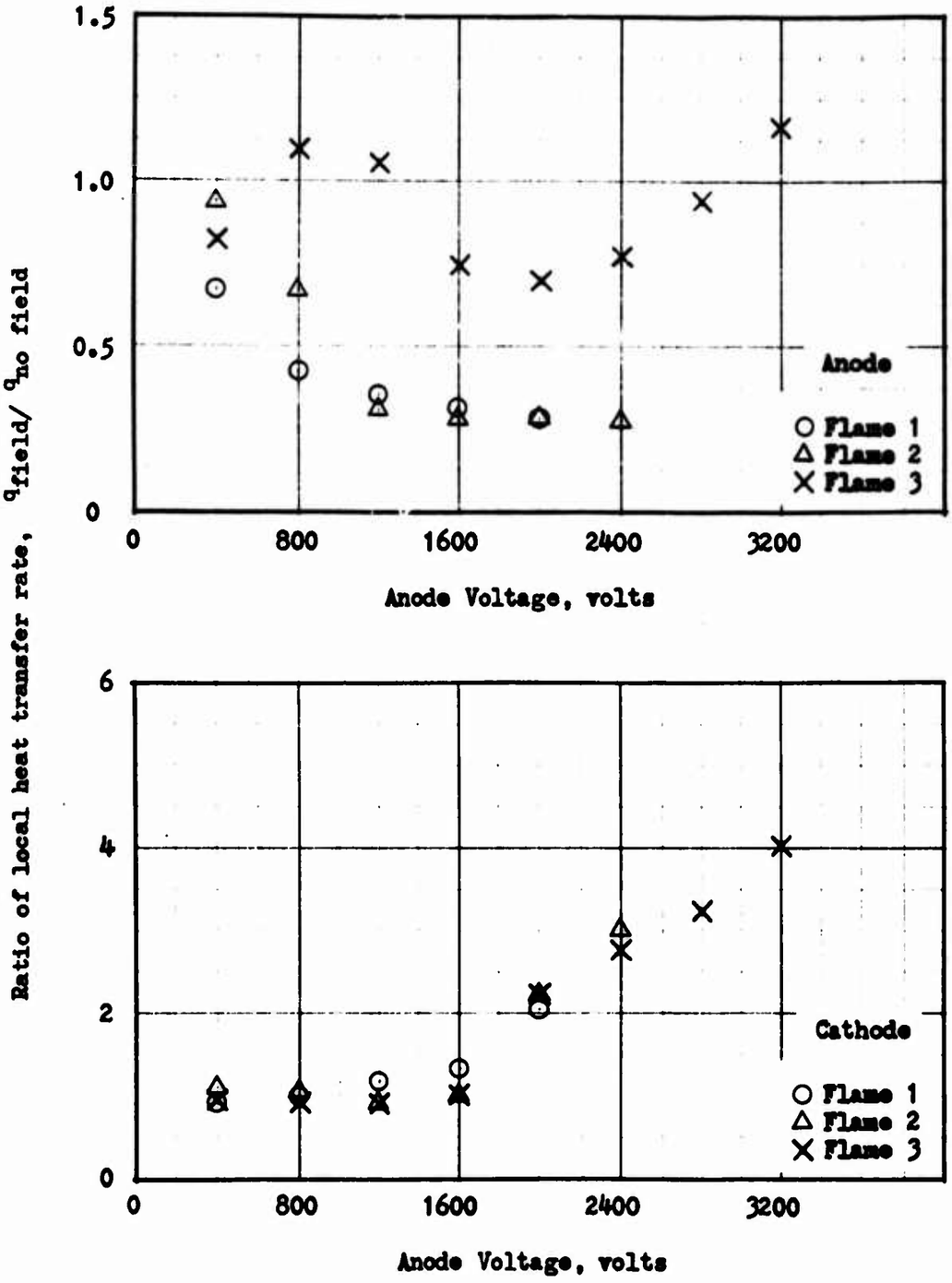

Fig. 50 The effect of the electric field on the heat transfer rate, y = 1.875 inches

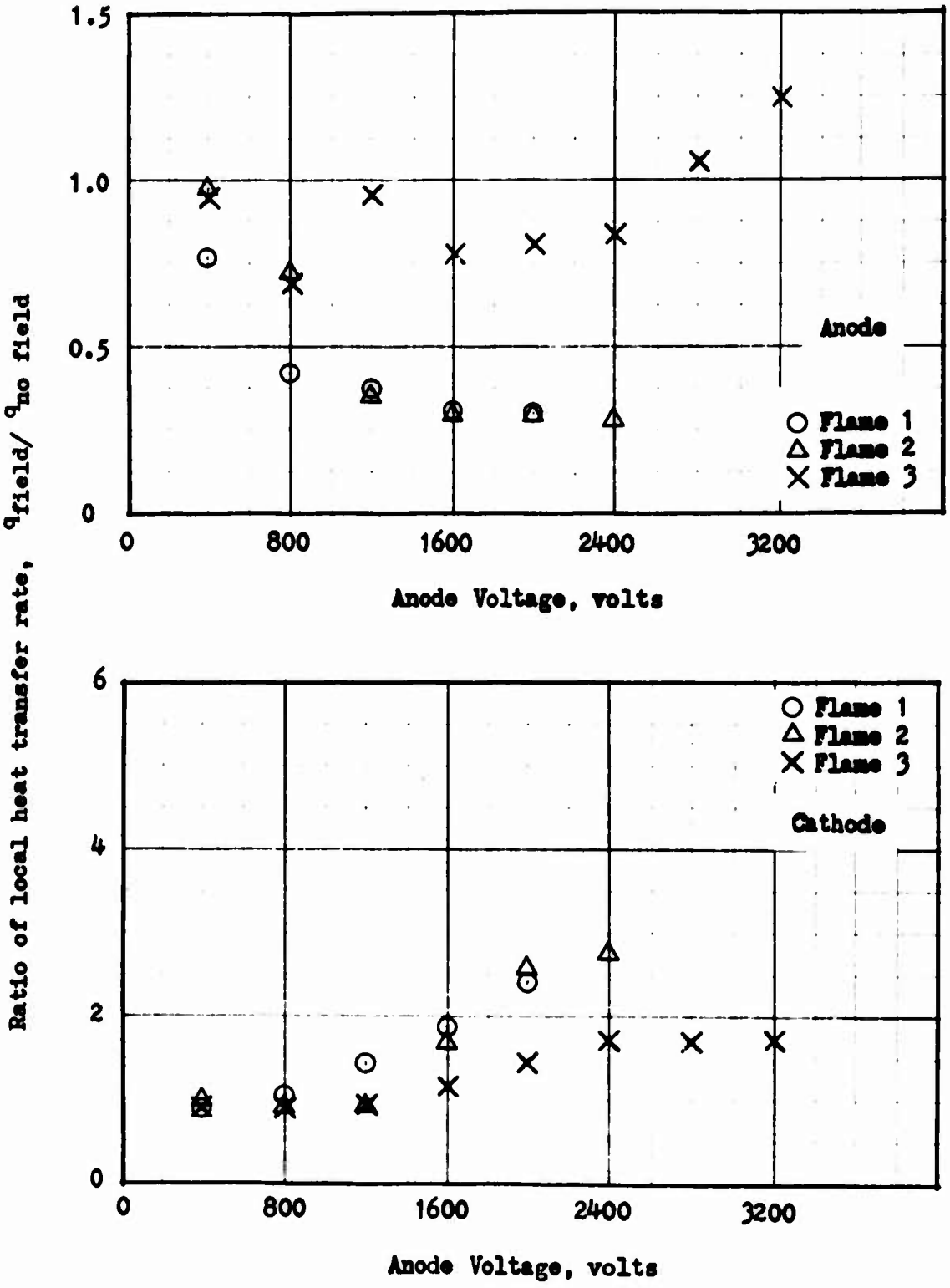

Fig. 51 The effect of the electric field on the heat transfer rate, y = 3.0 inches

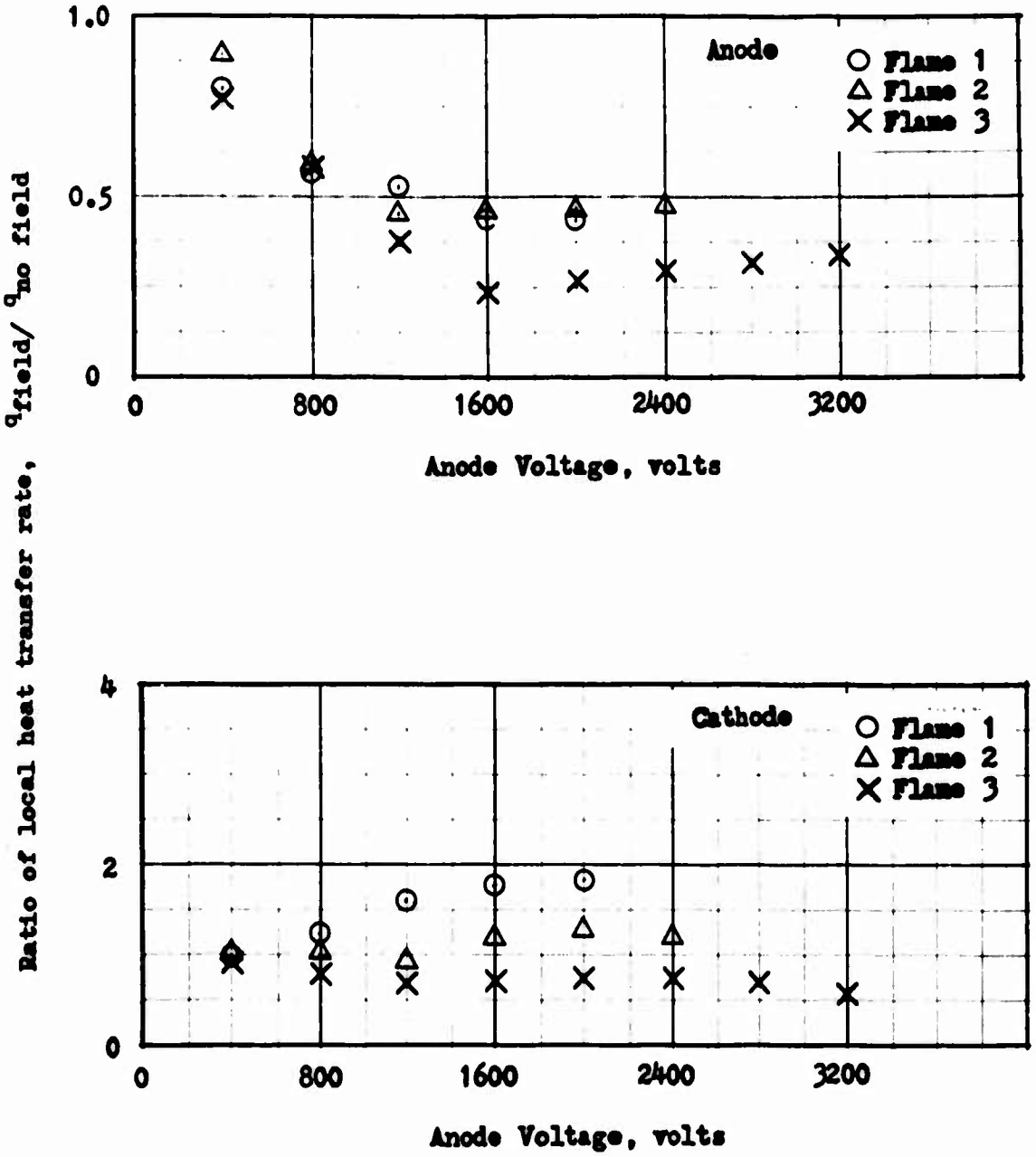

Fig. 52 The effect of the electric field on the heat transfer rate, y = 4.125 inches

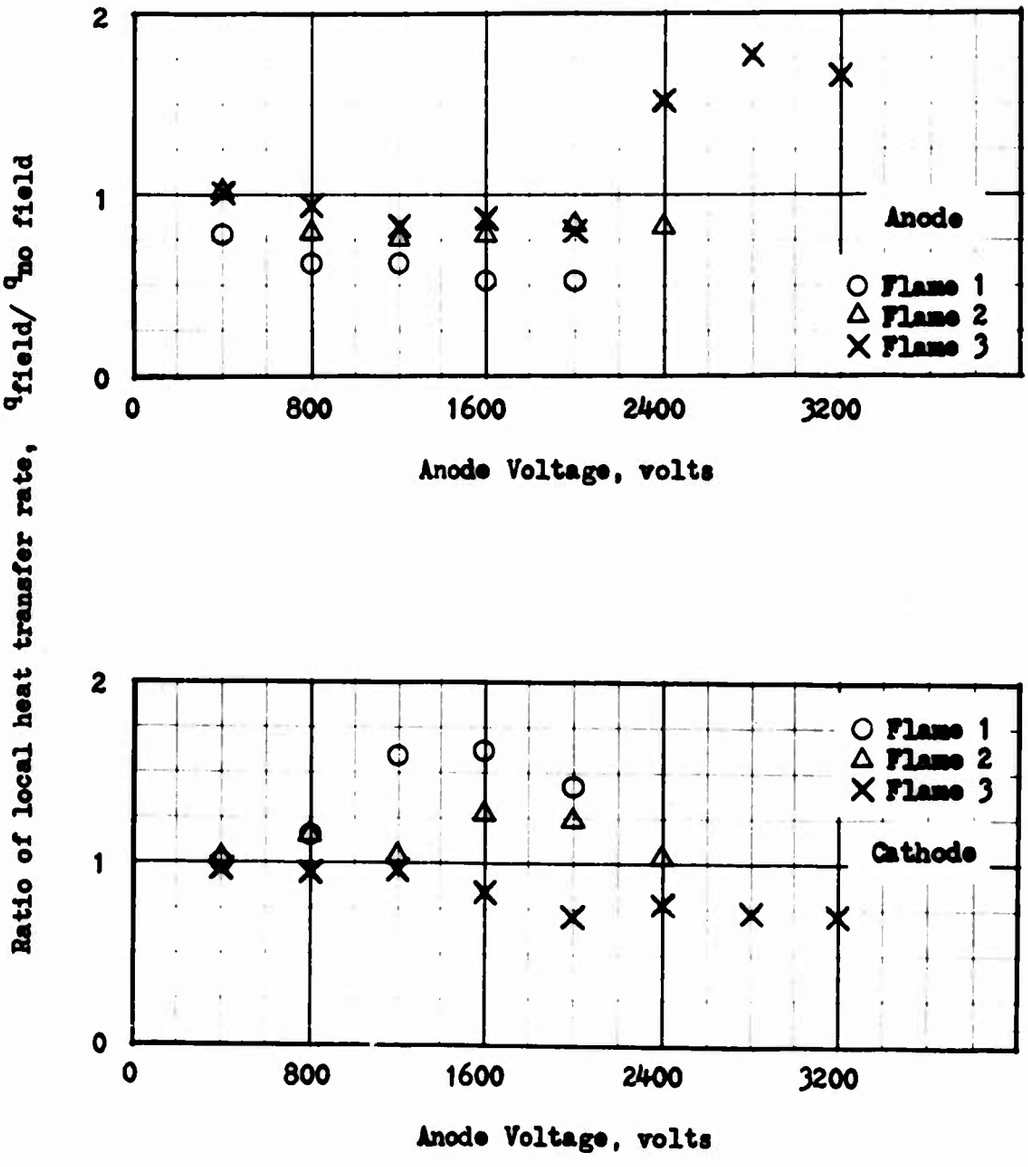

Fig. 53 The effect of the electric field on the heat transfer rate, y = 5.25 inches

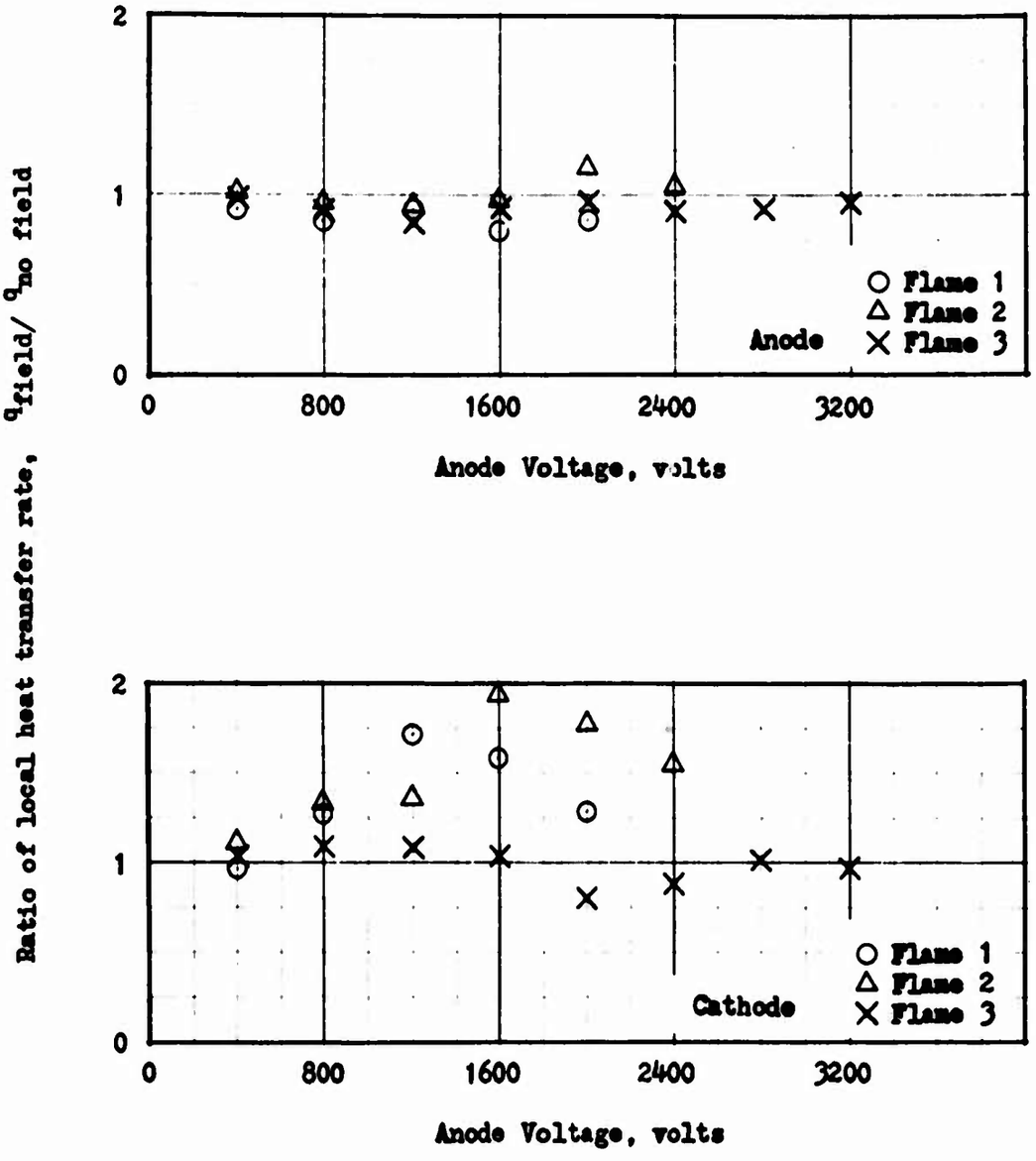

Fig. 54 The effect of the electric field on the heat transfer rate, y = 6.375 inches

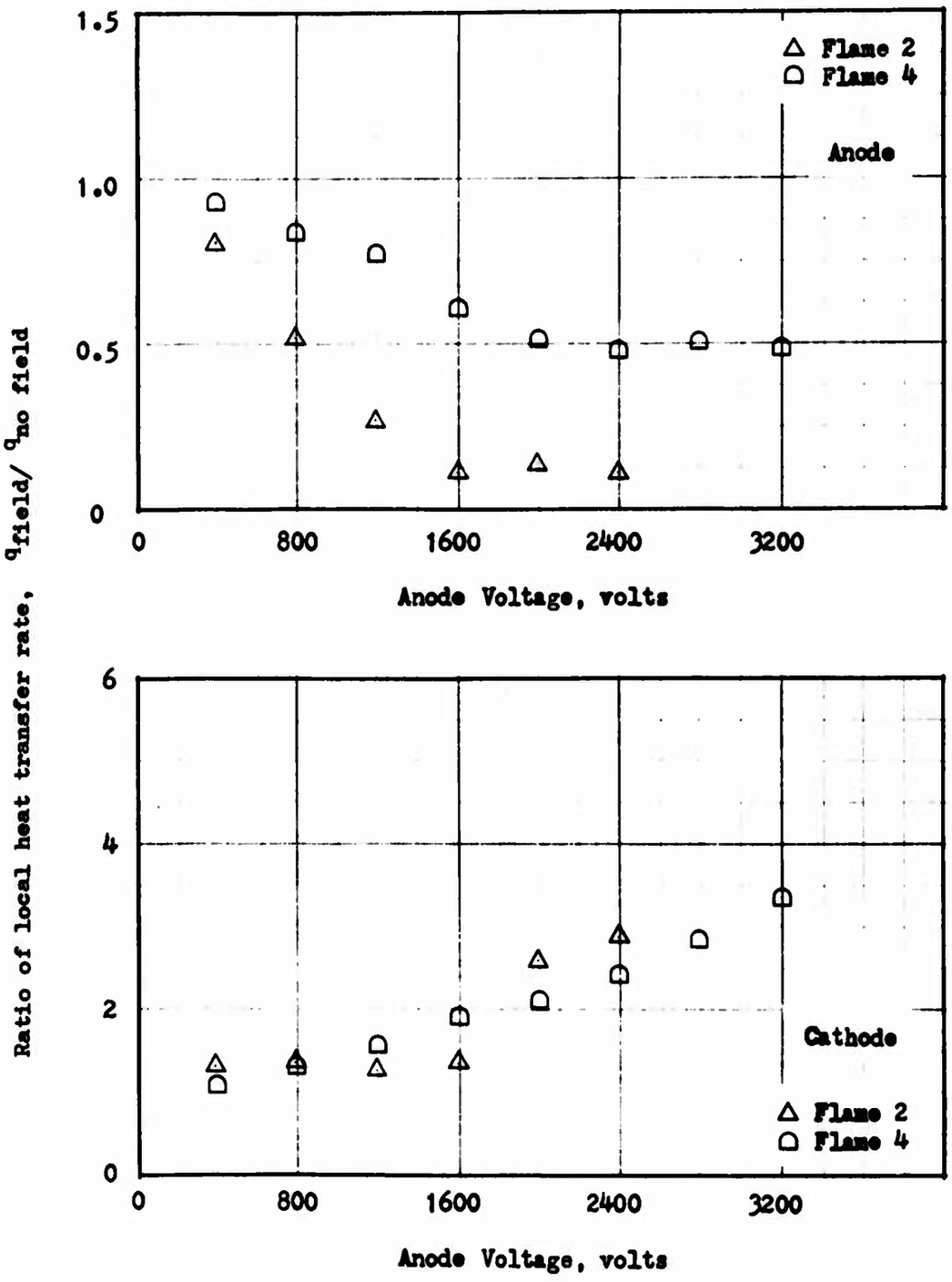

Fig. 55 The effect of the electric field on the heat transfer rate, y = 0.75 inches

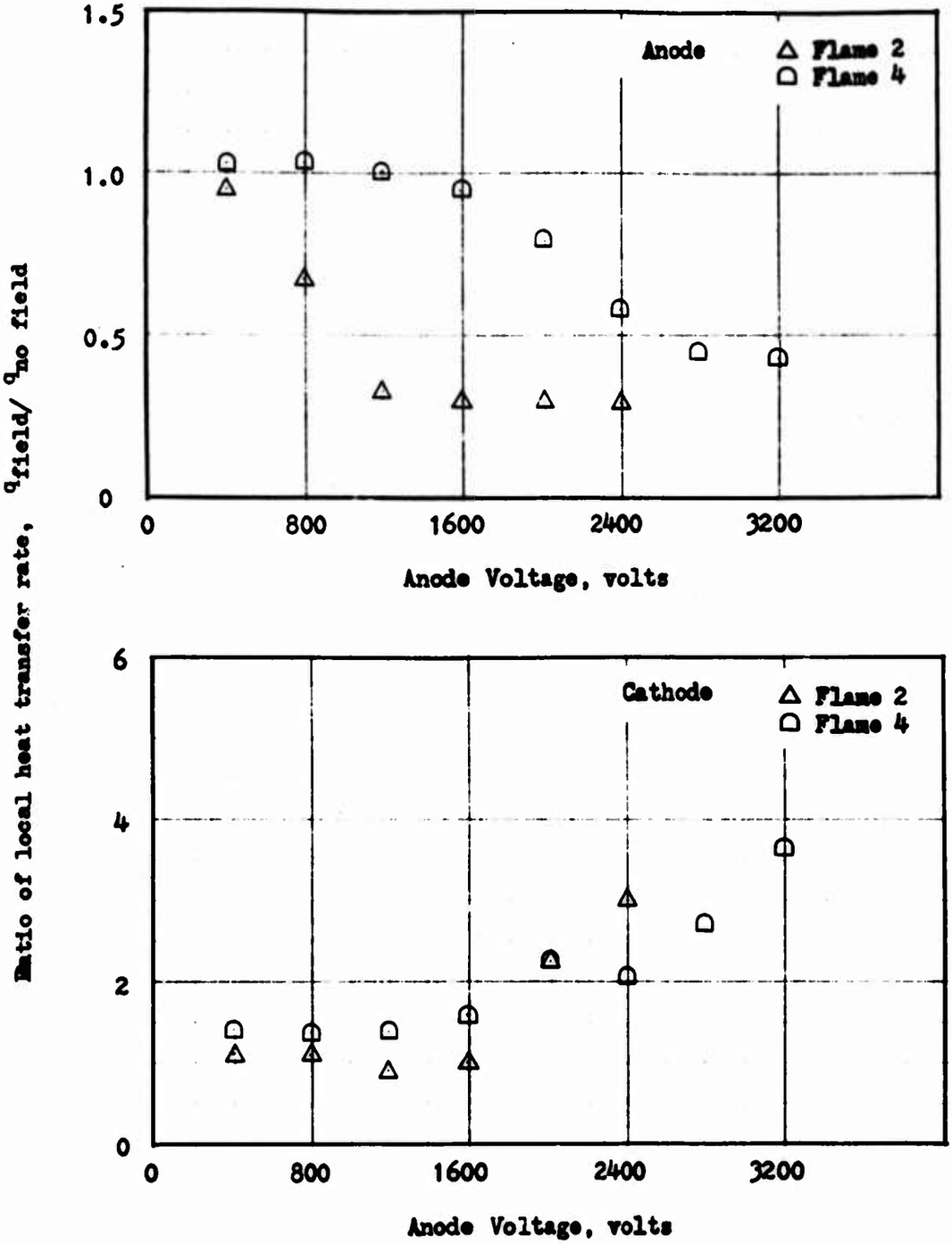

Fig. 56 The effect of the electric field on the heat transfer rate, y = 1.875 inches

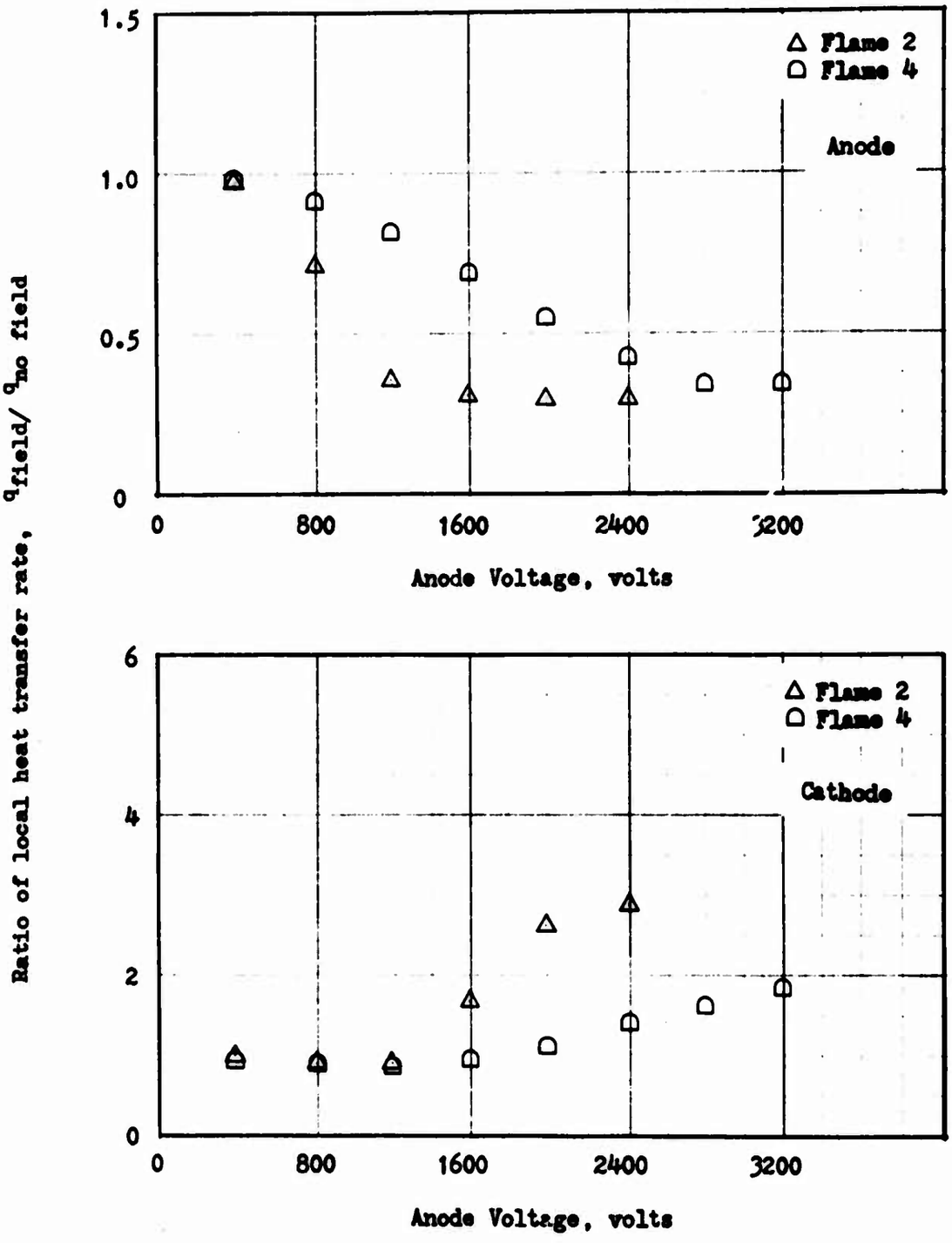

Fig. 57 The effect of the electric field on the heat transfer rate, y = 3.0 inches

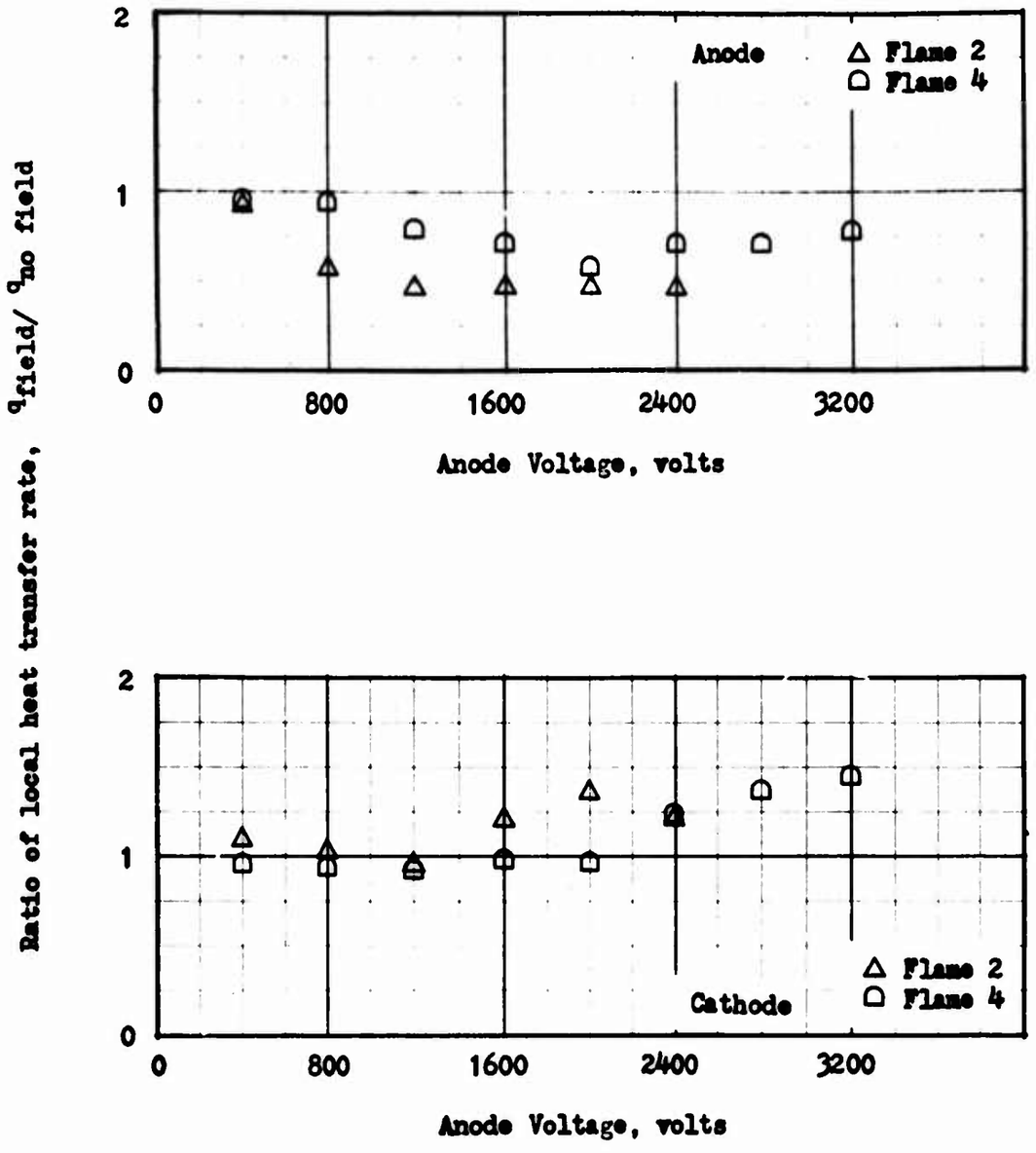

Fig. 58 The effect of the electric field on the heat transfer rate, y = 4.125 inches

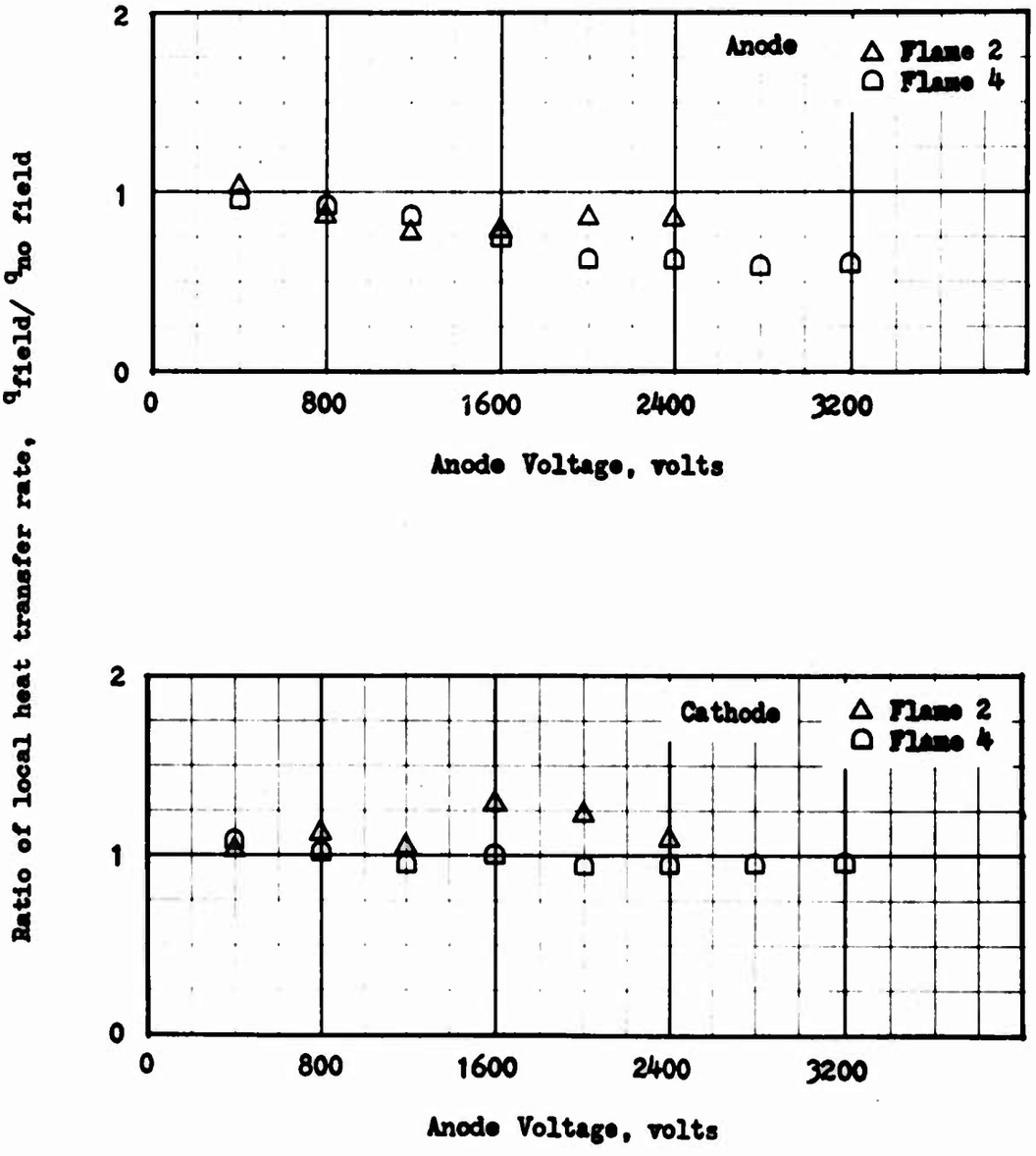

Fig. 59 The effect of the electric field on the heat transfer rate, y = 5.25 inches

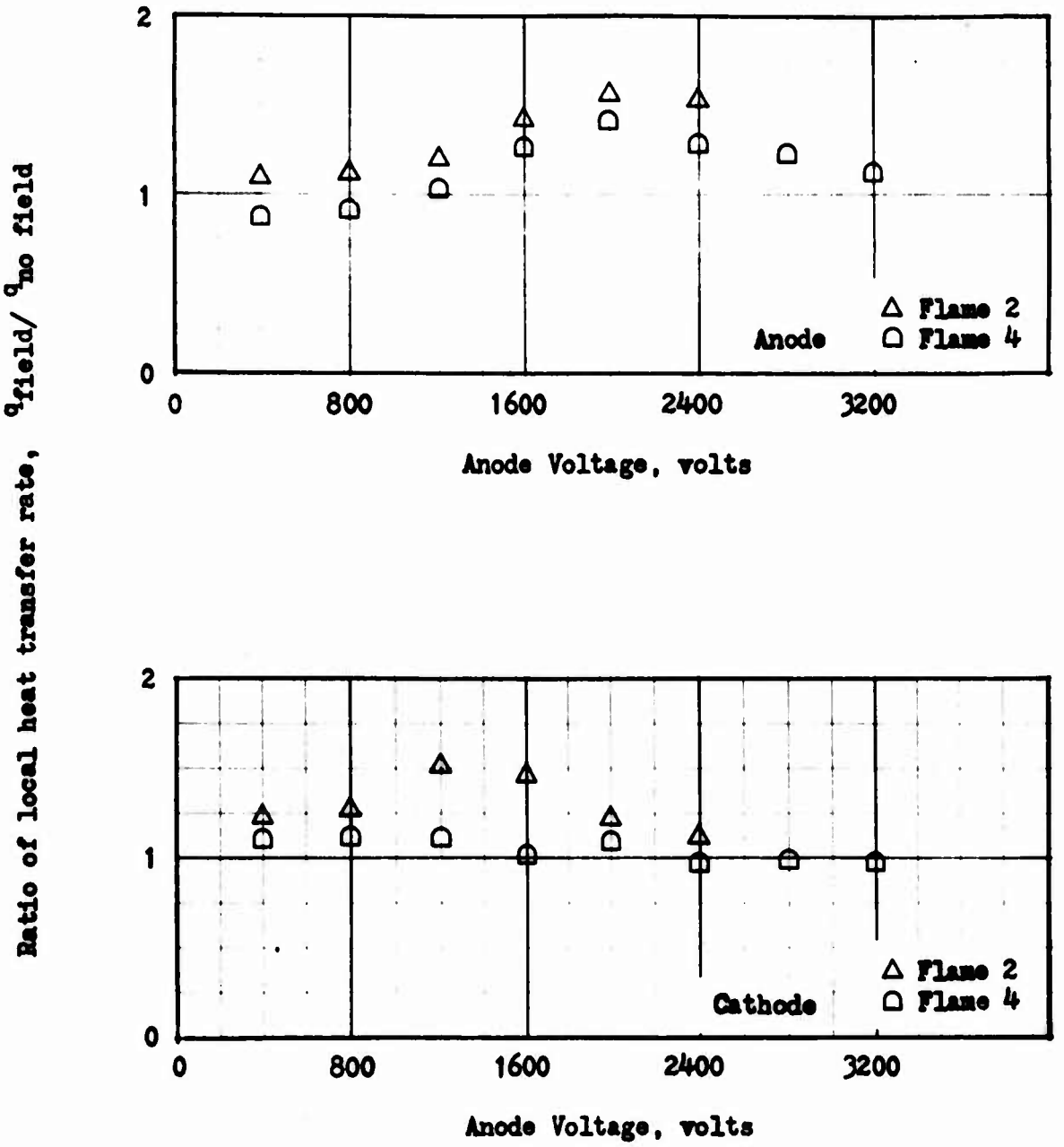

Fig. 60 The effect of the electric field on the heat transfer rate, y = 7.5 inches

increased up to a factor of six within the range of voltages applied. At progressively higher levels of the flames the electric effect on the heat transfer is reduced, as can be seen from the curves in Figs. 49-60.

A comparison of the results on flames 2 and 4, the same mixtures but different velocities, shows a trend which was observed before in Chapter 8 on electric measurements. For several curves the electric effect on the higher velocity flame 4 is seen to "lag" that of flame 2; i.e., a more rapid increase or decrease of heat transfer ratio occurs at a higher voltage for flame 4. This same effect was noticed in the current density curves, and it was also noted from oscilloscope traces that flame 4 began to flicker at a higher voltage than flame 2. Thus there is some evidence to support the statement that aside from induced flame movement, the onset of electrically induced flame flicker produces a first order effect on the heat transfer from the flame.

The data on Figs. 49-60 may be plotted to show the distribution of heat transfer ratio along the electrodes at constant voltage, as is shown in Figs. 61-64 for 1200 and 2000 volts. As mentioned earlier. both the decrease in anode heat transfer and the increase in cathode heat transfer diminishes at higher levels of the flame. The luminous flames also show some values of anode heat transfer ratio greater than one at upper parts of the flame. This trend indicates that electron attached carbon particles are active in reversing the flame movement existing at lower levels of the chamber.

While the maximum heat transfer effects are observed to occur at lower parts of the flame, and current densities are similarly a maximum there, the current level itself is not a direct source of increased transfer. Electrical energy input to the chamber is less than one percent of the heat transfer measured, and the energy associated with the the work functions and ionization potentials is insignificant.

At the highest voltage applied, the cathode heat transfer rate at the first segment, Figs. 49, 55, is increasing with voltage. At higher voltages it is therefore expected that even further increases in heat transfer would result. At these voltages the flame directly impinges on the cathode, and of course the model of a flat flame is no longer applicable. The flow situation more resembles stagnation flow, as evidenced by the flame photographs.

10.3 HEAT BALANCE

A heat balance was calculated for each flame at various electrode voltages and is shown in Figs. 65 and 66. The heat transfer to the anode and cathode represents the sum total of the indicated heat inputs from Eq. (10.1). The maximum decrease in total anode heat transfer was about 30 to 40% of the anode heat transfer at zero voltage. For flame 3 the maximum decrease occurred at 2000 volts, and at higher voltages the

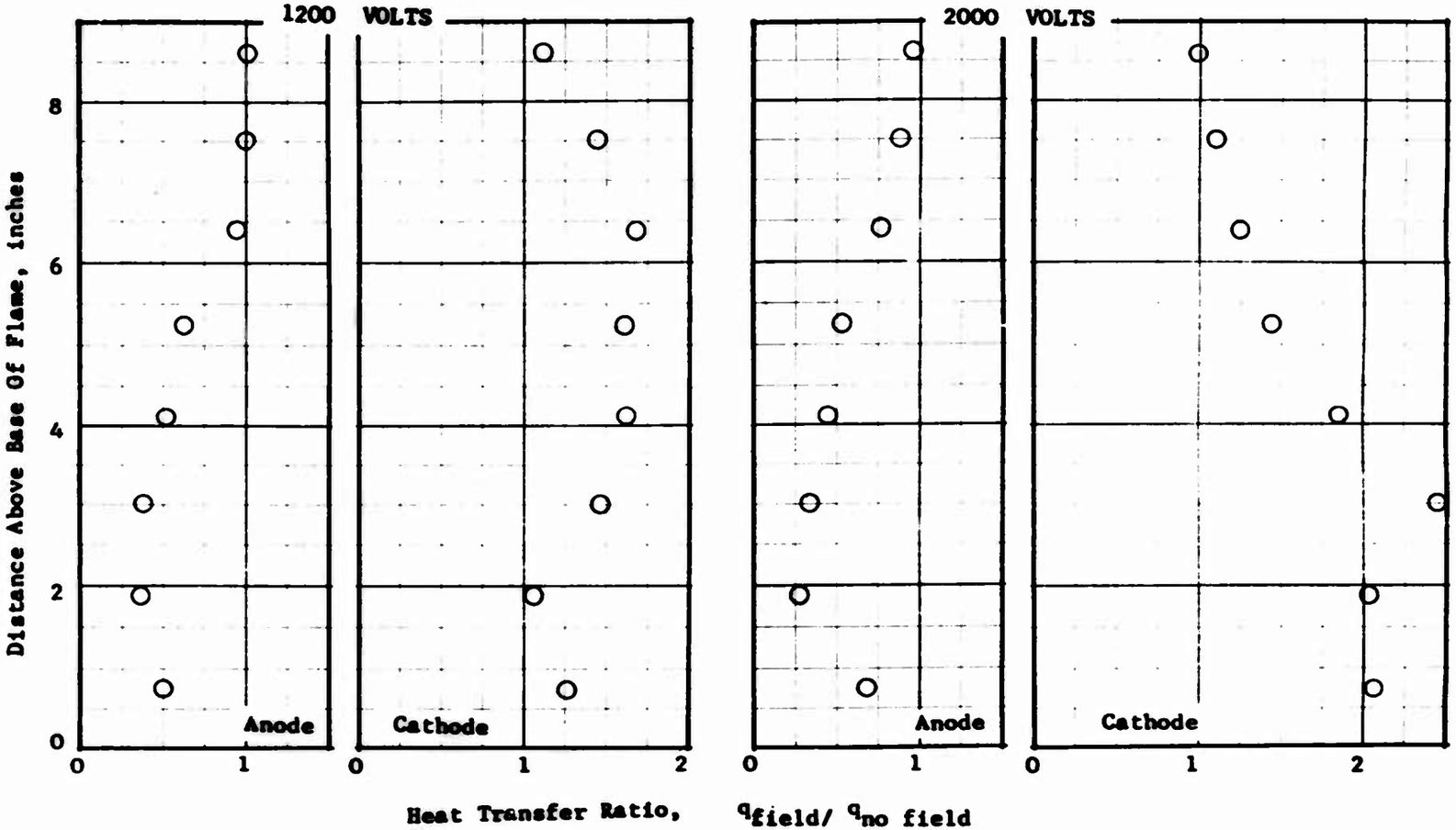

Fig. 61 Distribution of heat transfer ratio along electrodes, flame 1

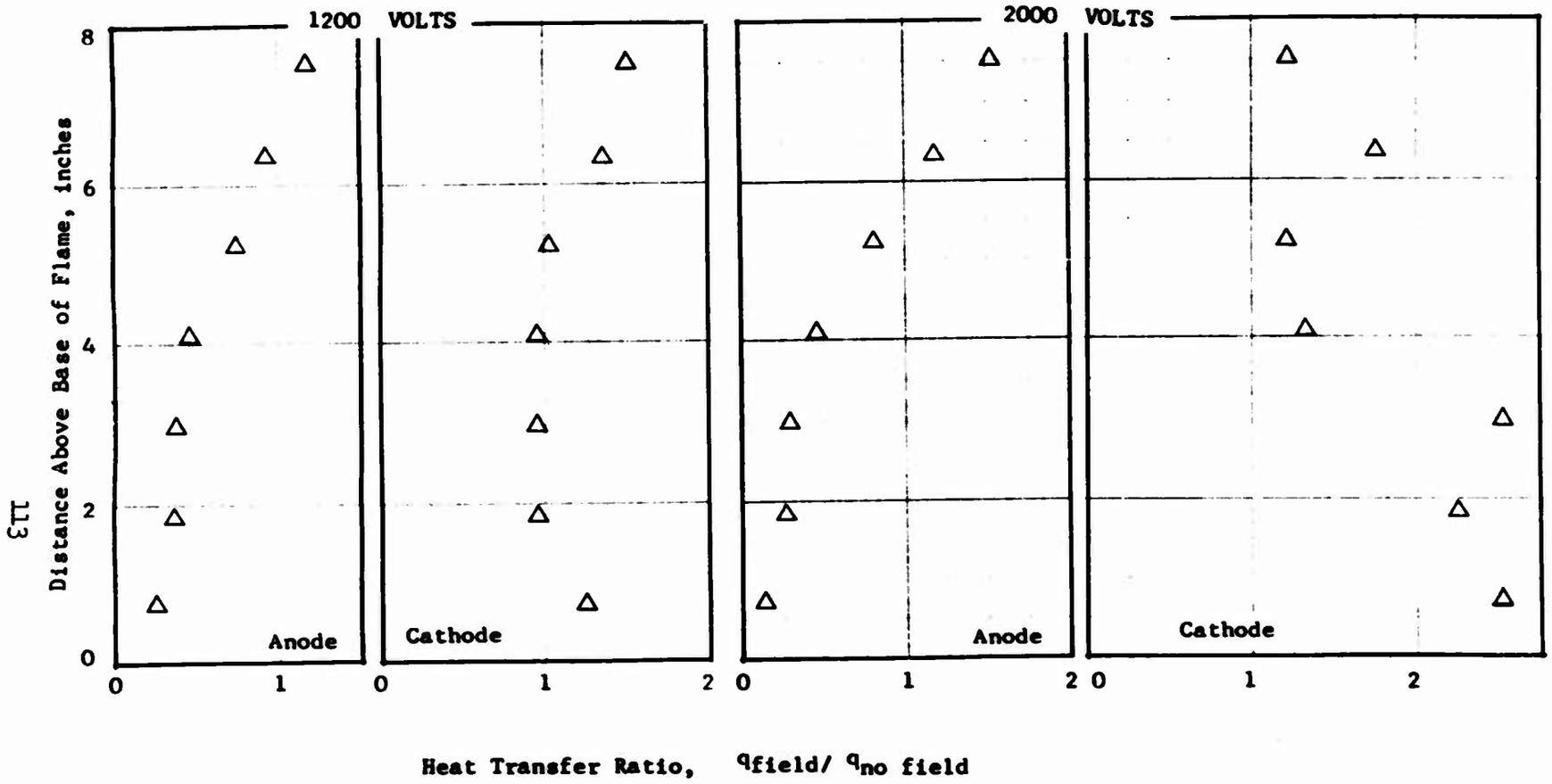

Fig. 62 Distribution of heat transfer ratio along electrodes, flame 2

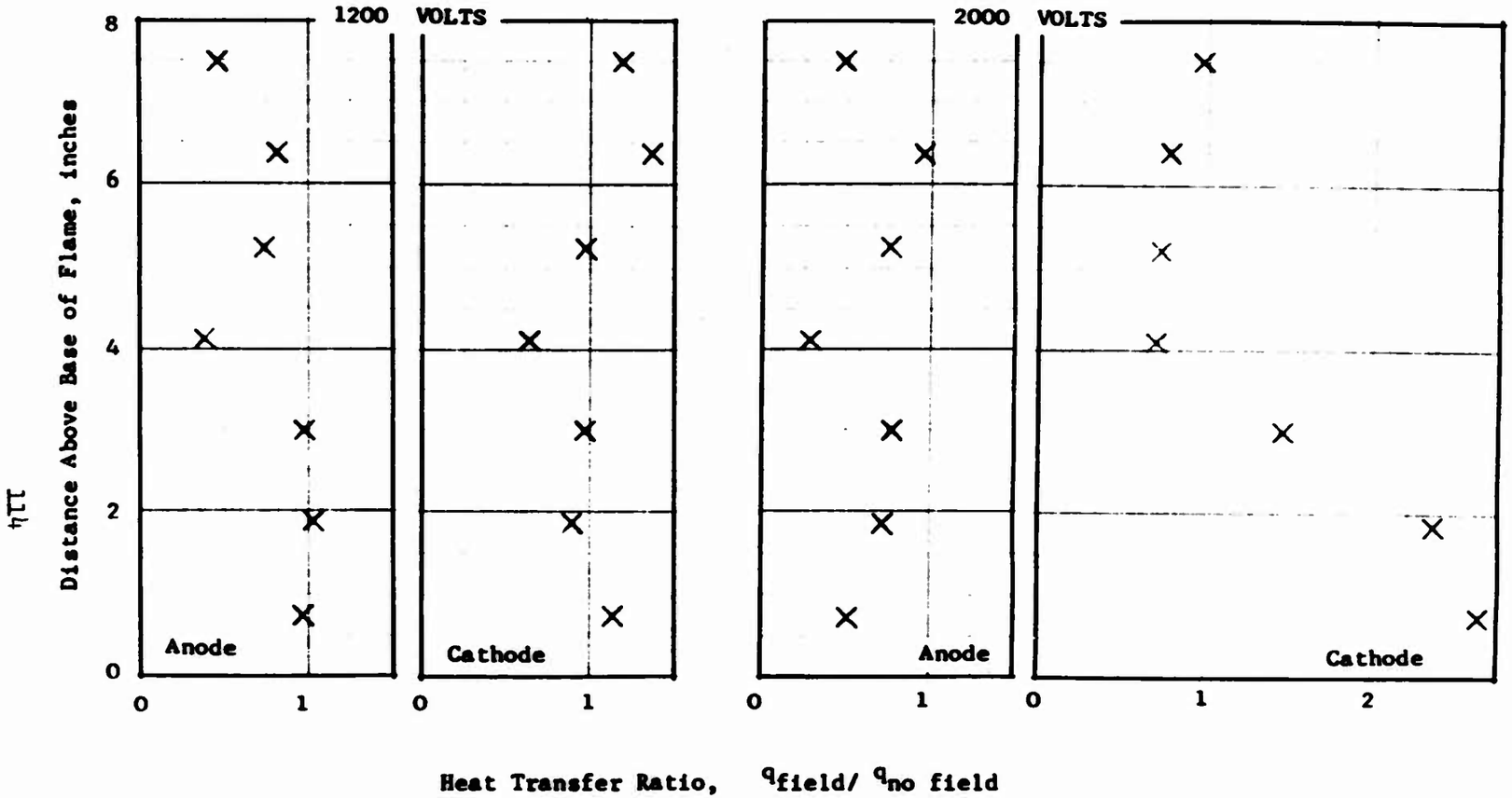

Fig. 63 Distribution of heat transfer ratio along electrodes, flame 3

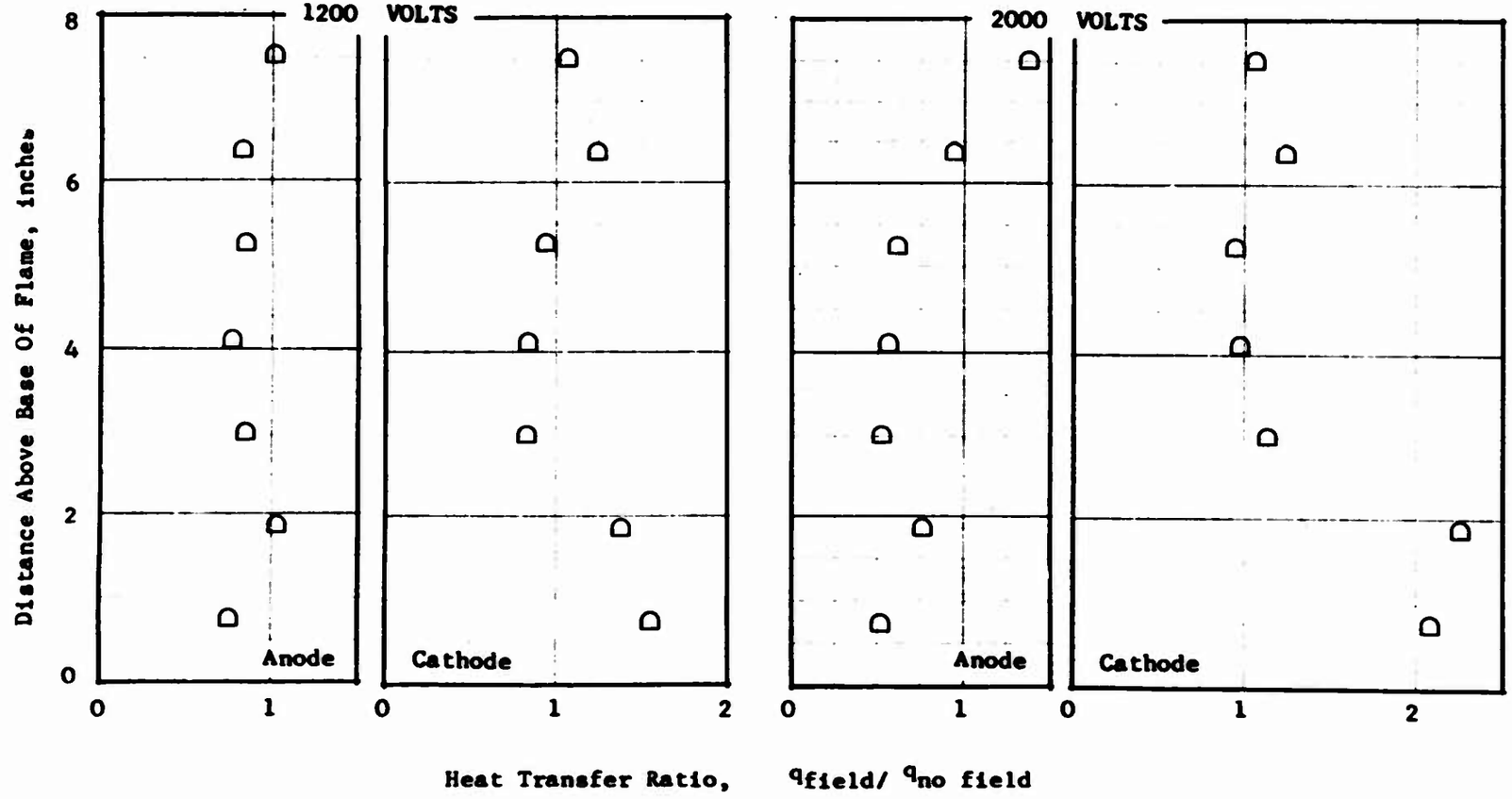

Fig. 64 Distribution of heat transfer ratio along electrodes, flame 4

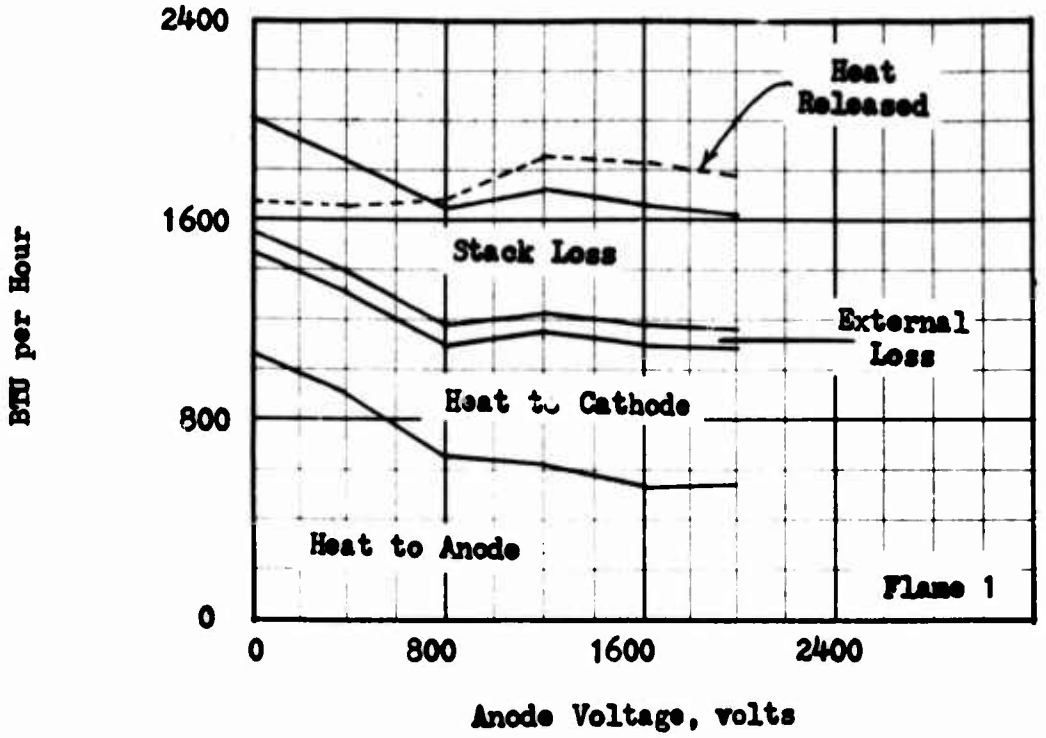

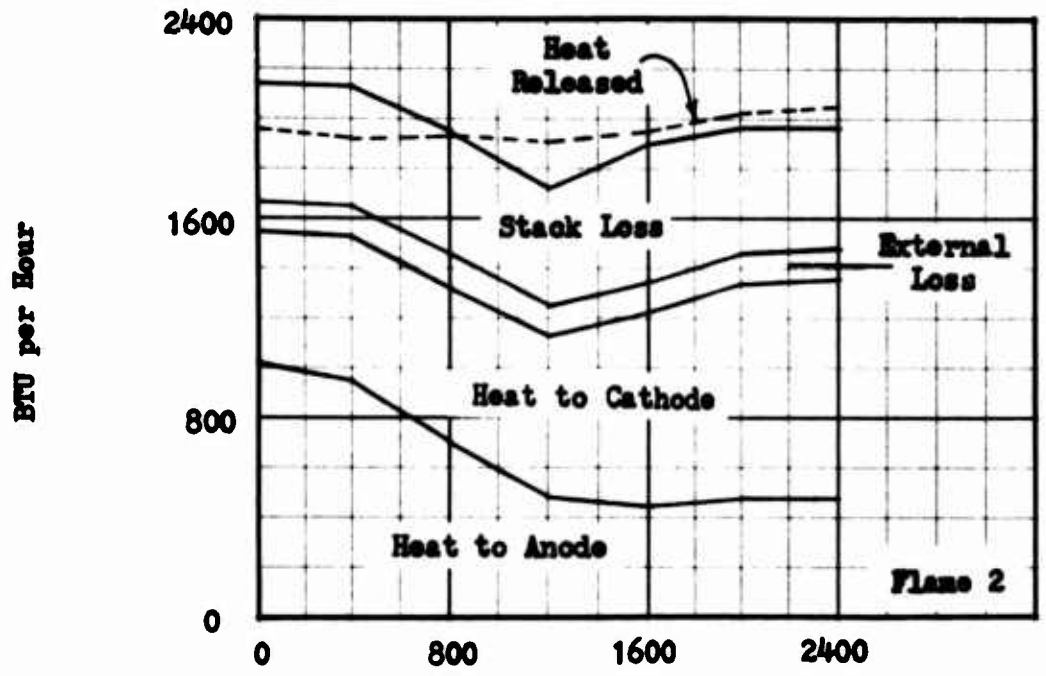

Fig. 65 Heat balance for flames 1 and 2

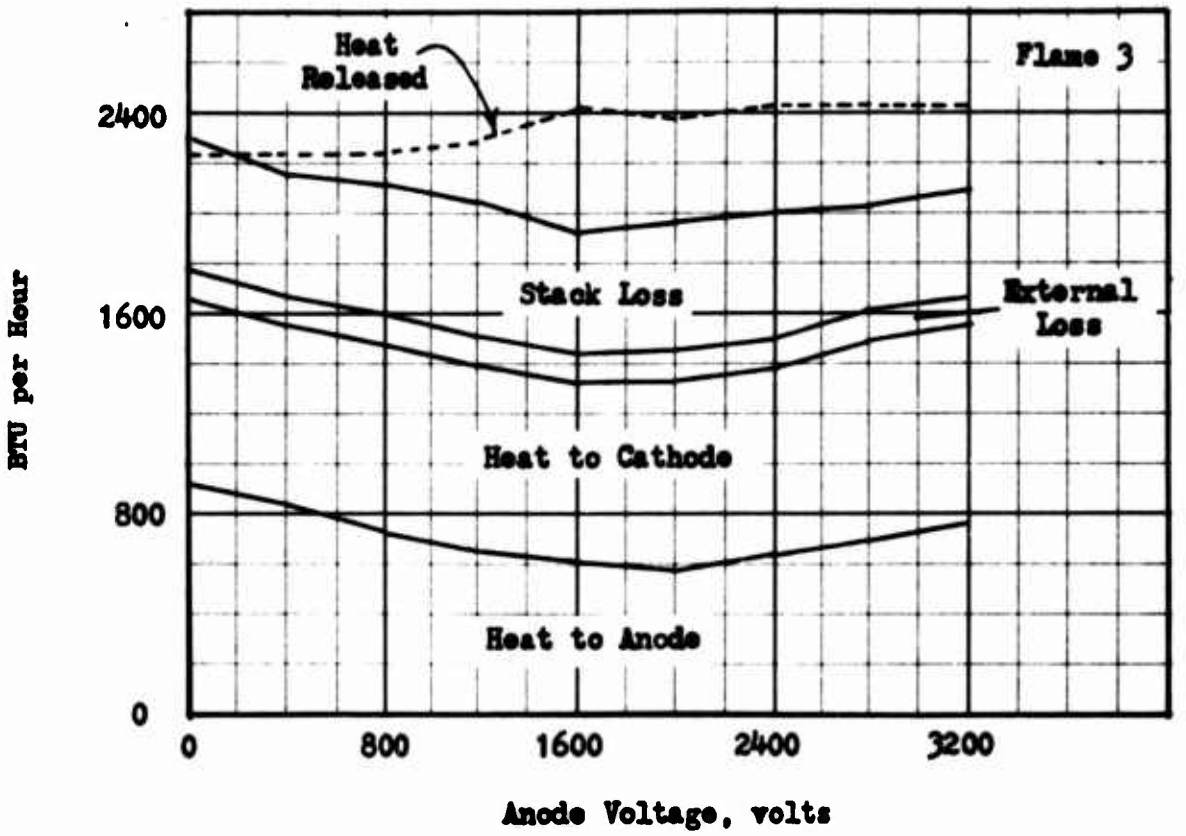

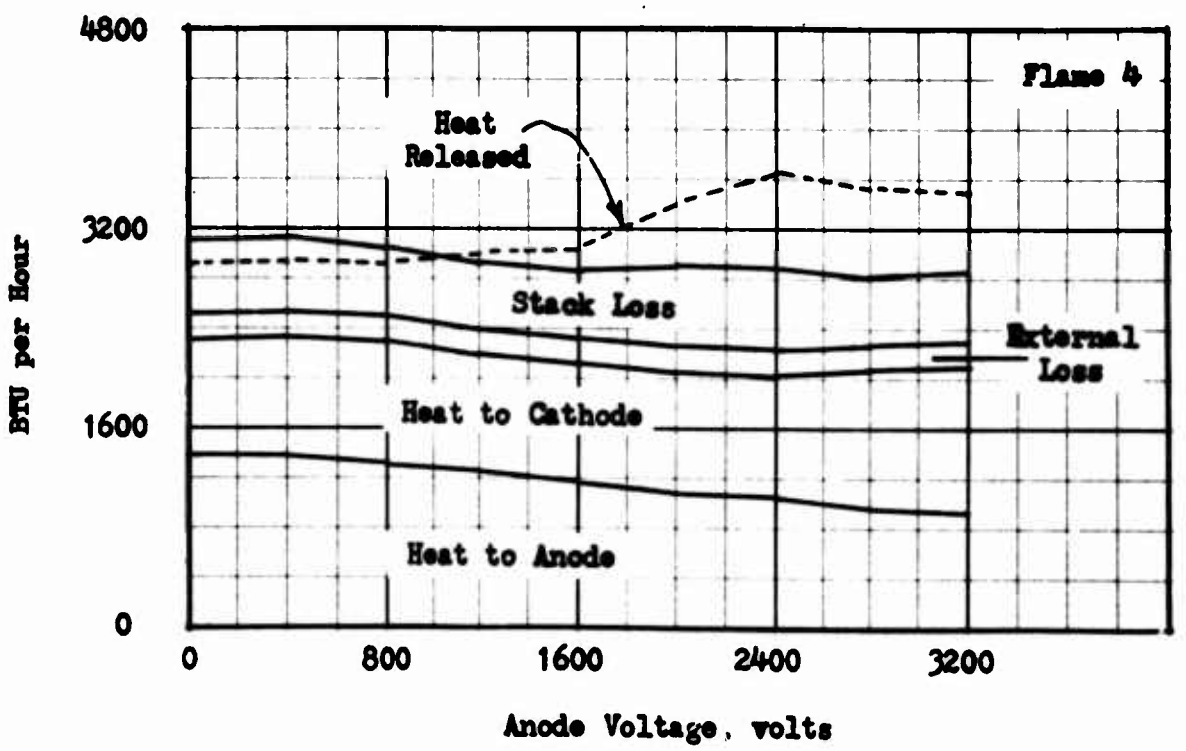

Fig. 66 Heat balance for flames 3 and 4

anode heat transfer increased, presumably because of the effect of carbon particles discussed earlier.

The maximum increase in the cathode heat transfer was greatest for flames 1 and 2, about 30 to 40%, but a much smaller change was found for flames 3 and 4. In every case the sum of the total anode and cathode heat transfer was reduced by the applied voltage.

Because each electrode segment was at a temperature higher than ambient, unavoidable heat loss occurred through convection and radiation. For each flame one average value of heat loss was determined. An average electrode temperature was first determined by taking the average segment temperature at zero volts, and at the maximum voltage applied. Radiation loss was figured by assuming perfect radiation from the average temperature to a sink at ambient temperature. The combustion chamber was located in a fume hood with an exhaust fan drawing air over the external surfaces at a measured velocity of one foot per second. The convection loss was estimated as the heat loss from a flat plate at the average temperature in a uniform stream of air at one foot per second at ambient temperature. The total external loss was small but not a negligible fraction of the total heat transfer.

The energy loss in the exhaust gases was calculated as follows: First the exhaust temperature was obtained from twelve iron-constantan thermocouples spaced over the flow cross section above the electrodes and connected in parallel to a millivolt recorder. The average exhaust temperature had a rapid fluctuation as indicated in the plot of the exhaust temperature versus voltage, Figs. 67 and 68. The composition of the exhaust gas was taken to be the measured quantities of CO, CO_2, unburnt hydrocarbon, and the input quantity of nitrogen. All the hydrogen in the burnt hydrocarbon was assumed to be oxidized to water and exhausted as vapor. Even though some liquid water was observed in the base of the chamber, the quantity was only a small portion of the total water formed. Solid carbon formed was assumed to be gas borne with the exhaust products. The stack loss represents the energy required to raise the exhaust products from the inlet temperature to the exhaust temperature, flowing at the measured or calculated flow rate. The stack loss was found to be relatively constant with voltage, and an appreciable part of the heat balance.

The chemical energy released by combustion was calculated from the lower heating value of the burnt propane and is shown as a dashed line in Figs. 65 and 66. These dashed lines should ideally coincide with the upper solid lines on these figures in order to account for all the energy transfer. These lines for each flame cross once and show a reasonable heat balance considering all the measured and calculated quantities. Flame 3 shows the worst agreement in the total heat balance. The major source of error in all the heat balances is probalby in the input amount of propane, which could slowly vary during a test by around one percent of the desired value.

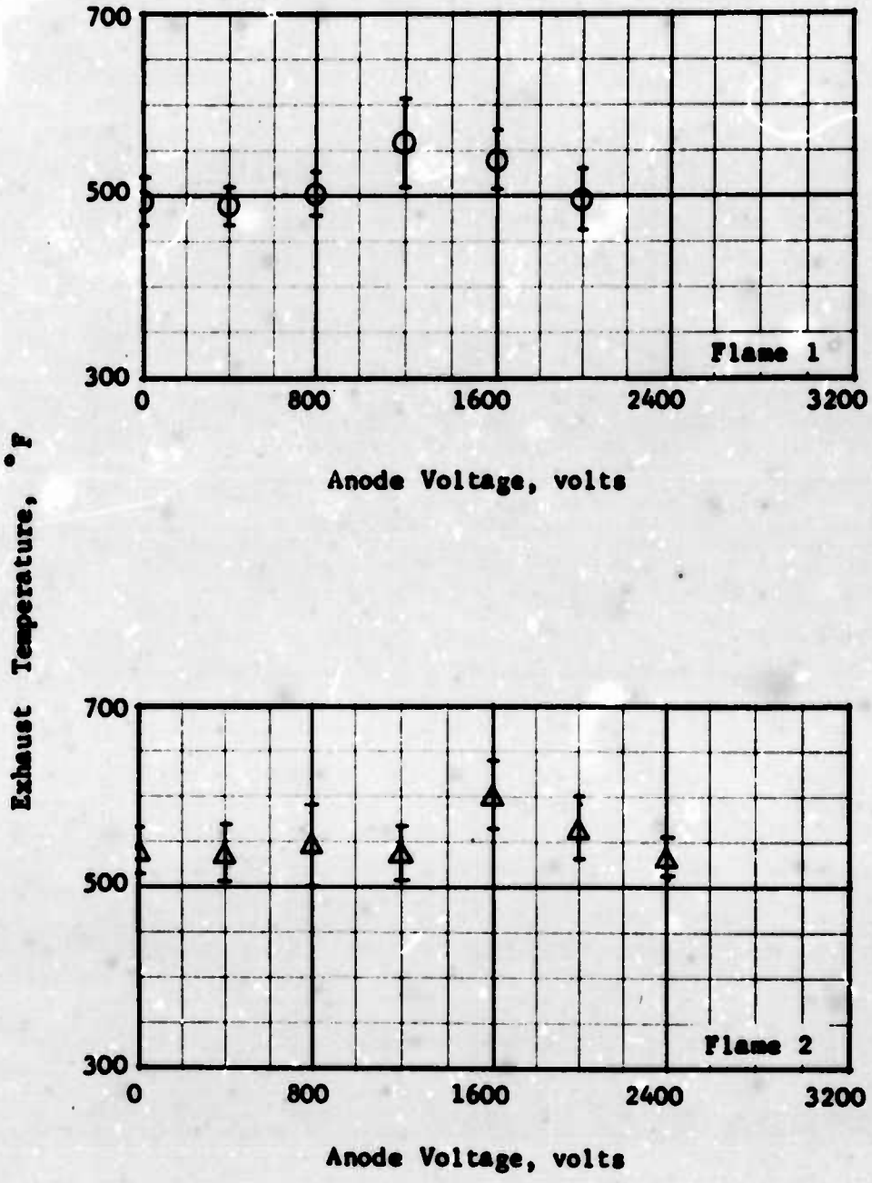

Fig. 67 Exhaust temperature as a function of anode voltage

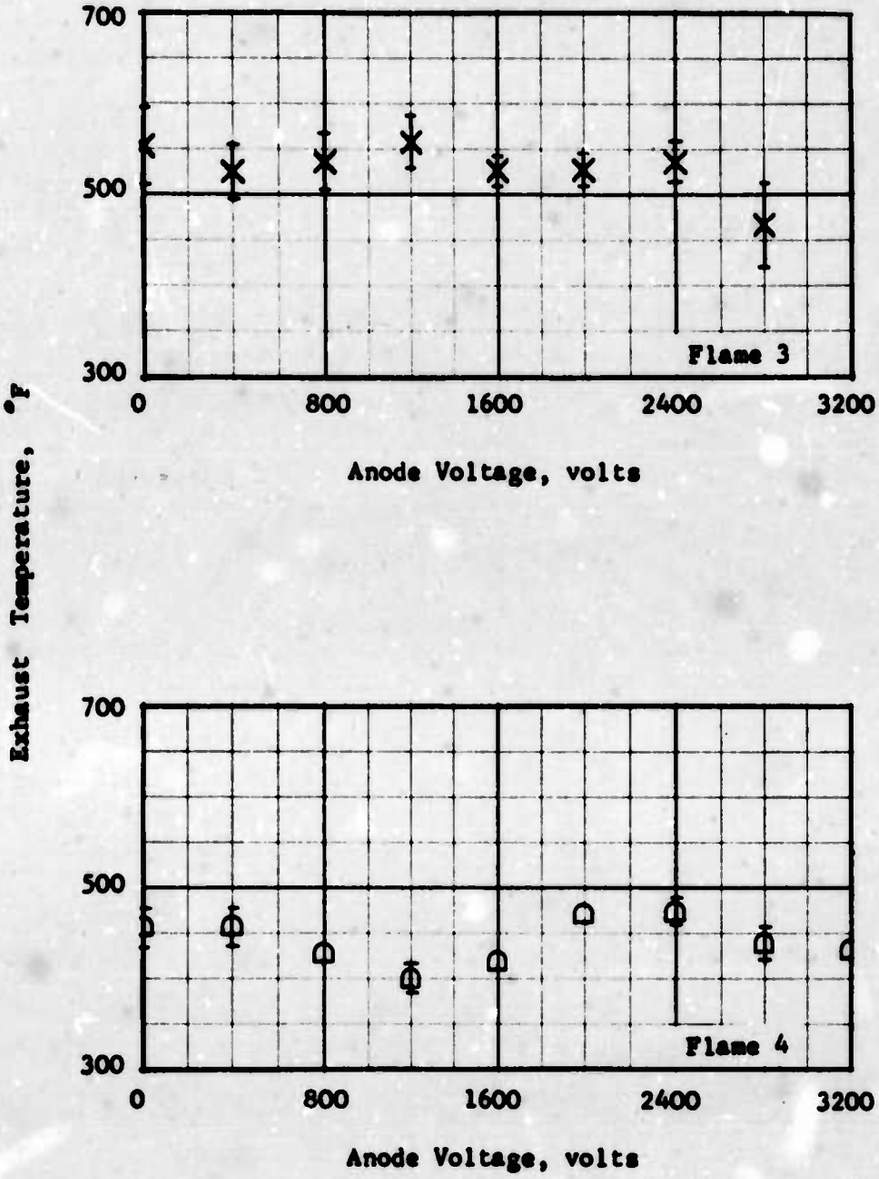

Fig. 68 Exhaust temperature as a function of anode voltage

10.4 DISCUSSION OF RADIATIVE TRANSFER

Radiative heat transfer from flames depends to a great extent on the emissivity. For nonluminous flames the energy is radiated in specific bands of wavelengths, whereas for luminous flames where carbon particles are present and achieve a high temperature, continuous radiation at a higher emissivity generally takes place. In some industrial applications radiative transfer is desirable and foreign particles are injected into the flame to increase the emissivity (51). Although a detailed study of radiative transfer was not made in the present study, and there were indications that radiation was secondary to convection in this case, there is in the general case of luminous flames a possible strong mechanism for an electric effect on radiative transfer. There is evidence that a field can greatly affect the growth and distribution of carbon particles in flames (2, 24). A theoretical study (52) has shown that large variations in emissivity are obtained by changes in carbon particle size and distribution. An indication of the magnitudes of the effect of carbon particles on emissivity is given by Tables 10 and 11, which show results from Reference 52. It appears that if carbon particle size and quantity can be effectively changed electrically, then a large heat transfer effect may be expected in flames that are primarily radiative because of carbon.

Table 10. Flame Emissivity for Various Carbon Particle Sizes and Wavelength at a Surface Density of 10^{13} Particles cm^{-2}

Particle Size	Wavelength, microns			
	2	6	10	16
50 A	0.15	0.02	--	--
200 A	1	0.8	0.4	0.2
500 A	1	1	1	0.96

Table 11. Flame Emissivity for Various Carbon Particle Sizes and Surface Density at a Wavelength of 6 Microns

Particle Size	Flame Surface Density, Particles cm^{-2}				
	10^{11}	10^{12}	10^{13}	10^{14}	10^{15}
50 A	--	0.01	0.02	0.2	0.9
200 A	0.02	0.13	0.8	1	1
500 A	0.2	0.92	1	1	1

CHAPTER 11

SUGGESTIONS FOR FURTHER RESEARCH

The present investigation was limited to consideration of steady applied voltages. Alternating electric fields could also affect flames, and, because of the field reversal, result in fundamentally different interactions with the flame. The frequency conceivably would be an important parameter since it would determine the length of travel of any given ion before the ion reversed direction in response to the field. Three possible regimes of action would occur when the field and ion mobility are such as to reverse the direction of ion motion when the ion has traveled a distance less than the flame thickness, less than the combustion chamber width, or greater than the combusion chamber width.

The high voltage equipment available could only supply either steady or 60 cycles per second output. Figure 69 shows photographs of two flames with 60 cycle voltages applied to the electrodes. The results were the same whether the fuel side electrode or the air side electrode was impressed with the voltage and the other side grounded. The sequence of photographs reveal a flame movement toward the electrode on the air side of the flame. At intermediate voltages one of the flames possesses a peculiar wavy shape.

Free carbon in the flame gases appears to be significant, although a flame movement toward the air side was present with an entirely nonluminous flame. The lower sequence of photographs in Fig. 69 shows a flame relatively rich in fuel with a corresponding large amount of free carbon. At the highest voltage the flame is seen to be spread out across the width of the combustion chamber. It is speculated that charged carbon particles may have a mobility low enough that they oscillate between the electrodes, inducing a turbulence which results in a flame more characteristic of a premixed flame rather than a diffusion flame.

It is suggested that further study be applied to the interaction of flames with controlled frequency electric fields; in this connection luminous hydrocarbon flames may be particularly interesting.

Fig. 69 Flame Photographs with Alternating Voltages

CHAPTER 12

SUMMARY AND CONCLUSIONS

Flat parallel diffusion flames of propane and air were formed in a flat combustion chamber; the wall on the fuel side served as an anode and the wall on the air side was the cathode across which a D.C. voltage of up to 3200 volts was impressed. Four flames were investigated; three flames at equal velocities with various proportions of propane and one flame at a higher velocity. The leanest mixturew was nonluminous and the richest mixture very luminous. The combustion chamber had segmented anode and cathode walls and was instrumented to measure local current density, local heat transfer rate, electric pressure, exhaust composition, and exhaust temperature as a function of applied voltage. The flames could be viewed through a window in the edge wall of the combustion chamber.

The applied electric field was found to affect the flame through three different mechanisms. It was shown that a gradient in current density along the flame was responsible for an induced gas motion away from the flame in the zone containing positive ions. Such an induced motion affected the concentrations of fuel and air in the chamber so as to cause the flame to move toward the cathode.

Another interaction between the field and the flame was the onset of a flickering condition which, with increasing voltage, appeared at upper parts of the flame first. A parameter for describing flame instability was set up which indicated that conditions near the saturation voltage of the flame favored instability. A stabilizing parameter proportional to the concentration gradients in the combustion chamber was defined which indicated that the flame gets less stable in the regions further downstream. Onset of stability was detected by an unsteadiness in the flame current observed on an oscilloscope.

A third mechanism was the attachment of electrons to carbon particles or molecules in upper parts of the flame. The resulting electrically induced drift of the negative ions tended to reverse the trend of induced motion toward the cathode at lower parts of the flame.

The electric interactions with the flame were found to affect greatly the heat transfer rates, especially near the base of the flame. At the highest voltages applied, the flame was observed to impinge directly on the cathode with increase in local heat transfer over the no voltage case of up to a factor of 6. The anode heat transfer rate near the base of the flame was found to be reduced up to 85%. At progressively higher

parts of the flame the electric effect decreased. It is, therefore, concluded that heat transfer rates can be either increased or decreased in a controlled manner by the application of fields.

The maximum current density from the flames were only of the order of eight microamperes per square inch of flame surface and, therefore, direct effects of current such as recombination were extremely small compared to the heat transfer rates.

Appreciable decreases in the amount of carbon monoxide and unburnt hydrocarbon were found to be obtained by the application of voltage; solid carbon formation was found to increase. A possible explanation for the increase in solid carbon is the electron attachment to carbon particles in the pyrolysis zone with a subsequent movement away from the flame, favoring escape of the particle from combustion.

There were indications that the heat transfer was convection controlled, but a possible strong mechanism for an electric effect on luminous flames was outlined. It may be possible to control the emissivity of flames through the influence of the electric field on the formation, growth, or combustion of charged particles in the flame.

In the present investigation an electric field was applied across the combustion chamber from the fuel side toward the air side. From the mechanisms described, if the applied voltage were reversed in polarity, flame movement toward the electrode on the fuel side would be expected. In this case, however, carbon particles would be present mostly in a region of positive ions, and, therefore, ion attachment to particles would add to the effect of the moving positive ions.

APPENDIX

ONE-DIMENSIONAL ELECTRIC EQUATIONS OF A FLAT FLAME BETWEEN ELECTRODES

Derivation of Eq. (3.14)

Integration of Eq. (3.12) yields

$$J_+ = rs + \text{constant}$$

But $J_+ = 0$ for $s < s_1$, so the constant above is $-rs_1$, hence

$$J_+ = r(s-s_1)$$

The current density measured at the electrodes is

$$J_{O+} = r(A-s_1)$$

and also

$$J_s = rA$$

Combining the above two equations

$$s_1 = A\left[1 - \frac{J_{O+}}{J_s}\right]$$

which is Eq. (3.14).

Derivation of Eq. (3.18)

The voltage drop across the ionization zone is

$$V_2 = \int_{\left(1-\frac{J_O}{J_s}\right)A}^{A} \left[\left[\frac{J_s A}{k\epsilon}\right]^{1/2}\left[\frac{J_O}{J} - 1\right] + \left[\frac{J_s}{k\epsilon A}\right]^{1/2} s\right] ds = \left[\frac{J_s A}{k\epsilon}\right]^{1/2}\left[\frac{J_O}{J_s} - 1\right]s$$

$$+ \left[\frac{J_s}{k\epsilon A}\right]^{1/2} \frac{s^2}{2}\Bigg|_{\left(1-\frac{J_O}{J_s}\right)A}^{A} = \frac{1}{2}\left[\frac{J_O^4 A^3}{J_s^3 k\epsilon}\right]^{1/2}$$

which is Eq. (3.18).

Derivation of Eq. (3.28)

From Eq. (3.15)

$$\frac{dE}{ds} = \frac{n_+}{\epsilon}$$

But

$$J_+ = rs$$

and

$$n_+ = \frac{J_+}{\epsilon k_+ E}$$

Therefore

$$\frac{dE}{ds} = \frac{rs}{\epsilon k_+ E}$$

Integrating,

$$E^2 = \frac{rs^2}{k_+ \epsilon} + \text{constant}$$

But $E = E_f$ at $s = A$, and substituting $J_s = rA$,

$$E = \left[E_f^2 - \frac{J_s}{k_+ \epsilon A} (A^2 - s^2) \right]^{1/2}$$

which is Eq. (3.28).

Derivation of Eq. (3.29)

$$V_2 = \int \left[E_f^2 - \frac{J_s}{k\epsilon A} (A^2 - s^2) \right]^{1/2} ds$$

Rearranging,

$$V_2 \left[\frac{J_s A^3}{k\epsilon} \right]^{-1/2} = \int \left[E_f^2 \frac{k\epsilon}{J_s A} - 1 + \frac{s^2}{A^2} \right]^{1/2} d\left(\frac{s}{A}\right) = \frac{s}{2A} \left[\frac{E_f^2 k\epsilon}{J_s A} - 1 + \frac{s^2}{A^2} \right]^{1/2}$$

$$+ \frac{1}{2} \left[\frac{E_f^2 k\epsilon}{J_s A} - 1 \right] \ln \left[\frac{s}{A} + \left[\frac{E_f^2 k\epsilon}{J_s A} - 1 + \frac{s^2}{A^2} \right]^{1/2} \right] \Bigg|_0^1$$

Evaluating the above equation results in

$$V_2 = \frac{E_f A}{2} + \frac{1}{2}\left[\frac{J_s A^3}{k\epsilon}\right]^{1/4}\left[\frac{E_f^2 k\epsilon}{J_s A} - 1\right]\operatorname{csch}^{-1}\left[\frac{E_f^2 k\epsilon}{J_s A} - 1\right]^{1/4}$$

which is Eq. (3.29).

Justification of Eq. (3.35)

Equation (3.34) can be written

$$V\left[\frac{J_s A^3}{k\epsilon}\right]^{-1/4} = \left[E'^2 - 1\right]^{1/4}\frac{L}{A} + \frac{E'^2}{2} + \frac{1}{2}\left[E'^2 - 1\right]\operatorname{csch}^{-1}\left[E'^2 - 1\right]^{1/4}$$

$$+ \frac{1}{3}\left[\frac{2(R-L-A)}{A} + E'^2\right]^{3/2} - \frac{E'^3}{3}$$

where E is the nondimensional field strength $E' = E_f\left[\frac{J_s A}{k\epsilon}\right]^{1/4}$

For the particular case when (R-L) = L = 50 A and E' = 2 the right side of the above equation is

$$50 + \frac{1}{2} + 0.82 + 344 - \frac{8}{3}$$

The second two terms are small and therefore Eq. (3.35) is justified on an order of magnitude basis.

REFERENCES

1. Wilson, H. A., "Electrical Conductivity of Flames," Review of Modern Physics, Vol. 3 (1931).

2. Payne, K. G., Weinberg, F. J., "A Preliminary Investigation of Field Induced Ion Movement in Flame Gases and Its Applications," Proceedings of the Royal Society, Vol. 250A (1959), p. 316.

3. Papoular, R., Electrical Phenomena in Gases, American Elsevier Publishing Co., (1965), p. 148.

4. Calcote, H. F., King, J. R., "Studies of Ionization in Flames by Means of Langmuir Probes," Fifth Symposium (International) on Combustion, Reinhold Publishing Co., New York, N. Y. (1955).

5. Calcote, H. F., "Ion Production and Recombination in Flames," Eighth Symposium (International) on Combustion, Williams and Wilkins Co., Baltimore, Md. (1962), p. 184.

6. Calcote, H. F., "Ion and Electron Profiles in Flames," Ninth Symposium (International) on Combustion, Academic Press, New York, N. Y. (1963) p. 622.

7. Mukherjee, N. R., et. al., "Ions in Flames," Eighth Symposium (International) on Combustion, Williams and Wilkins Co., Baltimore, Maryland (1962) p. 1.

8. Shuler, K. E., Weber, J., "A Microwave Investigation of Ionization of Hydrogen-Oxygen and Acetylene-Oxygen Flames," Journal of Chemical Physics, Vol. 22, No. 3 (March, 1954) p. 491.

9. Singer, J. M., Grumer, J., "Carbon Formation in Very Rich Hydrocarbon Air Flames," Seventh Symposium (International) on Combustion, Butterworths, London (1959) p. 559.

10. Nakamura, J., "Effect of the Electric Field upon the Spectra of the Hydrocarbon Diffusion Flame," Combustion and Flame, Vol. 3, No. 3, (September, 1959).

11. Calcote, H., Kurgius, S., Miller, W., "Negative and Secondary Ion Formation in Low Pressure Flames," Tenth Symposium (International) on Combustion, The Combustion Institute, Pittsburgh, Pa. (1965).

12. DeJaegere, S., Deckers, J., Van Tiggelen, A., "Identity of the Most Abundant Ions in Some Flames," Eighth Symposium (International) on Combustion, Williams and Wilkins Co., Baltimore, Md., (1962) p. 155.

13. Dimmock, T. H., Kineyko, W. R., "The Low Pressure, Combustion Gas Plasma," Combustion and Flame, Vol. 7, (Sept., 1963).

14. Wortberg, G., "Ion Concentration Measurements in a Flat Flame at Atmospheric Pressure," Tenth Symposium (International) on Combustion, The Combustion Institute, Pittsburgh, Pa., (1965) p. 651.

15. Calcote, H. F., Reuter, J. L., "Mass Spectrometer Study of Ion Profiles in Low Pressure Flames, "Journal of Chemical Physics, Vol. 38, No. 2, (1963) p. 310.

16. King, J. R., "Recombination of Ions in Flames," Air Force Office of Scientific Research, Contract AF 49(638)-650, Project 9751, Task No. 37510 (1962).

17. Van Tiggelen, A., "Experimental Investigation of Ionization Processes in Flames," Air Research and Development Command, U. S. Air Force, Contract No. AF 61(052)-398, AD-258050, (May, 1961).

18. Deckers, J., Van Tiggelen, A., "Ion Identification in Flames," Seventh Symposium (International) on Combustion, Butterworths, London (1959).

19. Kinbara, T., Nakamura, J., Ikegani, H., "Distribution of Ions in Low Pressure Flames," Seventh Symposium (International) on Combustion, Butterworths, London, (1959) p. 263.

20. Pancelet, J., Berendsen, R., Van Tiggelen, A., "Comparative Study of Ionization in Acetylene-Oxygen and Acetylene-Nitrous Oxide Flames," Seventh Symposium (International) on Combustion, Butterworths, London (1959) p. 256.

21. Smith, H., Sugden, J. M., "Studies on the Ionization Produced by Metallic Salts in Flames," Proceedings of the Royal Society, Vol. 211 A (1952).

22. Becker, A., "Die Elektrischen Eigenschaften der Flamme," Handbuch Der Experimentalphysik, Vol. 13, Part 2, Leipzig, Germary (1959).

23. Lawton, J., Weinberg, F., "Maximum Ion Currents from Flames and the Maximum Practical Effects of Applied Electric Fields," Proceedings of the Royal Society, Vol. 277 A, p. 468 (1964).

24. Place, E. R., Weinberg, F., "Electrical Control of Flame Carbon," Proceedings of the Royal Society, Vol. 289 A (1966) p. 192.

25. Payne, K. G., Weinberg, F., "Measurements on Field-Induced Ion Flows from Plane Flames," Eighth Symposium (International) on Combustion, Williams and Wilkins Co., Baltimore, Md. (1962) p. 207.

26. Parker, T. A., Heinsohn, R. J., "The Effect of a Transverse Electric Field on Bluff Body Flame Extinction Limits," Third Conference on the Performance of High Temperature Systems, Pasadena, California (December 7-9, 1964).

27. Heisohn, R. J., "Studies of a Flat Flame under Impressed Electric and Magnetic Fields," Ph. D. Thesis, Michigan State University, (June, 1963).

28. Heisohn, R. J., Lay, J. E., "Studies of a Flat Flame under Impressed Electric and Magnetic Fields," ASME Paper 64-WA/Ener-2, (December, 1964).

29. Rezy, B. J., Heinsohn, R. J., "The Increase in the Maximum Heat Release Rate and Apparent Flame Strength of Opposed-Jet Diffusion Flames under Impressed Electric Fields," ASME Paper 65-WA/Ener-3 (November, 1965).

30. Cook, M. A., Gwyther,T., "Influence of Electrical Fields on Shock of Detonation Transition," AF OSR-56, AD No. 629 239 (1965).

31. Bone, W., Frazer, R., Wheeler, W., Transactions of the Phil. Society (London) Vol. 735A (1935).

32. Guenault, E., Wheeler, R., "Propagation of Flame in Electric Fields," Vol. 135 (1932) p. 2788.

33. Richardson, D., Karlovitz, B., "A Burner with an Electrical Discharge Superimposed on the Combustion Flame," ASME Paper 61-WA 251 (December, 1961).

34. Harker, J. H., "Electrically Augmented Flames," Industrial and Process Heating, Vol. 3, No. 12, (1963).

35. Davies, R. M., "Heat Transfer Measurements on Electrically-Boosted Flames," Tenth Symposium (International) on Combustion, The Combustion Institute, Pittsburgh, Pa. (1965).

36. Calcote, H., King, J., "Studies of Ionization in Flames by Means of Langmuir Probes," Fifth Symposium (International) on Combustion, Reinhold Publishing Co., New York, N. Y. (1965) p. 423.

37. Burke, S., Shumann, E., Ind. Eng. Chem., Vol. 20 (1928) p. 998.

38. Powell, H. N., Browne, W. G., "Some Fluid Dynamic Aspects of Laminar Diffusion Flames," Sixth Symposium (International) on Combustion, Reinhold Publishing Co., New York, N. Y. (1957) p. 124.

39. Malkus, W., Veronis, G., "Surface Electroconvection," Physics of Fluids, Vol. 4, No. 1 (January, 1961).

40. Rose, D., Clark, M., Plasmas and Controlled Fusion, John Wiley and Sons, New York, N. Y., (1961).

41. Melcher, J. R., Field Coupled Surface Waves, Massachusetts Institute of Technology Press, Cambridge, Mass. (1963).

42. Cobine, J. D., Gaseous Conductors, Dover Publications, New York, N. Y. (1958).

43. Papoular, R., Electrical Phenomenon in Gases, American Elsavier Publishing Co., New York (1965) p. 189.

44. Sherman, R. A., "Heat Transfer by Radiation from Flames: A Summary of the Work of the International Flame Research Foundation," Trans. of the A.S.M.E., Vol. 79, (1957) p. 1727.

45. Thring, M. W., The Science of Flames and Furnaces, John Wiley and Sons, New York, N. Y. (1952).

46. Godridge, A., Thurlow, G., Wallis, J., "A Method of Studying the Influence of Flame Characteristics on Heat Transfer in Furnaces," Journal of the Institute of Fuel, Vol. 31 (1958) p. 491.

47. Tailby, S., Ashton, M., "Heat Transfer from Town Gas Flames to Water Jacketed Horizontal Tubes," Transactions of the Institution of Chemical Engineers, Vol. 36 (1958).

48. Tailby, S., Clutterbuck, E., "Heat Transfer in Horizontal Town Gas Immersion Tubes," Trans. of the Inst. of Chemical Engineers, Vol. 92 (1964).

49. Zartman, W., Churchill, S., "Heat Transfer from Acoustically Resonating Gas Flames in a Cylindrical Burner," A.I.Ch.E. Journal (December, 1961) p. 588.

50. Tailby, S., Berkovitch, J., "The Effect of Sonic Vibrations on Heat Transfer from Town Gas Flames," Trans. Inst. of Chemical Engineers, Vol. 36, (1958).

51. DeWerth, D., Zalavadia, J., "Effects of Particle Injection on Natural Gas Flame Radiation," ASME Paper 65-WA/Fu-2, (November, (1965).

52. Stull, V. R., Plass, G., "Emissivity of Dispersed Carbon Particles," Journal of the Optical Society of America, Vol. 50, No. 2 (February, 1960) p. 121.

UNCLASSIFIED
Security Classification

DOCUMENT CONTROL DATA - R & D

(Security classification of title, body of abstract and indexing annotation must be entered when the overall report is classified)

1. ORIGINATING ACTIVITY *(Corporate author)*
The Ohio State University Research Foundation, Columbus, Ohio

2a. REPORT SECURITY CLASSIFICATION
Unclassified

2b. GROUP
N/A

3. REPORT TITLE
Effects of a Transverse Electric Field on the Characteristics and Heat Transfer of a Diffusion Flame

4. DESCRIPTIVE NOTES *(Type of report and inclusive dates)*
Technical

5. AUTHOR(S) *(First name, middle initial, last name)*
Pejack, Edwin R.; Velkoff, Henry R.

6. REPORT DATE
November 1967

7a. TOTAL NO. OF PAGES
145

7b. NO. OF REFS
52

8a. CONTRACT OR GRANT NO.
DA-31-124-ARO-D-246

b. PROJECT NO.
2001050B700, 1D12, 40A142

c.

d.

9a. ORIGINATOR'S REPORT NUMBER(S)
Technical Report # 8

9b. OTHER REPORT NO(S) *(Any other numbers that may be assigned this report)*

10. DISTRIBUTION STATEMENT
Distribution of this document is unlimited.

11. SUPPLEMENTARY NOTES

12. SPONSORING MILITARY ACTIVITY
US Army Research Office - Durham
Durham, North Carolina

13. ABSTRACT

Effects of a transverse electric field on a parallel flow diffusion flame in a flat combustion chamber were investigated. Various mixtures of propane, nitrogen, and air were introduced separately at the base of an experimental combustion chamber and burned in a diffusion flame sheet located between flat walls of the chamber which served as anode and cathode. The electrode walls were instrumented to measure the local heat transfer rate, local current density, and pressure.

It was found that the application of a voltage difference across the electrodes moved ions out of the burning zone and resulted in a current at the electrode walls. The heat transfer rate near the base of the flame was considerably increased on the cathode and decreased on the anode; at positions further from the base of the flame the electric effect was lessened.

Flame distortion was thought to be caused by electrically induced gas motion derived from a gradient in current density in the flow direction and by the onset of an electrically induced flame flickering. An analysis of the products of combustion revealed that the applied electric field acted to increase the amount of unburnt solid carbon and decrease the quantities of unburnt fuel and carbon monoxide.

DD FORM 1 NOV 1473

Unclassified
Security Classification

Unclassified
Security Classification

14. KEY WORDS	LINK A		LINK B		LINK C	
	ROLE	WT	ROLE	WT	ROLE	WT
1. ombustion 2. eat transfer 3. combustion heat transfer 4. electrostatic effects on combustion 5. electrostatic effects on heat transfer 6. electrostatic effects on combustion heat transfer						

Unclassified
Security Classification